UNIVERSITY OF CALIFORNIA

Santa Barbara

An Experimental Toolkit for Analysis of Single Monoaminergic Axons in the Mouse Brain

A Dissertation submitted in Partial Satisfaction of the requirements for the degree of Doctor of Philosophy in Psychological and Brain Sciences

by

Kasie Chanel Mays

Committee in charge:

Professor Skirmantas Janusonis, Committee Chair

Professor Benjamin Reese

Professor Kathleen Foltz

Professor Kenneth Kosik

December 2022

The dissertation of Kasie Chanel Mays is approved

_____

Professor Benjamin Reese

_____

Professor Kathleen Foltz

_____

Professor Kenneth Kosik

_____

Professor Skirmantas Janusonis, Committee Chair

December 2022

ACKNOWLEDGMENTS

I would like to thank the following people, without whom I would not have made it through my Ph.D. program.

The Neuroscience and Behavior faculty at the University of California- Santa Barbara, especially my PI and advisor, Skirmantas Janusonis. Without your unwavering support, mentorship, patience, and guidance, I never would have made it in graduate school and definitely would not have achieved as much as I have today. A special thanks to Justin Haiman for being the best research assistant whose support allowed me to go the extra mile—cheers to Disney music and long hours of science. Thank you to the ARC staff and our fantastic veterinarian, Manny Garcia, for training me and all your support to researchers and animals alike. Many thanks to the microscopy facilitator, Ben Lopez, for his training, expertise, and invaluable help while we struggled through troubleshooting our imaging process. And to all the countless people at UCSB that cheered me on and lifted me up when I fell—you are the true heroes. Chris McFerron, you are the heart of PBS.

The biggest and loudest THANK YOU goes out to my wonderful family and specifically, my amazing kids. You are my heart and were so patient with me during this long journey. You are my biggest support system, and I could not have done this without you guys.

This dissertation is dedicated to my extraordinary and beautiful parents.

In loving memory of Robert & Shirley Stark.

I know you would have done anything to have been here… I did it <3

VITA OF KASIE CHANEL MAYS

December 2022

EDUCATION

Bachelor of Science, University of South Dakota, May 2017 (summa cum laude)

Certificate in College and University Teaching, University of California, Santa Barbara, June 2022

Doctor of Philosophy in Psychological and Brain Sciences, University of California, Santa Barbara, December 2022 (expected)

PROFESSIONAL EMPLOYMENT

2017-2018: Teaching Assistant, Department of Psychological and Brain Sciences, University of California, Santa Barbara

Summer 2019: Instructor of Record, Summer Discovery Program, University of California, Santa Barbara

2020-2022: Associate Instructor, Department of Psychological and Brain Sciences, University of California, Santa Barbara

2022: Graduate Career Advisor, Career Services, University of California, Santa Barbara

PUBLICATIONS

Serotonergic Axons as 3D Walks Janusonis S., Mays KC., Hingorani M, ACS Chemical Neuroscience, 2019

AWARDS

Harry J Carlisle Award, University of California, Santa Barbara, 2022

Nasser Graduate Student Memorial Scholarship, University of California, Santa Barbara, 2022

Graduate Opportunity Fellowship, University of California, Santa Barbara, 2021 – 2022

Nomination for Excellence in Teaching, University of California, Santa Barbara, 2020 & 2021

Graduate Student Researcher Fellowship, University of California, Santa Barbara, 2018 – 2019

Soroptimist Women's Opportunity Scholarship Recipient, University of South Dakota, 2014

FIELDS OF STUDY

Major Field: Neuroscience and Behavior

Studies in Serotonergic Axonal Research with Professor Skirmantas Janusonis

ABSTRACT

An Experimental Toolkit for Analysis of Individual Monoaminergic Axons in the Mouse Brain

by

Kasie Chanel Mays

The current understanding of monoaminergic neurotransmission relies upon the ability to image and analyze the components of these systems. Yet, the efforts to understand these systems are inhibited from a combination of the unique properties of axons that release monoamines and limitations in imaging technologies. Axons from monoaminergic cells can be thin (~ 1 μm in diameter) and cannot be viewed directly, requiring both fluorescent labeling and high-resolution imaging. Adding further complications are that the axons travel the entirety of the brain, appear to intertwine freely with each other, and are often difficult to track individually. Here, we successfully designed an experimental process for monoaminergic axon research that endows the ability for axon differentiation with the use of Brainbow AAV and Cre technologies. These approaches were validated with a new algorithm that can reliably trace individual axons in various brain regions. To complement these methods and provide information on axon trajectories in the natural 3D-space, we also designed a process for high-resolution light-sheet microscopy using tissue clearing technologies for imaging of axons without sectioning tissue combined with machine learning

algorithms for automated tracing. These methods allow for unprecedented access to individual axon trajectories and support their modeling as paths of spatial stochastic processes. This project focused on the serotonin system, however, these methods can be extended and applied to research using other monoamines. This is the first research on serotonin or monoamines in general with the capability of individual axon discrimination and can help answer many previously elusive questions within this field of research.

TABLE OF CONTENTS

Certificate of Approval of Dissertation.....*ii*

Acknowledgments.....*iii*

Vita of Kasie Mays.....*iv*

Abstract.....*vi*

Introduction.....1

Chapter 1: Background Information.....3

Anatomy of the Serotonergic System.....3

Brief Overview of Serotonergic Functions.....5

i. Neuroplasticity.....5

ii. Respiration and Body Temperature.....7

iii. Sexual Behaviors.....9

iv. Compulsivity, Impulsivity, and Learning.....10

Serotonergic Axonal Development.....13

Fiber Morphological Diversity and Varicosities.....17

i. Morphology.....17

ii. Varicosities.....17

5HT Synthesis and Release.....19

Neurotransmitter Co-Release.....19

Serotonin Receptors.....22

Serotonin Fiber Terminal Field Densities.....24

Serotonin Fiber Plasticity.....25

Serotonin and Psychological Disorders.....27

Chapter 2: Research Aims.....31

Chapter 3: Conceptual and Historical Overview of Methods.....32

Mouse Models.....33

i. Cre-LoxP.....33

ii. Brainbow.....34

iii. Adeno-Associated Viruses.....36

iv. Brainbow AAV.....37

Manual and Automatic Tracing.....37

i. Manual Tracing.....37

ii. Automatic Tracing.....37

iii. Brainbow nTracer.....43

iv. Machine Learning (TrailMap) 44

Analysis Methods.....45

i. Von-Mises Fisher Model.....45

ii. Fractional Brownian Motion.....48

Tissue Clearing.....50

Chapter 4: Experiments.....52

Experiment 1: Imaging and Tracing of a Transgenic Fluorescent Mouse Model.....52

Ex1.1 Verification of Transgene Expression.....52

Ex1.2 Signal Amplification and Imaging.....59

Ex1.3 Fiber Tracing and Analysis.....62

Experiment 2*:* Creating a Model for Axon Differentiation.....67

Ex2.1 Verification of Transgene Expression.....67

Ex2.2 Signal Amplification and Imaging.....70

Experiment 3: A Model for Axon Differentiation with Brainbow AAV.....72

Ex3.1 Surgical Transfection of the Brainbow AAV.....73

Ex3.2 Signal Amplification and Imaging.....74

Experiment 4: Visualization of Serotonergic Fibers in a 3D Environment.....80

Ex4.1 Tissue Clearing.....81

Ex4.2 Testing Immunohistochemistry on Cleared Tissue.....83

Ex4.3 Light-Sheet Imaging.....87

Chapter 5: Discussion.....92

References.....102

Monoaminergic neurotransmission influences numerous processes in the brain such as motivation, self-control, reactivity to stress, mood regulation, and cognitive performance. The specific neurotransmitters classified as monoamines are serotonin, dopamine, adrenaline, and noradrenaline, each of which has roles in specific neurological functions and psychological disorders. A unique characteristic of the monoaminergic system is their cell bodies (somata) can only be found in the brainstem and send extremely long axons to innervate nearly every area of the brain. Our current understanding of monoaminergic neurotransmission is based on our ability to image and analyze the components of the system on multiple scales. However, this effort is hindered by limitations in imaging technology. A particular challenge is collecting information about something that is very small (e.g., axons may be less than 1μm in diameter), yet travels the entirety of the brain. Morphologically, it is similar to trying to find a specific street when looking at a map of an entire state. Even if we zoom in to just looking at a map of a city, finding the specific street is still challenging. Once we have obtained the magnification that is needed to find the specific street, we have then lost a lot of information about how the street fits into the city and the state. We face the same issues when imaging these systems. Once we obtain the magnification needed to visualize individual axons, we have lost the larger picture of how the axons taken together create dense meshworks in the brain. This problem can be viewed as a problem of self-organization (Figure 1).

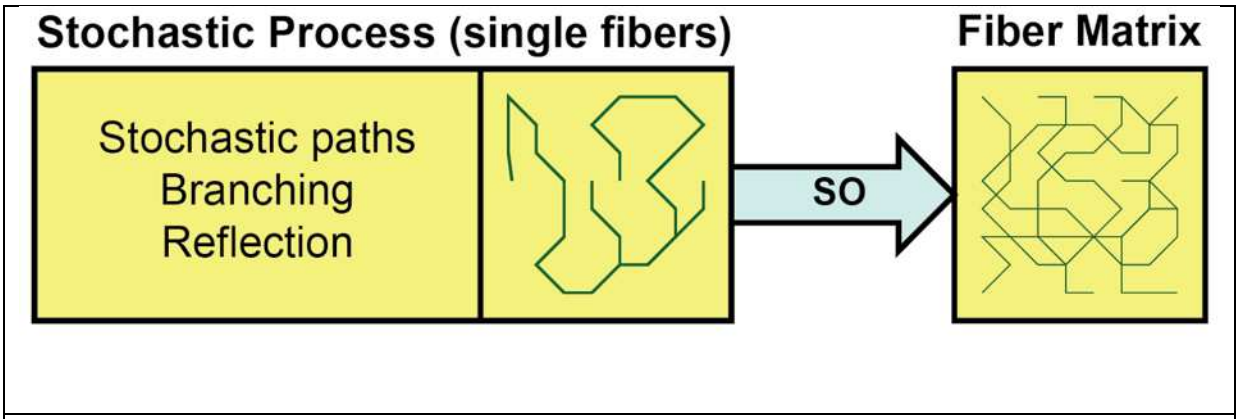

Figure 1: Self-organization (SO) of the serotonergic meshwork (matrix), a typical monoaminergic meshwork.

Due to the inability for monoaminergic axons to be viewed directly, fluorescent labeling is added through a method called immunohistochemistry (IHC), which comes with limitations of its own. First, IHC labels all cells of the same type with the same color and therefore reduces the ability to differentiate between axons of individual cells for accurate and precise tracing. Second, IHC primarily labels varicosities (which contain a high concentration of neurotransmitter) and leaves the inner-varicose segments weakly labeled. These segments often fall below the detection threshold, causing axons to appear segmented. Current methods for studying monoaminergic axons are not able to address these challenges; raising the question: Can a method be developed that allows for both differentiation and long-distance tracing of axons within intact tissue? In this project, we develop a toolkit for analyzing monoaminergic neurotransmitters using the serotonergic system that allows for axon differentiation through a transgenic mouse construct; we use cutting edge techniques of Brainbow adeno-associated viruses (AAV's), tissue clearing, light-sheet microscopy and automatic axon tracing.

CHAPTER 1: BACKGROUND INFORMATION

ANATOMY OF THE SEROTONERGIC SYSTEM

Serotonergic (5HT) neurons are among the earliest generated neurons in the brain. Developmental studies show that they are produced during mid-gestation in rodents and from the fifth-to-seventh week in humans (Deneris & Gaspar, 2018). In mice, serotonergic neurons are born between embryonic day 10 (E10) and at E12 from separate progenitor pools which span both transcriptionally and anatomically defined hindbrain segments called rhombomeres (R1–R11) and the 'isthmus' (also known as R0) (Simon et al., 2005; Jensen et al., 2008). All rhombomeres express the transcription factor *Pet1,* yet are distinguishable through the expression of an additional transcription factor. *Pet1* encodes an ETS (erythroblast transformation specific) family transcription factor and strongly overlaps with the expression of the rate-limiting enzyme for serotonin synthesis, tryptophan hydroxylase 2 (Tph2), in defining the serotonergic neuron identity. For instance, R0 and R1 express *En1-Pet1*, R2 expresses *Rse2(HoxA2)-Pet1*, R3 and R5 express *Erg2-Pet1*, R4 expresses *Hoxb1-Pet1,* and R6-R11 express *Tac1-Pet1* (Okaty et al., 2019). Serotonergic cells originate close to the floor plate of the neural tube ventricular zone and, following aggregation, migrate to the pial raphe surface using somal translocation, creating the characteristic sigmoidal shape of the raphe (Lidov & Molliver, 1982; Hawthorne et al., 2010 Deneris & Gaspar 2017). At this time, the newborn serotonergic neurons are in an immature state, have not yet migrated to their adult raphe locations, have yet to develop axonal and dendritic structures, and have not made connections with neuronal targets and afferents. Furthermore, complex upstream and downstream gene expression has been shown during this timeframe, suggesting that

maturation of serotonergic neurons results from the induction of specific genes. For example, RNA sequencing of flow-sorted serotonergic neurons followed by hierarchical clustering revealed that expression of the peptide genes *Sst, Penk, Pdyn,* and *Nts,* were low at embryonic day 11.5 (E11.5) when the serotonergic transmitter identity is acquired, but subsequently increased by two to three-fold through the remaining fetal stage and into early postnatal life (Wyler et al., 2016).

The resulting anatomy of the serotonergic system in the mammalian brain consists of raphe nuclei clusters that are located solely in the brainstem and are a component of the ascending reticular activating system (ARAS) (Jacobs and Azmitia, 1992; Okaty et al., 2019). There are different grouping and labeling nomenclatures that have been used for naming the cells of this system with some referring only to the serotonergic neurons and some referring to cytoarchitectonic structures that contain serotonergic neurons. The first one divides the raphe into 9 groups of nuclei, named B1-B9, that extend from the medulla to the pons then up to the rostral midbrain (Dahlstroem & Fuxe, 1964). The second model (Figure 2) broadly categorizes the clusters of serotonergic neurons into two brainstem groups that are further subdivided into nuclei. First is the rostral (midbrain/pons) group which consists of four main subdivisions: the caudal linear nucleus (CLi), B9 (from the original nomenclature), the dorsal raphe (DR), and the median raphe (MR). The DR is further subdivided into the dorsal, ventral, lateral wings, interfascicular, and caudal parts. The MR is further divided into the prepontine (PPnR), pontine (PnR), and paramedian parts. The second major brainstem division is the caudal (medulla) groups. This group also has four subdivisions: the nucleus raphe magnus (RMg)—with dorsal and ventral subdivisions, the nucleus raphe obscurus

(ROb), the nucleus raphe pallidus (RPa) and the ventrolateral medulla (VLM) (Jacobs & Azmitia, 1992).

Ultimately, these two nomenclatures are parallel to some extent, but the raphe nuclei contain a variable mix of serotonergic and non-serotonergic neurons. For instance, the

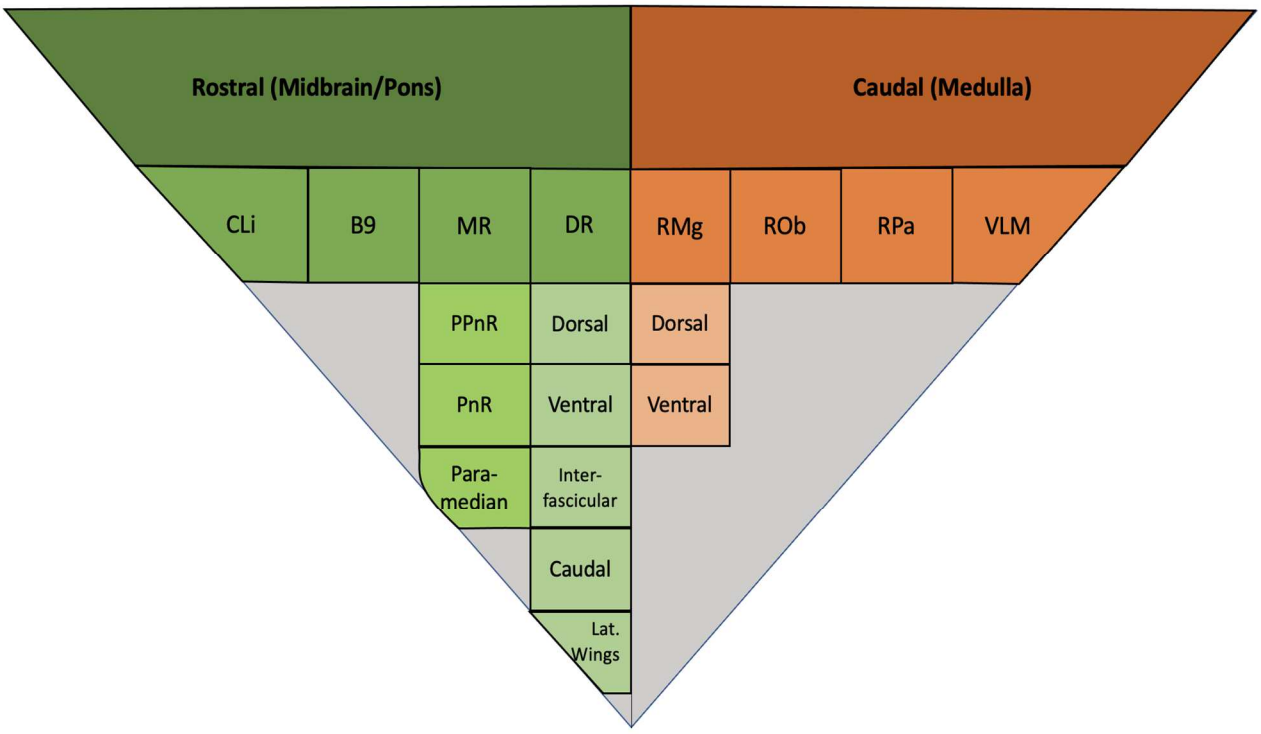

proportion of serotonergic neurons ranges from 50% in the DR, to 21% in the MR, and less than 10% in the paramedian raphe (Sos et al., 2017).

Figure 2: Overview of serotonergic neuronal organization and nomenclature

A BRIEF OVERVIEW OF SEROTONERGIC FUNCTIONS

i. NEUROPLASTICITY

A relationship between serotonin and different types of neuroplasticity appears to be well established, including learning and memory, brain derived neurotrophic factor (BDNF) release, interactions with cell adhesion molecules, and the critical period in the development of the visual system. Neuroplasticity is an umbrella term referring to the

brain's ability to adapt, structurally, to changes in either the internal or external environment (Pascual-Leone et al., 2005; May 2011). One part of neuroplasticity is neurogenesis which refers to newly born neurons. Another aspect is synaptic plasticity, which is the brains' ability to sense, assess, and store information used ultimately for modification of synaptic transmission. It can be achieved through the regulation of the number of synapses (synaptogenesis), which is a crucial part of neuronal development in early life.

Another aspect of serotonin's involvement in plasticity is its interactions with BDNF and cell adhesion molecules. For example, while BDNF administration to cell cultures promotes the growth of serotonergic neurons and dendrite lengths; on the other hand, serotonin increases BDNF mRNA in raphe neuronal cultures (Homberg et al., 2014). Another line of evidence suggests that serotonin interacts with synaptic adhesion molecules. Serotonin increases the polysialylated form of the neural cell adhesion molecule (PSA-NCAM), which has a role in synaptogenesis and neurite remodeling. Moreover, PSA-NCAM is considered a marker of developing neurons with decreasing expression during maturation. Additionally, fluoxetine (a selective serotonin reuptake inhibitor (SSRI)) has been demonstrated to increase the expression of PSA-NCAM in the prefrontal cortex and alter the morphology, connectivity, and plasticity of cortical interneurons (Varea et al., 2007; Guirado et al., 2014).

Perhaps the most interesting evidence of the role serotonin may play in plasticity stems from a large-scale randomized clinical trial of SSRIs in acute stroke patients which found that initiating fluoxetine after an ischemic stroke improved motor outcomes at 90 days (Chollet et al., 2011). In fact, a meta-analysis of over 4000 stroke patients showed a

similar benefit of SSRIs in recovery (Mead et al., 2012). Adding to this evidence are animal studies showing that SSRIs are capable of reopening the critical period for ocular plasticity in adulthood (Maya Vetencourt et al., 2008; Guirado et al., 2016). Critical periods are timeframes in neural development characterized by the potential for large-scale synaptic plasticity and cortical reorganization. With regard to the role of serotonin in reopening critical periods, serotonin can modulate the homeostatic response of visual circuits by decreasing inhibition and therefore, tipping the excitatory–inhibitory balance in favor of excitation (Baroncelli et al., 2010; Guidotti et al., 2012). Similarly, SSRIs have been shown to decrease the overall inhibitory tone in the adult rat visual cortex in a serotonin-dependent manner by decreasing extracellular GABA and reducing the number of GABAergic interneurons (Maya Vetencourt et al., 2008; Ohira et al., 2013; Ng et al., 2015). With SSRIs decreasing the inhibitory tone of the circuit, the cortex becomes hyperexcitable, creating an environment permissive for novel visual experiences to affect circuit organization in a way that is not typically seen in adulthood (Vialou et al., 2015). Finally, serotonin has been shown to have a role in reversal learning and synaptic plasticity (see section on Compulsivity, Impulsivity, and Learning).

ii. RESPIRATION AND BODY TEMPERATURE

Serotonin was perhaps first linked to respiration in 1951 when Reid & Rand noted that intravenous injections of serotonin induced apnea in cats (Reid & Rand 1951). Over time, the link of serotonin to respiration was further defined to a role in the chemoreflex—a physiological phenomenon where increases in carbon dioxide (CO_2) lead to an increase in respiration in an effort to eliminate CO_2, thereby restoring the CO_2-pH

homeostasis. In fact, serotonin neurons are located in close proximity to arteries entering the brainstem as well, placing them in an ideal position to detect changes in CO_2 levels (Kumar and Prabhakar, 2012). Adding more evidence to the role serotonin has in respiration is an *in vitro* study on the brainstem-spinal cord of a newborn rat found that serotonin facilitated respiratory rhythms through the 5-HT receptors in the rostral VRC of region in the medulla and motor neurons through 5-HT_2 receptors (Di Pasquale et al.1992). Further studies continue to link serotonin to respiration while improving our understanding of the mechanisms underlying this phenomenon. For instance, both *in vivo* and *in vitro* studies have shown serotonin neurons increase their firing rate in response to hypercapnia (increased CO_2 in the bloodstream), while lesions of serotonin neurons decrease this response (Feldman et al., 2003; Nattie et al., 2004; Dias et al., 2007).

Studies on serotonergic neuron activity during anesthesia from isoflurane administration indicate that DR neurons may in fact, facilitate emergence from general anesthesia. While experimental manipulations activating or inhibiting serotonergic neurons have revealed little-to-no influence on anesthetic induction times, these manipulations do have a significant impact on regaining consciousness following anesthesia (emergence). The activation of serotonergic neurons (electrically and agonistically) significantly shortens emergence times while their inhibition has the opposite effect—prolonging the time to regain consciousness following anesthesia (Ao et al., 2021). Supporting this finding, while monitoring activity levels through calcium signaling, this group also found that activity levels of serotonergic neurons decrease as expected during the initiation of isoflurane anesthetic yet recover activity levels prior to the animal regaining consciousness (Ao et al., 2021). Taken together, these results

indicate serotonergic neurons may have a role in facilitation of emergence from anesthesia.

In addition to the role serotonin has in respiration is the role it plays in thermoregulation. This link has been primarily elucidated through studies on a transgenic mouse model that targeted Lmx1b (f/f/p). LIM homeobox transcription factor 1 beta (Lmx1b), is a conditional knock-out mouse where Lmx1b is only deleted in Pet1-expressing serotonergic neurons and nearly all central serotonin neurons fail to survive (Zhao et al., 2006). When exposed to cold environments, these mice display either a decreased or abolished shivering response that is typically observed in warm blooded animals for thermogenesis (Hodges & Richerson, 2008, 2010). The serotonin inputs contributing to gating the spino-parabrachial thermoafferent pathway provides an optimal interaction between thermoregulation and the respiratory response for serotonin, indicating that the lateral parabrachial nucleus of the dorsolateral pons may be a crucial component for this response (Song & Poon, 2009).

iii. SEXUAL BEHAVIOR

Multiple lines of research have implicated serotonin in the regulation of sexual behaviors. Research in rodent models shows compounds that increase serotonin levels lead to a decrease in sexual behavior, while the opposite is true for compounds that decrease serotonin levels (Moll & Brown, 2011; Uphouse, 2014). An example of this effect was seen by Kang et al., when they treated male rats with DA 8031 (an SSRI) and found an increase in ejaculation latency and reduced number of ejaculations (Kang et al., 2014; Angoa-Perez & Kuhn, 2016). A possible underlying mechanism for the role

serotonin plays in sexual behavior is the 5-HT_{1A} receptor; however, it has curiously been shown to facilitate sexual behavior in male rats while inhibiting sexual behavior in female rats. Therefore, there may actually be a divergent role of the 5-HT_{1A} receptors by gender (Eelke et al., 2013). The association of serotonin with sexual behavior is further supported by reports that SSRIs reduce sexual desire in both human males and females (Burri et al., 2012). A recent double-blind study looked at treating individuals dealing with a sexual addiction with an SSRI (Citalopram) and found that after 4 weeks of treatment, compared to a placebo group, individuals treated with 30-60 mg of Citalopram significantly reduced sexual desire, use of pornography, and masturbation frequency (Malandain et al., 2020). Our understanding of the influence serotonin has on sexual behavior has also led to several studies using SSRIs as a therapeutic treatment for premature ejaculation in human males (De Jong et al., 2006; Malandain et al., 2020). These studies show that SSRIs exert only a minimal ejaculation delay in the first week that is often not clinically relevant, with clinical relevancy of ejaculation delay occurring gradually after 2–3 weeks of treatment—which interestingly corresponds with the time-lapse for reducing depressive symptoms (Olivier et al., 2010). Taken together, the research in both rodents and human subjects indicates that increased serotonin levels decrease sexual behaviors.

iv. COMPULSIVITY, IMPULSIVITY, AND LEARNING

Studies using invertebrates such as *Aplysia* first linked serotonin to a role in learning when it was found that alterations in serotonin levels influenced short-term facilitation (STF). Specifically, knocking down a serotonergic receptor (5-HT_{apAC1}) completely

blocked STF while stimulation of serotonergic functions facilitated STF through interactions with adenylyl cyclase (Lee et al., 2009). Further supporting the role serotonin has in learning is a study on *D. melanogaster* which provided compelling evidence serotonin is required for place memory (Sitaraman et al., 2008). Short- and long-term plasticity in invertebrates have also been reported, notably in *Drosophila*, *Apis mellifera,* and honeybees (Blenau & Thamm, 2011). In mammals, serotonin has been implicated to have a role in three separate areas contributing to learning/memory: compulsivity, impulsivity, and reversal learning.

Compulsivity is a type of disturbance in behavioral control defined as a tendency to respond in a preservative manner that is situationally inappropriate and maladaptive (Robbins & Crockett, 2010). It is also clinically distinguished from impulsivity; however, there is significant overlap in the possible roles' serotonin plays in each of these and therefore will be covered together (Hollander & Rosen, 2000). Overall, the 5-$HT_{2A/C}$ receptors have been implicated as the underlying mechanisms for each of these. Current understanding of compulsions was advanced by research on compulsive cocaine seeking in rats. The criterion for compulsive behavior in this paradigm is the persistence of cocaine-seeking behavior despite adverse consequences of punishment via electric foot-shock and showed that the rats had reduced forebrain 5-HT and that the compulsive cocaine seeking could be reversed with an acute dose of citalopram (an SSRI), or with a 5-$HT_{A/C}$ receptor agonist (Pelloux et al., 2012). Significantly, the compulsive cocaine seeking behavior could even be simulated in normal rats with either a treatment of a selective 5-HT_{2C} receptor antagonist or by blocking a selective 5-HT_{2A} receptor antagonist. A particularly important advancement in our understanding of serotonin's role

in impulsivity arose from several lines of evidence demonstrating that individual differences in impulsive action reflect variations in cortical 5-HT_{2A} receptors (Fink et al., 2015). These studies showed that rats screened to be highly impulsive on the 5-choice Serial Reaction Time Task, exhibited a greater head-twitch response following administration of a 5-HT_{2A} receptor agonist, DOI. Furthermore, the rats exhibited a greater sensitivity to a reduction in impulsive responding after administration of the 5-HT_{2A} receptor antagonist. Notably, this is the same pattern of effects as seen for impulsive behavior, suggesting a shared substrate for compulsive behavior, yet it is distinct from the opposite profile seen in reversal learning. Procedures for measuring compulsivity in humans and animals tend to involve modifications of reinforcement rules so that persistent responding becomes suboptimal and reversal learning is a common procedure based upon this approach. In reversal learning procedures, subjects are typically required to discriminate between two stimuli, one of which is associated with positive reinforcement and the other with the omission of reinforcement. When discrimination of these stimuli has been learned to a high level of performance, the reinforcement rules are switched, so that the previously rewarded stimulus is now never rewarded and vice versa. Continued responses at the previously correct stimulus are termed 'perseverative errors' and can be taken as an index of compulsive responding. Mechanisms involved in the regulation of synaptic serotonin levels have been heavily implicated in reversal learning. For instance, one study found numerous serotonin alterations in the orbitofrontal cortex of a population of rats identified as having high preservation (low reversal learning) rates. These alterations consist of reduced serotonin metabolite levels, abnormal 5-HT_{2A} receptor binding, as well as abnormal expression of

monoamine oxidase genes in the DRN (Barlow et al., 2015). This finding is consistent with previous research on vervet monkeys which found individual differences in monoamine levels (including serotonin) in the orbitofrontal cortex were able to explain individual variation in reversal learning performance (Groman et al., 2013). Additional evidence for the role of serotonin in reversal learning stems from genetically modified mice lacking the serotonin transporter exhibiting fewer preservative errors on reversal learning compared to controls. Neurobiological recordings of serotonin neuron activity in head-fixed mice during a reversal learning task showed close resemblance to the characteristic prediction-error neural activity seen in midbrain dopamine neurons, indicating that serotonergic cells may convey information on reinforcement related events, including reward-predictive cues (Matias et al., 2017).

SEROTONERGIC AXON DEVELOPMENT

An important feature of serotonergic neurons is that their axons produce convoluted trajectories and innervate nearly every area of the brain. Due to their extremely long trajectories, these axons are typically referred to as serotonergic "fibers." Serotonergic fiber development is outlined using the original B1-B9 nomenclature. It begins following migration when serotonin cell groups are distributed in nine groups (B1–B9). The posterior groups (B1-B3) mainly consist in raphe magnus sending projections to the medulla, the spinal cord, and the periphery, while the dorsal raphe (B6, B7) and the median raphe (B5, B8) contain ascending serotonergic fibers projecting to the telencephalon and diencephalon. In the mouse, as early as embryonic day 12 (E12) serotonin neurons start to elongate their axons rostrally in the medial forebrain bundle (mfb). Starting from E13, serotonergic axons

begin making their way to their target regions by initially traveling together along the mfb before diverging to their specific destinations at either the fasciculus retroflexus (fr) (toward the habenula), the hypothalamus (hyp), the striatum, or the septum (se) (Vitalis et al., 2013). At this point, fiber trajectories become more tortuous and increasingly "random", ultimately reaching their targets by the end of gestation. Morphologically, at birth fibers appear as thick and dot-shaped enlargements with few detectable connections. As they mature, fibers progressively become smoother and more uniform along their length up to postnatal day 28 (PND 28) (Maddaloni et al., 2017).

During postnatal development, the serotonergic system undergoes terminal field development—a massive and progressive increase in the amount of serotonergic fibers within the target region (Lidov & Molliver, 1982). Studies measuring the total length of developing serotonergic fibers have identified distinct developmental patterns showing progressive or transient increases in fiber length with region-specific timing. For example, total fiber lengths (within a 3D stack) progressively increased in the caudate putamen (CPu), basolateral amygdala (BLA), dorsal lateral geniculate nucleus (DLG) and substantia nigra (SN). However, in the BLA and SN, the total length of serotonergic fibers started increasing at PND 7 while fibers in the CPu and DLG regions began increasing on PND 14. All regions had a peak in fiber length at PND 28 which remained unchanged up to adulthood (Maddaloni et al., 2017).

Underlying these growth and innervation patterns are a handful of specific axon guidance molecules that have been shown to act in the selective orientation and targeting of the serotonin raphe axons. For instance, wingless-related integration site (WNT) is a secreted morphogen that controls neuron specification and axon growth and has been shown to play a

major role in the initial polarity and orientation of serotonergic axons along the anterior to posterior axis (Fenstermaker et al., 2010). For example, gain- and loss-of-function experiments indicate that WNTs act as chemoattractants for both the ascending and the descending serotonin raphe neurons. Providing further evidence of WNT's role, other studies show that E11 - E12 serotonergic raphe neurons express WNT receptors (FRIZZLED3, CELSR3, and VANGL2) and mice deficient for one or another of these receptors appear to have abnormal orientations of raphe serotonin axons. Specifically, rostrally oriented axons appeared misrouted laterally and caudally while serotonin axons arising from the posterior cluster showed aberrant rostral orientation of their axons. This ultimately resulted in an abnormal ingrowth of serotonin axons in an area normally devoid of them—the R4 region (posteroventral cochlear nucleus and rostroventral part of the dorsal cochlear nucleus) during early embryonic development (Fenstermaker et al., 2010).

Another guidance molecule involved in serotonergic fiber development is ephrin—a type of Eph protein which belongs to the superfamily of transmembrane tyrosine kinase receptors. Eph proteins were initially identified from an overexpression discovered in human carcinomas, triggering a large number of studies aimed at describing their function. The role the Eph proteins play as signaling molecules arise from their ability to allow for short distance cell-to-cell communication, activating signaling pathways affecting cellular cytoskeletons and resulting in cell repulsion (and cell adhesion in some circumstances). Specifically, some of the decision-making steps in long distance growth cone guidance depends on ephrin-Eph signals. In turn, these signals drive regional differences in actin dynamics within growth cones and resulting in growth cone turning or ultimately, the choice of a particular axon trajectory (Kania & Klein, 2016). In the matter of ephrin's role in

serotonergic fiber development, expression of a specific Eph receptor gene, EphA5, is unequally distributed across the raphe nuclei with a high expression found in the DR and low expression in the MR. Growth cones from axons with the EphA5 receptor have been shown both *in vitro* and *in vivo* to be repelled by *ephrinA*, explaining why DRN axons avoid innervating areas with high *ephrinA* expression while MRN axons innervate these areas freely (Teng et al., 2017). Supporting this theory, studies using EphrinA5 knockout mice show that serotonin axons originating in the DRN end up innervating regions with high *ephrinA* expression (Deneris & Gaspar, 2017). Overall, these studies indicate that ephrin may be involved in selective targeting of axons originating from the DRN vs the MRN.

Protocadherins, Lmx1b and BDNF have also been shown to be involved in axonal growth and development. Protocadherin clusters are the largest family in the cadherin superfamily. The murine cluster of protocadherins are further divided into 3 subfamilies (α, β, γ, or pcdha, pcdhb and pcdhg respectively) based upon their position in the gene cluster. The Pcdha subfamily is of particular interest for the development of the serotonergic system as high expression levels of these transcripts have been found in raphe nuclei from embryonic stages to adulthood (Katori et al., 2009). Additionally, when pcdha is knocked out in mice, serotonin axons approach their target regions as normal but do not form the same arborizations as wild type mice do—resulting in an abnormal distribution pattern of axons in adulthood. The role for Lmx1b in axonal growth was briefly outlined in the previous section covering serotonin and respiration. BDNF may have a trophic role of supporting axonal growth and remodeling in the adult brain as chronic BDNF infusions into the serotonergic terminal fields of PCA treated rats stimulated regenerative sprouting (Mamounas, et al., 2000).

FIBER MORPHOLOGICAL DIVERSITY AND VARICOSITIES

i. MORPHOLOGICAL DIVERSITY

In the adult mouse brain, two unique morphologies of serotonergic fibers have been described, the D fibers, and the M fibers. The D fibers are the more abundant of the two and are characterized by their thin appearance and fusiform homogenous varicosities. Conversely, the M fibers are thick and have large, oval varicosities (Kosofsky & Molliver, 1987). Another layer of complexity of these fibers is they have been shown to be highly collateralized (branched) with these patterns varying across terminal regions (Waselus et al., 2011; Gagnon & Parent, 2014; Ren et al., 2018). These collateralizations endow individual serotonergic neurons with the possibility of modulating multiple regions alone. For example, some DR neurons have been shown to fire in a time-locked manner to the hippocampus theta rhythm (Hyman et al., 2005; Jones & Wilson, 2005), while individual DR neuron reconstructions utilizing single-color, intracellular tracer injections have shown projecting collateralizations innervating both the prefrontal cortex and the hippocampus (Gagnon & Parent, 2014), suggesting the activity in both structures can be modulated by a single DR neuron. Extensive literature review has not revealed any publications further describing collateralization frequencies or patterns of individual serotonergic axons more definitively.

ii. VARICOSITIES

Along serotonergic axons are enlarged, or dilated portions called *varicosities*—which are the primary sites of serotonin release. Research exploring the dynamics of varicosities appears to be limited; however, some studies have suggested a relationship between

extracellular serotonin levels with the size and distribution of their varicosities (Daubert et al., 2010). Varicosities have been assumed to be evenly distributed to ensure serotonin can reach all targets in an efficient manner (Bunin and Wightman, 1998). However, a study by Chen and Condron (2008) found that the varicosity distribution in *Drosophila* was not as uniform as expected. In fact, recent findings from multiple research groups indicate that varicosities may be much more dynamic than previously thought—motivating a systematic study into their structure and dynamics. One such study found a significant increase in the number of large varicosities (>9 μm2) in all layers of the prefrontal cortex in aged A53T α-synuclein expressing mice (a mouse model for Parkinson's Disease) (Wihan et al., 2019). An increase in enlarged varicosities has also been shown in *Drosophila* with excess serotonin levels (Daubert et al., 2010). On the other hand, a study that compared rats injected with kainate to induce post-status epilepticus (post-SE) with saline-injected controls has shown a loss of small varicosities (Maia et al., 2019). This same study also found an increase in the density of large varicosities in infralimbic layers II/III and in all subdivisions of the dentate gyrus (Maia et al. 2019). The gap in knowledge surrounding the developmental mechanisms behind varicosities started to be answered in a very recent study looking at axonal growth following TBI's, which points to the induction of these swellings being caused by transverse compression (Sun et al., 2022). However, this is yet to be explored specifically in serotonergic axons. Another interesting study suggests that the development of new serotonergic varicosities may be a mechanism in the long-term facilitation of learning (Upreti et al., 2019).

5-HT SYNTHESIS & RELEASE

Serotonin synthesis is a two-step process that occurs within the neuron. First, the essential amino acid, tryptophan, is converted into 5-hydroxytryptophan (5-HTP) by tryptophan hydroxylase. Next, 5-HTP is converted into serotonin (5-HT) through decarboxylation by the enzyme, aromatic amino-acid decarboxylase (AADC). Once serotonin is synthesized, it is transported into synaptic vesicles by a vesicular monoamine transporter, VMAT2, and stored in varicosities along serotonergic fibers. When an action potential is received, the synaptic vesicles then undergo exocytosis and fuse with the membrane to release serotonin. From here, there are a few different paths that serotonin molecules can take. Initially, some of the serotonin will bind to postsynaptic receptors while some will leave the synaptic cleft through diffusion. Alternatively, some of the serotonin can be taken back into the cell via a reuptake mechanism mediated by the serotonin transporter (SERT), where it will either loaded back into synaptic vesicles by VMAT2 or converted by monoamine oxidase (MAO) into 5-hydroxyindoleacetic acid (5-HIAA) (Mosienko et al. 2015).

NEUROTRANSMITTER CO-RELEASE

Studies utilizing several approaches (e.g., immunohistochemistry, transcriptional profiling, *in-vitro* systems) have indicated that many serotonergic neurons may co-release other neurotransmitters such as glutamate, GABA, and neuropeptides.

The potential for co-release of glutamate from serotonergic cells has the most supporting evidence of these three. The earliest evidence stems from an immunohistochemical co-localization study in 1983 that targeted serotonin and glutamate

(Storm et al., 1983). However, the detection of glutamate is not enough evidence to prove that serotonergic cells are co-releasing it. As outlined in the previous section, the ability to package the neurotransmitter into vesicles is also needed for release. The identification of the glutamate vesicular transporter, *Vglut3*, in serotonergic neurons has addressed this gap (Gras et al., 2003). In fact, studies have shown that *Vglut3* is expressed both at the mRNA and protein level by a set of cell groups in the rat brain, including serotonergic neurons in the DR and MR (Herzog et al., 2004). Further investigations found that roughly 80% of serotonergic neurons in the rat ventromedial DR and MR express *Vglut3* (Hioki et al., 2010). On the other hand, other studies have reported a pronounced group of *Vglut3*-positive, but serotonin-negative neurons residing between the dorsal and ventral DR regions—suggesting not all DR *Vglut3*-expressing neurons produce serotonin (Commons, 2009). Rounding out the evidence of glutamate co-release is an *in-vivo* study in rats using acute slice, optogenetic electrophysiology and electron microscopy, showing that channelrhodopsin (ChR)–green fluorescent protein (GFP)-expressing fibers emanating from neurons in the MR formed functional synapses with hippocampal GABAergic interneurons, where they released serotonin and glutamate upon photo-stimulation (Varga et al., 2009). The co-release of serotonin and glutamate led to a rapid depolarization of postsynaptic hippocampal interneurons through the 5-HT_{3A} receptors, and the glutamate AMPA-type and NMDA-type receptors.

When it comes to serotonin and GABA co-release, studies have hinted toward this possibility from expressions of key GABAergic genes by certain serotonergic neurons (Okaty et al., 2015). Specifically, RNA sequencing studies in mice have found that serotonergic neurons have varying expressions of the synthetic enzymes for GABA

production—*GAD1* and *GAD2* (Niederkofler et al., 2016; Okaty et al., 2015). However, unlike the situation for serotonin and glutamate, there is an absence of the GABA vesicular transporter in *GAD1* and *GAD2* expressing neurons in the DR. Although this suggests that these cells do not package GABA for release, there are other methods that these cells may be utilizing for release as well as other explanations for the expression of *GAD1* and *GAD2*. First, these serotonergic neurons may release GABA through reversal of the GABA membrane transporter (GAT1) (Wu et al., 2007). Other studies have shown that midbrain dopaminergic neurons can release GABA through VMAT2 vesicular transport instead of VGAT, meaning the absence of VGAT in serotonergic neurons does not preclude the possibility of synaptic GABA release (Titsch et al., 2012). One more explanation for the expression of *GAD1* and *GAD2* is that GABA could have some other role in these serotonergic neurons such as intracellular signaling.

The last category of possible co-release from serotonergic neurons is with neuropeptides. In mice, much of the evidence arose from detection of mRNAs encoding neuropeptides. A recent study in the mouse MR found both mRNA and peptide expression for *Penk, Tac1*, TRH (thyrotropin-releasing hormone), CALCA (calcitonin gene-related peptide), and CCK (cholecystokinin) in serotonergic neurons (Yan et al., 2013). One interesting finding was that *Tac1* co-expression with serotonergic neuron markers are detected in only a small subset of DR 5-HT neurons in mice, yet in humans, around 50% of DR and 25% of MR serotonergic neurons co-express *Tac1* mRNA (Okaty et al., 2015, Hennessy et al., 2017).

SEROTONIN RECEPTORS

The astounding variety of serotonin receptors is one of the factors that explains the wide spectrum of influence that serotonin has in the brain. There are seven families of serotonin receptors named 5-HT_{1-7} and 14 known distinct receptor subtypes (e.g., 5-HT_{2A}) (Bockaert et al. 2006). Apart from the 5-HT_3 ionotropic receptor, all other serotonin receptors are G protein-coupled receptors (GPCR) that couple to all three GPCR pathways ($G_{\alpha i/o}$, $G_{\alpha q/11}$, and $G_{\alpha s}$).

The first GPCR pathway is the $G_{\alpha i/o}$ pathway, which is pertussis toxin sensitive and couples negatively to adenylate cyclase; in cells, this may lead to membrane depolarization and inhibition of firing. Serotonin receptors that are coupled to the $G_{\alpha i/o}$ pathway include 5-$HT_{1A-B/D-F}$, along with 5-HT_{5A-B}. The function of the 5-HT_{1A} receptor differs based on its pre- or postsynaptic location. Pre-synaptic 5-HT_{1A} receptors are auto-receptors that inhibit further release of serotonin, while the postsynaptic receptors help modulate the postsynaptic neuron. For example, postsynaptic 5-HT_{1A} receptors may help modulate the release of postsynaptic dopamine (Meltzer & Roth, 2013). Due to this function, the 5-HT_{1A} receptor has been the target of pharmaceutical drugs to treat anxiety, depression, and have even been targets for anti-psychotics. The 5-HT_5 receptors are unique as they can only be found in human cortical layers and the cerebellum (McCorvy & Roth 2015). 5-HT_{5A} antagonists have been shown to impair memory and reduce acoustic startle (Gonzalez et al. 2013; Curtin et al., 2013).

The second GPCR pathway is the $G_{\alpha q/11,}$ in which receptors work by activating phospholipase-C and ultimately increase intracellular calcium levels. Serotonin receptors coupled to the $G_{\alpha q/11}$ pathway are 5-HT_{2A-C}. The 5-HT_{2A} receptor is widely distributed in the central nervous system and research has recently been revitalized due to its known

hallucinogen action and the promising effects of psychedelics in psychological disorders (Miranda et al., 2019). Generally, there is an abundance of research in both humans and rodent models on the possible roles the 5-HT_{2A} receptor has in learning and memory. In humans, polymorphisms in the HTR_{2A} gene result in significant impairments to memory recall (Zhang & Stackman, 2015). In rodents, stimulation of these receptors by DOI induces Ca^{2+}-dependent TG with downstream effects ultimately leading to an increase in dendritic spine size. This suggests that serotonin may influence its own dendritic spine morphology and plasticity (Bockart et al., 2021). The 5-HT_{2A} receptor has also been implicated in mental illnesses such as schizophrenia, depression, and Tourette Syndrome (Meltzer & Roth, 2013). The 5-HT_{2C} receptor on the other hand, has varied effects. It has been associated with the rewarding effects in antidepressants, shown to induce cell proliferation, and has been used as a target for appetite suppressants (Banasr, 2004; Thomsen, 2008; McCorvy et al. 2011).

The third group of serotonin GPCRs is coupled to the $G_{\alpha s}$ pathway. The $G_{\alpha s}$ pathway functions by positively coupling with adenylyl cyclase and increasing cAMP. Serotonin receptors that couple to this pathway are 5-$HT_{4/6\text{-}7}$. The 5-HT_4 receptor is mostly located post-synaptically and agonists for it have been shown to increase the release of neurotransmitters from GABAergic, dopaminergic, and serotonergic neurons. The 5-HT_6 receptors are expressed almost exclusively in the central nervous system (CNS) where the highest concentrations are in the limbic and cortical regions. Selective antagonists for this receptor likely work through de-inhibition of GABAergic inhibition to increase glutamate release. Finally, 5-HT_7 receptors are localized on the soma and axon terminals of GABAergic neurons and have been implicated in thermoregulation and activation of rapid-eye movement

(REM) sleep via the modulation of the suprachiasmatic nucleus neurons in functional studies (Thomas & Hagan, 2004; Quintero-Villegas & Valdes-Ferrer, 2022).

SEROTONERGIC FIBER TERMINAL FIELD DENSITIES

The meshworks formed by serotonergic fibers within their terminal fields can be highly variable in both the number of fibers that occupy them and the morphology of the individual fibers. For instance, in the medial prefrontal cortex (mPFC) and orbitofrontal cortex (ORB), cortical layers I, V and VI have higher densities than the intermediate layers (II-IV). However, fiber densities can vary across brain regions; for instance, in the granular layer IV of the insular cortex (INC) has the highest fiber density (Linley et al., 2013).

Numerous studies of serotonergic fiber densities have been conducted in multiple species including rats, mice, ferrets, hamsters, cats, multiple non-human primates, as well as humans. These studies have found a generally higher density of serotonergic fibers in layers I-III with lower densities in the intermediate layers (Vertes, 1991; Awasthi et al., 2020; Voigt & De Lima, 1991; Morin and Meyer-Bernstein, 1999; Leger et al., 2001; Foote and Morrison, 1984; Lew et al., 2019). Awasthi (2020) found an overall significantly higher density of serotonergic fibers in the nuclei of forebrain limbic structures in mice, suggesting serotonin could have modulatory effects on emotional and cognitive behaviors. Supporting this finding, a study by Lew (2019) looked at the innervation of serotonergic fibers in the amygdala of three evolutionarily closely related species with increasingly complex social behaviors (chimpanzees, bonobos, and humans) and found significantly greater serotonin fiber density and differential patterns of innervations within distinct subdivisions of the amygdala in humans and bonobos compared to chimpanzees which may support the greater

behavioral flexibility in response to social situations in these species. There were two specific findings in humans that suggest that the serotonin system may be specialized for reduced emotion reactivity and greater behavioral control. The first is the significantly greater density of serotonergic fibers in the central nucleus compared to the lateral nucleus, suggesting increased neuromodulation of projections out of the amygdala (critical to physiological mechanisms that contribute to emotional and behavioral responses) and the second is an increased fiber density in the accessory basal nucleus—a site for integration of information from the neocortex and regulatory centers—which may facilitate a greater integration of autonomic and cognitive circuitry.

Despite the random appearance of individual fiber trajectories and the apparent variability in the networks that they form, the overall serotoninergic fiber densities are relatively stable from person to person and across species (Awasthi et al., 2020). Indeed, a recent study has shown that even though regenerating serotonergic fibers do not follow their previous trajectories, they can still restore the layer-specific density (Kajstura et al., 2018; Jin et al., 2016; Hawthorne et al., 2011).

SEROTONERGIC FIBER PLASTICITY

It is a widely held notion that injured axons in the mammalian CNS do not have the capacity to regenerate. This is primarily due to the neuroinflammatory response to injury activating astrocytes. The activation of astrocytes results in the release proinflammatory molecules essential for healing, but at the same time, these astrocytes also tend to hypertrophy in response to injury over time—forming a physical barrier of glial scar tissue while also secreting inhibitory chondroitin/keratan sulfate proteoglycans. Together, the

physical and molecular barrier caused by the activated astrocytes is likely the leading cause of the long-term dystrophic state seen in the majority of non-regenerating axons (Robinson et al., 2016). However, there is mounting evidence indicating that serotonergic axons could be an exception. For instance, when Traumatic Brain Injury (TBI) was induced in mice by either open skull injury or controlled cortical impact (CCI), significant recovery of serotonergic axons was observed at one and three months after injury (Kajstura et al., 2018). In fact, regrowth of serotonergic fibers has been reported following several methods of injury induction, including neocortical stab injury (Jin et al., 2016), as well as both thermal and amphetamine lesions (Hawthorne et al., 2011; Mamounas et al., 2000). Studies on the underlying factors enabling this response in serotonergic fibers have revealed two key molecules: growth-associated protein 43 (GAP-43), and Brain Derived Neurotrophic Factor (BDNF). GAP-43 is a phosphoprotein associated with the membrane skeleton and is enriched in growing or regenerating axons (but it is typically downregulated in adulthood). GAP-43 is also an important protein for serotonergic development as it is required for proper terminal arborization in the forebrain, postnatally. Indeed, serotonin axons in GAP-43 knockout mice fail to innervate the cerebral cortex, stalling in subcortical brain areas (Donovan et al., 2002). It has also been shown that adult serotonergic neurons continue to make GAP-43 mRNA and have an increased expression in adulthood which could be priming serotonergic neurons to respond better to injury (Hawthorne, et al 2011). The other molecule possibly underlying serotonergic fiber regrowth is BDNF. BDNF is part of a family of neurotrophins that have a critical role in the differentiation and survival of neurons during development (Huang & Reichardt, 2001). However, even after development a high expression of BDNF remains in the brain due to its role in regulating both excitatory and inhibitory neurotransmission as well

as activity-dependent plasticity (Tyler et al., 2002; Wardle & Poo, 2003). The neurotrophic effects of BDNF arise from binding to tyrosine kinase receptor (TrkB) which promotes cell survival, facilitates long-term potentiation, and increases spine complexity (Volosin, 2006). In serotonin fibers, although BDNF fails to protect the fibers from degradation, it appears to stimulate sprouting of axons. In fact, BDNF treatment stimulated regrowth of serotonin axons up to a month following PCA induced degradation (Magdalena et al., 2019).

If serotonin fibers are not static and continue to grow in the adult brain as these studies have suggested, then what process allows for achieving a steady equilibrium of densities? It has previously been suggested that serotonin fibers may be routinely interrupted and that these interruptions may be associated with microglia (Figure 3).

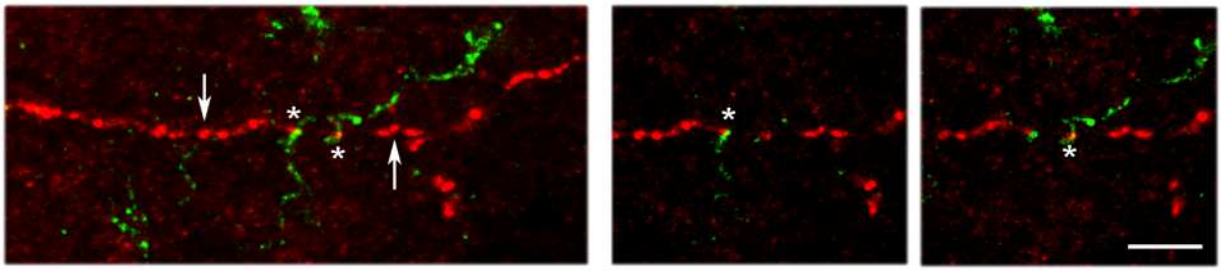

Figure 3: A Super-resolution (Leica, STED) image of possible contact (indicated by asterisks) from microglia processes (green), with a serotonergic fiber (red, arrows). The contacts delimit an apparent fiber break between asterisks. The image was obtained in a section of the mouse neocortex, visualized using immunohistochemistry methods detailed above. Scale bar = 3 µm. From Janusonis et al. (2019).

SEROTONIN AND PSYCHOLOGICAL DISORDERS

Parallel to its vast influence on behavior and physiological processes, serotonin has been implicated in an array of clinical disorders, including autism spectrum disorder (ASD), major depressive disorder (MDD), sudden infant death syndrome (SIDS), schizophrenia, anxiety disorders, and even impulse control disorders to name a few. Autism Spectrum Disorder is arguably the most difficult psychological disorder to study due to the notoriously wide array of clinical symptoms that patients exhibit along with high rates of comorbidity

with other disorders. These can range from seizures, anxiety and compulsive disorders to social/language deficits and even gastrointestinal problems. In fact, over 100 different genes and 44 genomic loci have been implicated in ASD (Betancur, 2011). However, there is a common factor behind these symptoms, as most of them have also been associated with abnormalities in the serotonergic system. Physiological and anatomical differences that have been observed in individuals with ASD provide further evidence for serotonin having a role in ASD. For instance, a physiological difference seen in many ASD individuals is hyperserotonemia (whole-blood serotonin levels exceeding the 95th percentile), which remains a stable biomarker in patients with an occurrence in roughly 30-40% of individuals with a confirmed diagnosis (Muller et al., 2016). Anatomical differences in the serotonin system have also been identified in ASD patients. For instance, decreased 5-HT_2 receptor binding has been found both peripherally and centrally in ASD patients. Platelet studies (Mcbride et al., 1989; Cook et al., 1993), a postmortem study (Oblak et al., 2013), along with two neuroimaging studies (SPECT and PET) (Murphy et al., 2006; Goldberg et al., 2009) all found decreased 5-HT_2 receptor binding in ASD patients. These consistent findings support the idea that peripheral changes in serotonin levels (such as hyperserotonemia), may be important markers for central abnormalities in ASD. Other anatomical changes in the serotonin system have also been described. Specifically, in another postmortem study, both the medial forebrain and the ansa lenticularis ascending serotonin fiber pathways had increased fiber densities when compared to controls. Increased counts of immunoreactive axons in these pathways, along with the globus pallidus pathway, were also reported in individuals with ASD. Since this increase is not confined to one brain region of the

serotonergic system, the results point towards a possible global increase of serotonergic axons in ascending serotonin pathways (Azmitia et al., 2011).

Another psychiatric disorder that has been associated with serotonin system abnormalities is major depressive disorder. In fact, several differences in the serotonin system have been linked to MDD. For example, gene association studies have linked polymorphisms of the $5HT_{1A}$ regulatory region to increased receptor levels in the brain and to an increased risk for depression (Nautiyal & Hen, 2017). A meta-analysis of 15 studies also has shown decreased SERT binding in the midbrain—a consistent phenomenon that was observed in several hundred patients (Gryglewski et al., 2014). Finally, contrasting with findings in ASD, a study on donated brains from suicide patients with a confirmed diagnosis of MDD, showed a significant decrease (24%) in serotonin fiber density in layer six of the dorsolateral prefrontal cortex compared to controls (Austin et al., 2002). This result corresponds with findings that individuals with MDD have decreased serotonin levels and provides support for the use of SSRIs as a drug therapy in MDD (Berger et al., 2009; Okaty et al., 2019).

Sudden infant death syndrome is a disease characterized by sudden death due to respiratory failure. Due to the role of medullary serotonergic neurons in respiratory chemoreception, serotonin has been implicated in sudden infant death syndrome (Richerson et al., 2001). Interestingly, this does not appear to be due to a reduction of serotonergic neurons that would be expected. In fact, the exact opposite has been found. A postmortem study has found a significant increase in the number and density of serotonergic neurons in the medulla (Bright et al., 2017). However, despite this increase in the number of serotonergic neurons, the ratio of 5-HTT binding to these neurons has been shown to be

reduced in SIDS cases when compared to controls (Paterson, et al., 2006). This suggests a relative decrease in expression of serotonin per serotonergic neuron count.

As important as the results regarding fiber densities from the ASD, MDD and SIDS studies are, they all possess a major limitation in the method used for the analysis of the fibers. These studies use optical densities, or the measurement of the cumulative signal densities above the background level. Historically, this has been the most common/preferred method for fiber analysis as it provides valuable information about the overall density of fibers in a given brain region. However, one flaw to this method is that the physical composition of individual fibers in a region can vary a great deal without changing the overall optical density. For example, a small tissue volume may contain many different small fiber segments, or it could contain just one fiber that is making many twists and turns (thus occupying more space) in that area, or the region could even consist of a mixture of both. Thus, even though optical density measurements provide important information regarding the overall serotonin "tone" in a region, without more information about the behavior of the individual fibers residing in these regions, we may never be able to fully understand if fiber density differences in psychological disorders such as ASD and MDD arise from differences in the total number of fibers, or if the density differences arise from the behavior (tortuosity) of single fibers. **Therefore, a method for the quantification of single fiber behavior is essential for advancement in our understanding of these disorders and to the fundamental neuroscience of these systems.**

CHAPTER 2: RESEARCH AIMS

The analysis of these fibers has been complicated by their high densities and their apparently random trajectories. The recent advances in high-resolution imaging methods, as well as the introduction of novel stochastic approaches (Janusonis et al., 2019; Janusonis and Detering, 2019; Janusonis et al., 2020), allow us to develop a predictive model of serotonergic fibers that we can combine with cutting edge technological methods to improve analysis capabilities. Leveraging these, three aims have been developed for this project to design an experimental toolbox for the analysis of individual fiber behavior.

SPECIFIC AIM 1 **will establish a procedure for reliable and automated fiber tracing and analysis**. We developed a transgenic (inducible Cre-based) approach to labeling individual serotonergic fibers independently of serotonin accumulation. An algorithm was also developed that can automatically and precisely trace labeled fibers in 3D-high resolution images and estimate their stochastic parameters in some brain regions (based on a random walk driven by the von Mises-Fisher directional probability distribution; further referred to as the vMF-walk).

SPECIFIC AIM 2 will form an **approach for separation of individual axons**. A more powerful approach utilizing Brainbow, and Cre-based technologies was developed which effectively expands the dimensionality of the analysis space, while supporting both single-fiber and population-level analyses. In this approach, individual fiber trajectories can be isolated more easily, and interactions among individual trajectories can be readily observed at lower magnifications. The algorithm developed in Specific Aim 1 can be adapted to include fluorophore information in decisions when two fibers intersect at distances that fall below the limit of optical resolution.

SPECIFIC AIM 3 will **ensure larger scale, density information is not lost** by obtaining longer fiber trajectories in their natural 3D-space using tissue clearing and high-resolution light-sheet imaging. This method is compatible with both transgenic approaches used in Specific Aims 1 and 2. To automatically segment fibers in light-sheet scans, we tested a recently introduced artificial neural network, with limited but promising results.

CHAPTER 3: CONCEPTUAL AND HISTORICAL OVERVIEW OF METHODS

The experimental methods described here were chosen to address our specific aims outlined above. First, multiple genetic manipulations were tested with the goal of obtaining individual fiber separation. Next, to preserve the natural 3D environment of the brain, tissue clearing methods along with refractive index matching were employed; and finally, different computational and tracing methods were tested to reduce time and bias while increasing accuracy (methodological overview in Figure 4).

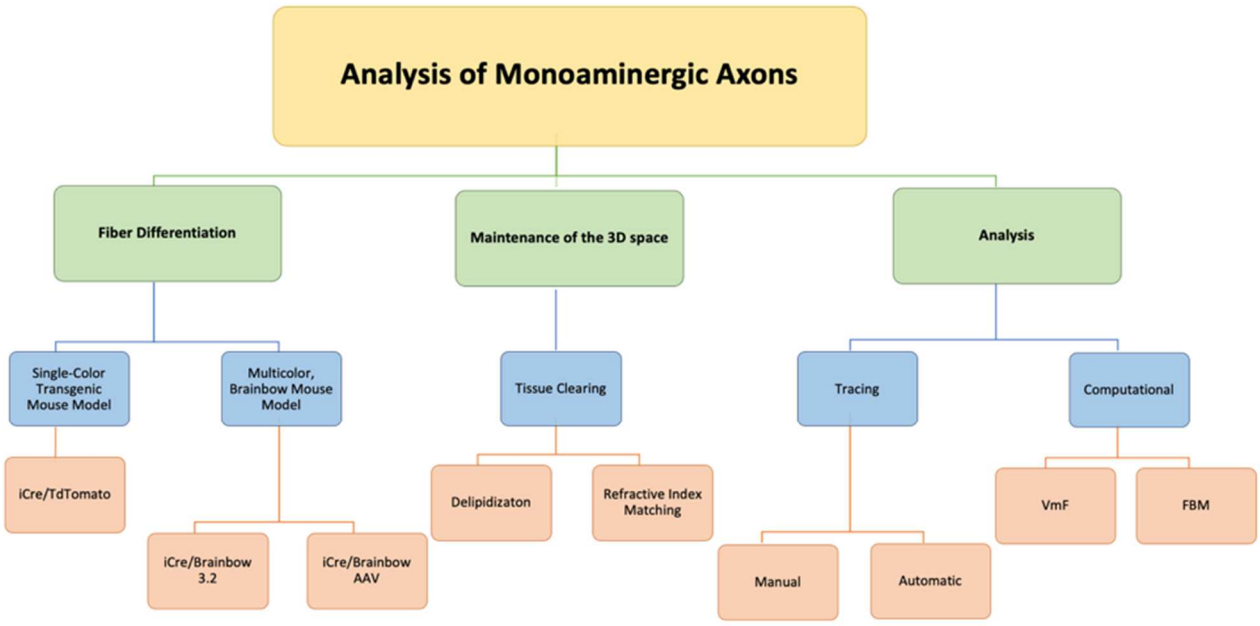

Figure 4: Methodological overview for analysis of monoaminergic axons.

MOUSE MODELS

i. CRE-LOXP MODELS

The cre-*lox*P mediated recombination system was first discovered in 1981 by Sternberg and Hamilton and is a powerful gene editing method that has become a popular technique for genetics and cell biology research. They were the first to describe that a recombinase enzyme isolated from the P1 bacteriophage can recombine DNA fragments. The Cre enzyme **c**auses **re**combination while the binding sites for *lox*P are the *locus of crossing over* **(x), P1**—resulting in the name, cre-*lox*P (Sternberg & Hamilton, 1981). Since the development of the cre-*lox*P system, over 3,000 reports have been published utilizing the technology (McLellan et al., 2017).

The cre-*lox*P system has aided in greatly advancing research and knowledge of biology by allowing for the targeting of specific gene functions in cell populations from a

wide range of tissues. It is also relatively simple to use—requiring only two elements. The first is a cell line or animal that is engineered to carry a genetic locus where DNA (often genomic) is flanked by two *lox*P DNA motifs (Sauer & Henderson, 1988). DNA segments flanked by *lox*P sites—referred to as "floxed" loci—can be generated in mice with relative ease by targeting embryonic stem cells (ESCs), followed by transplantation into blastocysts to generate transgenic mice (Hall et al., 2009).

The second requirement for the cre-*lox*P system is that a cell with floxed DNA must also express the Cre enzyme. The cell specificity of recombination is controlled by promoter and enhancer sequences that drive Cre expression in the cell or tissue type of interest, therefore removing the floxed genetic locus in the entire lineage (Gu et al., 1993, 1994). This system was improved even more with the inclusion of an inducible Cre system that is still controlled by cell-specific regulatory elements, but also allows for temporal control with induction by an exogenous inducer (such as tamoxifen or tetracycline) (Nagy, 2000; McLellan et al., 2017). The tamoxifen-inducible Cre system is achieved with a modified Cre protein fused with the estrogen receptor containing a mutated ligand binding domain (ER-LBD) (Brocard et al., 1997; Metzger & Chambon 2001; Kim et al., 2018). The fused Cre protein is called CreER recombinase, located in the cytoplasm in a form that binds to heat shock protein 90 (HSP90). This causes nuclear translocation of CreER and the interaction of Cre with *lox*P sites (Kim et al., 2018).

ii. BRAINBOW MODELS

The Brainbow transgenic line addresses the problem of identifying individual fibers by the inclusion of 3 or 4 fluorescent proteins into a transgene with *lox*P sites. This allowed

us to use the Cre-*lox*P recombination system to randomly combine these fluorophores in a *specific* cell type. By using this system, the combinatorial expression can give each neuron one of roughly 100 colors and thereby enable the distinction of individual neurons and their processes from other nearby cells (Cai et al., 2013).

The Cai research team were faced with two major hurdles that needed to be overcome when creating this new method. The first problem is that one of the fluorophores was being used as the default color (without recombination), which reduces the number of different colors one can obtain. Another difficulty was an uneven labeling of neuronal somata and processes. Since unmodified fluorescent proteins labeled somata so intensely, it was difficult to resolve nearby dendrites and axons. This was corrected by modifying the fluorescent proteins with farnesylated derivatives, which traffic more easily to the membranes of all neurites.

The Brainbow line that was used for this project is the newest version, Brainbow 3.2. This updated transgenic line is ideal for this project as it has corrected problems of previous Brainbow lines. In the first model, Brainbow 3.0, 15 fluorescent proteins were tested for their photostability, aggregation in-vivo, and stability with fixation using paraformaldehyde. From those tests, 7 were found to be suitable and then 3 were chosen from those that have the least spectral overlap and minimal sequence homology. The three fluorescent proteins used in this line are enhanced green fluorescent protein (EGFP) from a jellyfish with an excitation of 488 nm and emission of 507 nm, mOrange2 from a coral with an excitation of 549 nm and emission of 565 nm, and mKate2 from a sea anemone with an excitation of 588 nm and emission of 635 nm. The next generation model, Brainbow 3.1, was created to remove the issue of utilizing a default fluorescence as it reduces the diversity among recombined neurons

and the final model, Brainbow 3.2. was created to increase protein levels produced by viral vectors and transgenes by inserting the woodchuck hepatitis virus posttranscriptional regulatory element (WPRE), which stabilizes RNA (Cai et al., 2013).

iii. ADENO-ASSOCIATED VIRUS (AAV)

Adeno-associated viruses (AAV's) are part of the parvovirus genus (animal viruses) stemming from the Parvoviridae family and are dependent on co-infection with other viruses—particularly adenoviruses—for replication. The structure of AAVs' is relatively simple, consisting of a small, 4.8 kilobases (kb) of single-stranded DNA, protected by a protein shell. The single strand genome consists of three genes, *Cap* (Capsid), *Rep* (Replication), and *aap* (Assembly), giving rise to at least nine different gene products with alternative translation starting sites, three promoters, and differential splicing. The *Cap* expression creates the viral capsid proteins that form the outer capsid shell protecting the viral genome and is involved in cell binding (VP; VP1/VP2/VP3). This viral coat is estimated to constitute 60 proteins arranged into an icosahedral structure with the capsid proteins in a molar ratio of 1:1:10 (Samulski & Muzyczka, 2014). The *Rep* gene encodes four proteins that are required for genome replication and packaging (Rep40, Rep52, Rep68, Rep78), while *aap* encodes the assembly-activating protein and is believed to provide a scaffolding function for capsid assembly, while also being an alternate reading frame that overlaps with the *cap* gene (Naumer et al., 2012; Naso et al., 2017).

iv. BRAINBOW AAV

The team that created the Brainbow AAV had to first find a way to accommodate a slightly larger, 5 kb packaging size, while also achieving a high expression level. To achieve this, several tests were performed on promoter elements, polyadenylation sequence, as well as stop mechanisms. From these tests, the final Brainbow AAV architecture contains a human elongation factor alpha (EF1α) (shown to have a stronger expression over the 1kb hybrid promoter of CB6), *Lox*P left and right element mutants (LE-RE) mutant sites (shown to exhibit no Cre-independent expression), a 0.5kB human growth hormone polyadenylation sequence, the stop cassette of a tandem Myc epitope tag and a bovine growth hormone polyadenylation sequence (shown to produce multicolor labeling without Cre-independent expression), and farnesylated XFPs of EGFP, mCherry, and monoclonal teal fluorescent protein (mTFP) (Cai et al., 2013).

MANUAL AND AUTOMATIC TRACING METHODS

i. MANUAL TRACING

Z-stack images can be uploaded and manually traced using the Simple Neurite Tracer plug-in for ImageJ. Traces are then created by manually progressing through the stack to select/draw small segments to trace until either the end of the stack or the end of the trace is reached.

ii. AUTOMATIC TRACING

Our laboratory has recently developed an algorithm that analyzes local pixel intensities in a circular arc centered at the current location and bisected by the current

direction. Based on the distribution of the pixel intensities, the algorithm extends the trace and proceeds iteratively. Based on extensive testing, within an optical section (X-Y plane), the algorithm prioritizes the intensity peak closest to the current direction, while within a subset of optical sections (z-axis), it prioritizes the peak with the highest intensity value. The radius and angle of the arc are also dynamically adjusted so that the algorithm can handle multiple intensity peaks and fibers passing within close proximity, thus allowing for tracing in densely populated brain regions (Figure 5). This information can be used to simulate serotonergic fibers computationally (Figure 6).

In sparse or moderately dense areas, the trajectories of some individual serotonergic fibers can be followed visually, which allows for the verification of the general accuracy of various algorithmic approaches. These tests led to an empirically optimized algorithm that we describe in detail.

The z-stack of one fluorophore channel is imported as a series of high-resolution, grayscale TIFF images (with the xy-scaling of around 60 nm per pixel and the distance between two adjacent optical sections of around 300 nm). The images are auto-contrasted (with the brightness range of 0-1) and Gaussian-blurred using a one-pixel radius. The initial seed point on a fiber is selected in a specified ("current") optical section, manually or automatically, and the second point is automatically detected as the brightest point on a circle whose center is at the seed point and the radius is set at a fixed value (R). The second point becomes the "current point," and the "current direction" is determined by the vector connecting the two points. This initiates the tracing sequence.

In the current optical section, the brightness of pixels is examined on an arc that is centered at the current point. The radius (tracing step) and angle of the arc are given by R and

a fixed interval [-α, α], respectively, where the angle of 0° corresponds to the current direction. The number (*n*) of increments from -α to α should provide a sufficiently dense coverage of the arc; in particular, the "mini-arc" produced by the angle 2α/n should be less than one-half of the expected fiber width. By sampling the arc, brightness peaks ("hilltops") within a fixed brightness interval [*Bmin, Bmax*] are detected, but the peaks whose width (spatial extent) at *Bmin* falls below a set threshold (*Wmin*) are not kept. The latter procedure, along with the described Gaussian blur, efficiently eliminates pixels whose strong brightness is noise-related and does not extend to adjacent pixels. Of the remaining peaks, the peak closest to the current direction is selected (if there is more than one), and its point with the brightest value is recorded as the next candidate point.

In addition to the current optical section, this procedure is repeated for N sections above and N sections below the current optical section (if they exist), using the same arc. Among the next candidate points across the optical sections, the brightest point is selected. It becomes the next current point of the fiber. The next current direction is determined by the vector connecting the xy-coordinates of the two most recent points, and the procedure continues iteratively. It is automatically terminated when brightness peaks are no longer detected or when the edge of the stack is reached. It can also be terminated manually, after a fixed number of steps.

As described, the algorithm would not be able to handle transient interruptions in signal brightness that accidentally fall on the search arc. To prevent this, the algorithm can automatically extend its search radius to multiples of *R* (0.5*R*, 1*R*, 1.5*R*, 2*R*, …), if no brightness peaks are detected across the optical section subset. The set includes one radius that is smaller than the original radius. However, the increasing extensions (numbered i = 1,

2, 3, 4, …, *imax,* where $i = 2$ corresponds to the original R) increase the risk that the trace will jump to another fiber in the vicinity of the fiber that is being traced. Therefore, these extensions can be optionally accompanied by an automatically narrowing search angle, given by $\alpha(i) = \alpha_0 \exp(-k(i-2))$, where α_0 is the original α and k is a constant (the "narrowing strength"). The maximal number of extensions should be restricted (*imax*) to a small value, especially in dense areas. If the next point is detected with the extensions, in the next step the elongated R and the narrowed α revert to their original values.

Since the arc is set in a 2D-plane, the actual distances between adjacent points of the final trace (located in 3D) may differ from the original R. Extended R values also contribute to these deviations. However, such final traces can be automatically corrected with a 3D-step of a fixed length, by simply tracking a point that slides along the original trace and marking points that are the same Euclidean distance from the previous stop. Since the steps are typically small, the recalculated trajectory is nearly indistinguishable from the original one. However, the constant step is important in further calculation of the vMF-concentration parameter (κ).

Typical parameter values are given in Table 1. Note that the algorithm is "anisotropic" in that within each optical section it prefers a bright value that is closest to the current direction, but among the optical sections it prefers the brightest value in this set (which may not be closest to the current direction across the sections). It reflects the inherent properties of confocal imaging: confocal images are sets of 2D-images, not true 3D-images with an isotropic resolution.

Algorithm parameter	Meaning	Approximate value
R	default search radius (tracing step)	1.5-2.0 μm
$\alpha = \alpha_0$	default search angle (one side)	~π/2 (90°)
n	number of angle increments	~50
k	angle attenuation in extensions	0.0-0.1
i_{max}	maximal number of extensions	0-2
N	number of neighboring sections (one side)	R/(z-step)
B_{min}	minimal brightness	0.3-0.5
B_{max}	maximal brightness	~1.0
W_{min}	minimal peak width	0.1-0.3 μm

Table 1: Typical values of the tracing algorithm. They are based on stacks of grayscale images of 3144 × 3144 pixels, with the xy-scaling of 0.063 μm/pixel and the z-step of 0.333 μm.

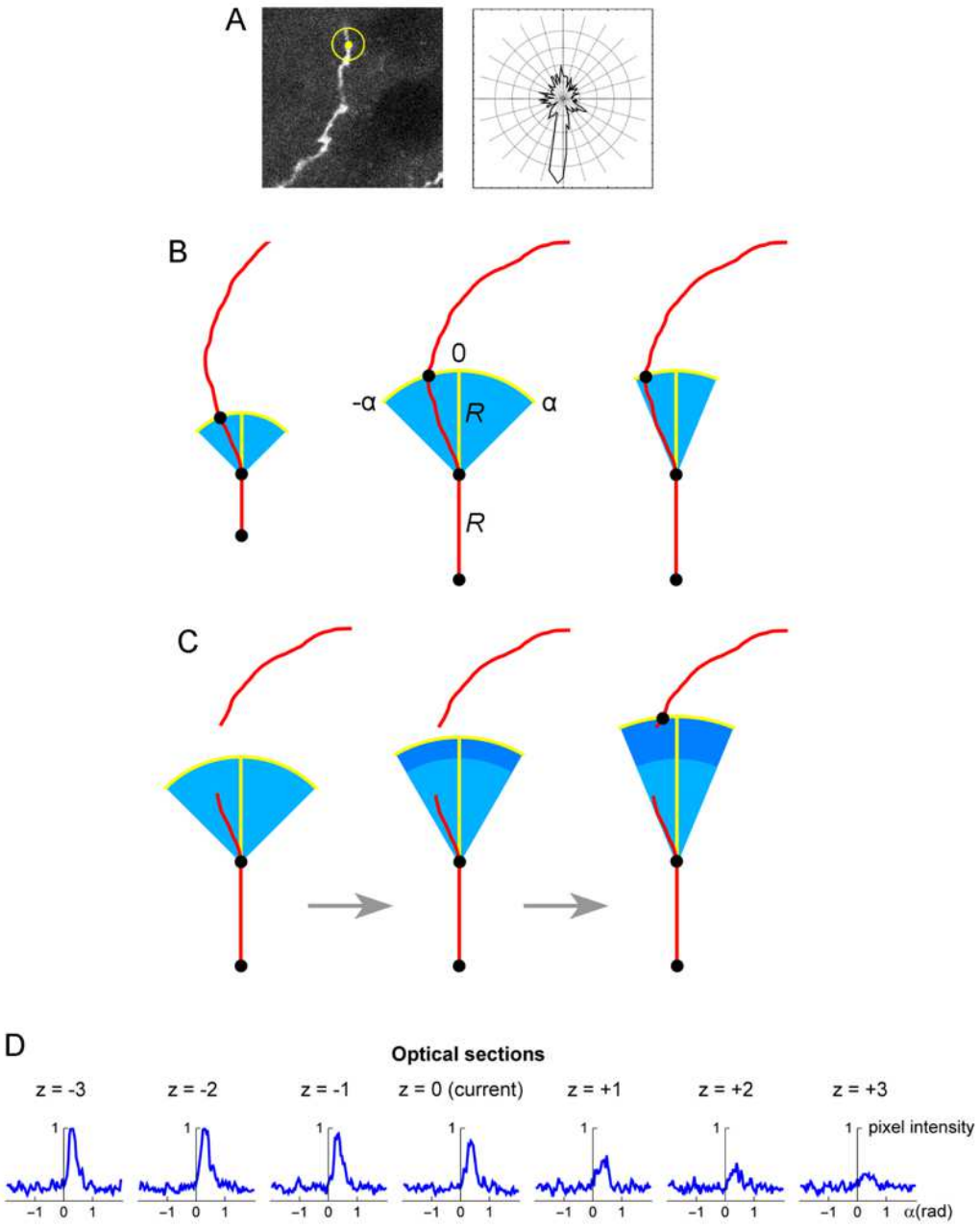

Figure 5: (A) A seed point (yellow) and the initial search circle around it (with a radius of around 2 µm; left), with a corresponding polar plot of the brightness values on the circle (where larger radii correspond to stronger brightness; right). The polar plot clearly indicates the position of the second point, which initiates the automated tracing procedure. (B) At each current fiber point (an xy-coordinate in a specific optical section), the "flashlight" tracing algorithm scans the intensity of the pixel values in an arc that is centered at this point, with a radius *R* and the subtended angle [-α, α]. The middle point of the arc (0) corresponds to the "expected" direction of the fiber (marked with the yellow segment), which is based on the current point and the point before it. The values of *R* and α can be adjusted to reflect the general tortuosity of the fiber. For clarity, the first segment is shown straight, and the value of *R* is greatly exaggerated (it is typically on the order of the fiber width). A specified number of optical sections above and below the current optical sections are also scanned in the same way. (C) If the algorithm fails to detect any intensity peaks in the subset of optical sections, the step can be automatically extended (the dark blue region). Since this extension increases the risk of false-positives (e.g., it may detect a segment of another fiber in the vicinity), the search angle can

be automatically decreased. The extended R is an integer multiple of the original R (0.5R, 1R, 1.5R, 2R, …); in the figure, it is shown smaller for compactness. (D) An example of a decision made by the tracing algorithm in one step. The center plot shows the pixel intensity values in the current optical section (z = 0) in an arc centered at the current xy-position, R = 2 μm, and α = 0.6π radians (the current direction is given by α = 0). The plots to the left and right of the middle plot show the corresponding pixel values at the same xy-position and direction in the three optical sections below and above the current optical section (typically, more adjacent sections are used). In this case, the trace turns slightly to the right and three optical sections down. The trace then resets to the new xy-position and direction.

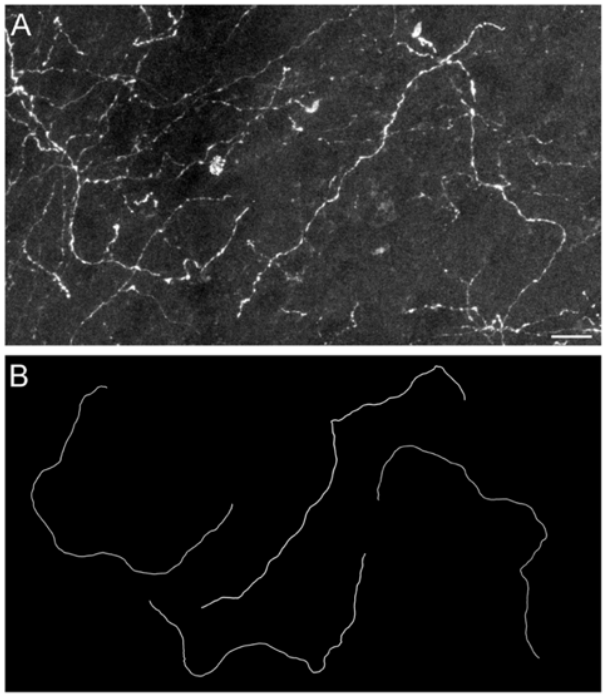

Figure 6: (A) EGFP-positive serotonergic fibers in the somatosensory cortex of a Tph2-iCre x LoxP-EGFP mouse. (B) Similar simulated fibers generated with a vMF-walk with κ = 170 and 1,000 steps.

iii. BRAINBOW TRACER (NTRACER)

Automated tracing in Brainbow images continues to be challenging despite improved axon differentiation due to nonuniform neurites and branching structures, as well as high levels of noise often present in multispectral 3D fluorescent Brainbow images. One possible solution is given by nTracer, a Brainbow-specific tracing system developed by another group (Roossien et al., 2019). The framework for the nTracer uses a combination of two key components: a denoising step and a Recurrent Neural Network (RNN) step, respectively. The RNN is an effective model to process sequential data. It learns complex dynamics by

mapping input sequences to a sequence of hidden variables. By passing the hidden variables recursively to the repeating module in the network, the RNN can memorize the previous information. Thus, RNN performs well in dealing with sequential data which have dependencies. In the image denoising step, nTracer adopts a VBM4D denoising strategy which is considered as a state-of-the-art denoising method for image stacks (Maggioni et al. 2012). During the RNN step, it utilizes Long Short-Term Memory (LSTM) to complete the automated neural tracing task. LSTM networks are a special kind of RNN, capable of learning long-term dependencies. LSTMs were specifically designed to avoid the long-term dependency problem, making remembering information for long periods of time practically their default behavior (Yan et al., 2018).

iv. MACHINE LEARNING (TRAILMAP)

Tracing axons in light-sheet images also poses unique challenge. With such large amounts of data, using other automatic tracers is no longer an option. Therefore, we attempted to trace serotonergic fibers in light-sheet images using a recently published machine-learning system called TrailMap (Friedmann et al., 2020). This system uses a convolutional neural network based on the 3D U-Net architecture. The system is designed for a lower resolution (typically used in light-sheet microscopy). However, at this resolution, serotonergic fibers cannot be reliably detected, which suggests that the network in the published form may not be ideal for tracing the goals of this project.

ANALYSIS METHODS

We have recently introduced **two stochastic models** for fiber analysis, one based on a stepwise random walk and the other based on a continuous, Brownian motion-like process (Janusonis and Detering, 2019; Janusonis et al., 2020). The advantage of the former process is that it does not require temporal information, but at the same time, it requires knowing the typical "step" of the process which is not natural biologically. The continuity of the latter process solves this problem, but it requires temporal information which is difficult to obtain in fixed tissue. These models are a stepwise walk based on the von Mises-Fisher directional distribution (vMF) and fractional Brownian motion (FBM), respectively. This research project is primarily based on the vMF-walk, with the expectation that future analysis may more heavily utilize the FBM model. Next, both models are briefly reviewed.

i. THE VON MISES-FISHER MODEL

A random walk is a mathematical model that describes a path of successive random steps in a mathematical 3D-space (Codling et al., 2008). In this framework, the behavior of serotonergic fibers can be thought of as a series of connected straight segments of the same length. Each of these segments has a restricted cone of possible directions that it can choose from (Figure 7A). When choosing the next direction, the *current direction* of the fiber can be considered as the *expected direction* of the next segment (therefore, the cone is oriented on the segment towards its current direction), with all other direction possibilities distributed around it (Janusonis and Detering, 2018). This cone representation is simple and intuitive, but fibers likely follow a probability density that has no hard deviation limits (e.g., individual fibers can occasionally make 90° turns). Therefore, a better model could use the current

direction as the expected direction, with all other directions still distributed around it, but with the key difference that the probability for these directions gradually decreases, the further they deviate from the expected direction (Figure 7B).

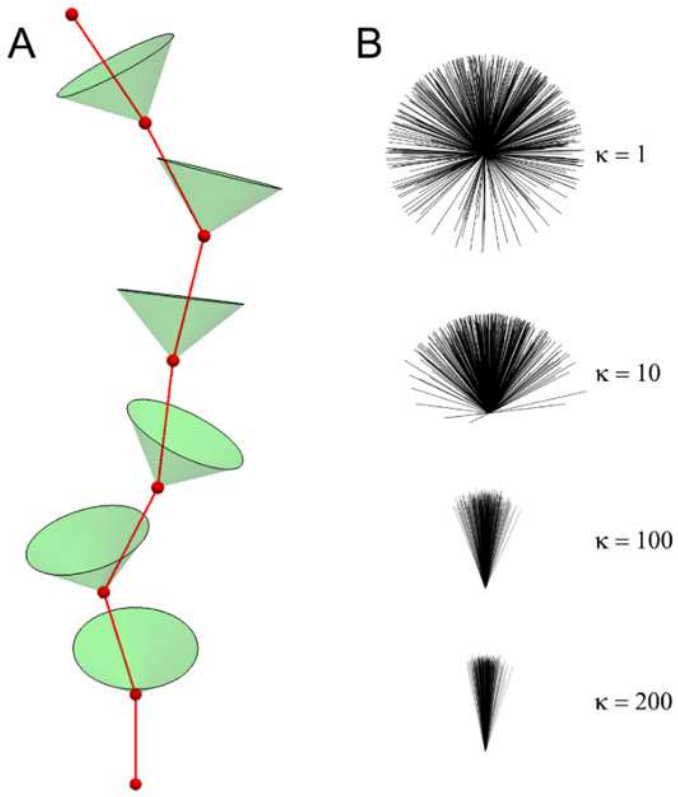

Figure 7: (A) A model of a fiber as a series of connected segments, each of which has chosen a random direction within its cone of possibilities. Note that each cone is centered at the current direction, but the next segment can deviate from it. Each realization will produce a unique fiber, but the fibers will appear qualitatively similar (if the width of the cones is kept constant). (B) Samples of 500 random directions drawn from the vMF distribution with different concentration parameter values (κ=10, 100, 200). With all κ values, all directions are theoretically possible, but some are highly unlikely.

Another obstacle is that the required probability distribution cannot be found among the ones used in standard probability theory and statistics (e.g., normal). The solution to this problem is the von Mises-Fisher distribution (vMF). The vMF distribution is a classical directional distribution that has the required properties for analysis of serotonergic fibers.

The vMF distribution is based on two parameters, the mean direction (μ), and the concentration parameter (κ). The mean direction is similar to the mean in a normal distribution, while the concentration parameter is comparable to the inverse of the variance of the normal distribution. The higher the κ, the tighter the concentration of directions are around the mean. Accordingly, at κ=0, all directions become equally probable. Another benefit of using the vMF distribution is that it allows for efficient analytical approaches using computer calculations, along with a quick and easy algorithm for the simulation of fibers based on the following steps:

1) Start with a random direction and draw the first segment

2) Set μ as the current direction

3) Draw a random direction from the vMF distribution with μ and a preselected κ

4) Add the next segment

5) Repeat from step 2 (Janusonis et al., 2019)

Within the terminal fields of adult brains, serotonergic fibers tend to show no directionality preference, thus making it possible to describe their behavior with only the concentration parameter (κ). Evidence to support this possibility has been shown using computer simulations that produce trajectories similar to those of serotonergic fibers imaged at high resolution with confocal microscopy (Janusonis and Detering, 2018). This raises an important question about how κ relates to differing fiber densities that have been described as relatively stable across different brain regions in healthy individuals. Since lower κ values tend to produce larger angle turns and thus spend more time in the given brain region, it is logical to conclude that different κ values may correspond to different fiber densities. Indeed,

computer simulations have shown that different κ values may correspond to fiber density variations (Janusonis and Detering, 2018). Due to the κ parameter containing all the information regarding individual fiber behavior, the use of κ values also allows for direct comparisons of the behaviors of individual fibers in not only different brain regions, but also in different conditions—including those affected by mental illness. This study measures these values in brain sections and whole brain preparations for the first time.

ii. FRACTIONAL BROWNIAN MOTION MODEL

Normal Brownian motion describes simple diffusion. Its scientific investigation dates back to the observation of water-suspended pollen grains by Robert Brown (a Scottish botanist) in 1827 and the pioneering theoretical work by Albert Einstein in 1905 (Gardiner, 2010). In normal Brownian motion, the spatial increments in any two non-overlapping time intervals are statistically independent, and particles that start at the same origin follow the normal (Gaussian) distribution in space – with the variance scaling linearly with time ($\sigma^2 t$, where $\sigma > 0$ is a constant parameter and t is time). FBM is a major theoretical extension of normal Brownian motion. It has several stochastic integral representations (Biagini et al., 2010) and dates to the data analyses of Harold Edwin Hurst (a British hydrologist) (Hurst, 1951) and the theoretical constructions by Andrey Kolmogorov (Biagini et al., 2010) and Benoit Mandelbrot with John Van Ness (Mandelbrot and Van Ness, 1968). In FBM, the spatial increments in non-overlapping time intervals are generally statistically correlated. In particular, the increment correlation between two consecutive time intervals of equal length is given by $2^{(2H-1)-1}$, where H is the Hurst index ($0 < H < 1$), a key parameter of the FBM process. Particles that start at the same origin follow the normal distribution, with the

variance now scaling as $\sigma^2 t^{2H}$. FBM is a time-continuous and self-similar process (i.e., it "looks the same" at all temporal scales). The regime at $H < 0.5$ is known as "subdiffusion" (characterized by anti-persistent trajectories, in which two consecutive increments are negatively correlated), and the regime at $H > 0.5$ as "superdiffusion" (characterized by persistent trajectories, in which two consecutive increments are positively correlated). Normal Brownian motion is recovered as a special case at $H = 0.5$. As H approaches 1, the trajectories approach straight lines, effectively losing their stochastic character (Figure 8).

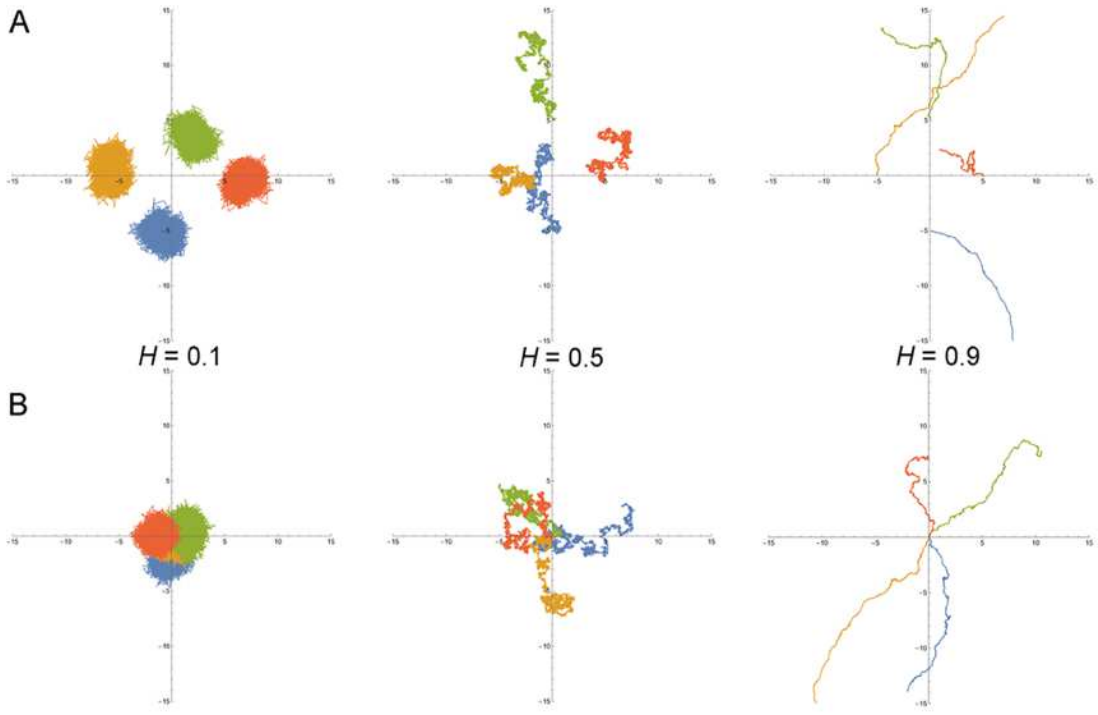

Figure 8: (A) Four FBM sample paths ($\sigma = 1$, T = 10, $\Delta t = 0.001$) starting at points (0, -5), (-5, 0), (0, 5), and (5, 0), with H = 0.1 (subdiffusion), H = 0.5 (normal diffusion), and H = 0.9 (superdiffusion). (B) Another realization of four FBM sample paths ($\sigma = 1$, T = 10, $\Delta t = 0.001$) starting at the same point (0, 0) to show the relative spread, with H = 0.1 (subdiffusion), H = 0.5 (normal diffusion), and H = 0.9 (superdiffusion).

TISSUE CLEARING

An important aspect in light microscopy is the refractive index (RI), a measure of how fast light travels through a tissue. In biological tissues, the RI is low because the tissue consists of multiple components, each with its own RI. Specifically, biological tissues contain 70-80% of water (RI: = 1.33), approximately 10% of proteins (RI: = 1.44), and approximately 10% of lipids (RI: = 1.45). These variations in RI cause incoming light to scatter, while endogenous pigments within the tissue (heme, riboflavin, melanin and lipofuscin) increase light absorption. Together, the increase of light absorption by pigments and light scattering by varying RIs are the components that limit tissue penetration in general microscopy imaging (Tainaka et al., 2016). Given this limitation, imaging of biological tissue can be accomplished by separating the tissue into thin sections before imaging. However, this method is problematic, as it is difficult to recreate the 3D environment from sections without their precise alignment (since they are processed separately, tissue distortions may occur).

The solution to this problem was first accomplished in 1914 by Werner Spalteholz with a process called tissue clearing (Spalteholz, 1914). The goals of tissue clearing methods are to homogenize the RIs of the tissue and remove the endogenous pigments while avoiding destruction or alterations of biological structures. Since then, numerous tissue clearing methods have been created that can be grouped into two categories: organic solvent-based clearing methods, or hydrophilic reagent-based clearing methods. Organic solvent-based methods can render tissue extremely transparent, which is particularly beneficial for light-sheet microscopy. However, the downside to organic based solvents is their tendency to quench fluorescent proteins, making them less useful for investigation of biological components that require fluorescent labeling for visualization. One organic solvent-based

method that has been explored for tissue clearing is with the reagent dibenzylether (DBE). However, DBE has been shown to cause considerable tissue shrinkage and deformations along with not preserving GFP fluorescence (Becker et al., 2012). Hydrophilic clearing methods use water-soluble reagents for tissue clearing and work by forming hydrogen bonds with components of tissues—such as proteins as well as surrounding water molecules, which can help to preserve the 3D structure of tissue components and, thereby, the signal of fluorescent proteins. One hydrophilic clearing method for tissue clearing is by using CLARITY, which has been shown to sufficiently clear tissue without alterations of biological structures; however, it was also not able to preserve GFP fluorescent signal (Chung et al., 2013). Another hydrophilic tissue clearing method is using *Scale*, which was able to preserve GFP signal and reach sufficient tissue clearing. Unfortunately, this only works when using small samples such as mouse hearts or embryos up to embryonic day 12.5 (Hama et al., 2011). A recent improvement in hydrophilic clearing methods has been achieved by Ueda and colleagues (Susaki et al., 2015), called CUBIC (Clear, Unobstructed Brain/Body Imaging Cocktails). CUBIC is a gentle method that has been shown not to cause shrinkage or expansion of tissue while preserving GFP signal. Another improvement of using CUBIC over other clearing methods is that it is able to remove heme pigments from samples, resulting in a more complete clearing and an overall improved RI (Mano et al., 2018)

CHAPTER 4: EXPERIMENTS

Experiment 1 - Imaging and Tracing of a Transgenic Fluorescent Mouse Model

Purpose: The primary goal for Experiment 1 was to create a fluorescent transgenic mouse model for tracing and analysis of serotonergic fibers. To analyze individual serotonin axon behavior, we utilized a single-color fluorescent transgenic mouse model. The first fluorescent mouse models (the "green mouse") were originally designed in 1997 utilizing the green fluorescent protein (GFP) to overcome the challenge of imaging live tissue without toxicity (Okabe, 1997). However, as soon as it was discovered that this genetic component increased labeling specificity and decreased "noise" from nonspecific background staining, the transgenic mouse became the "superior" or preferred method for IHC. An additional improvement transgenic models bring when working with monoamines is the labeling expression is independent of serotonin accumulation within the axons. This improves labeling continuity as well as enhancing signal reliability as axon segments or branches are labeled regardless of serotonin levels. For this experiment, we used an EGFP (enhanced green fluorescent protein) transgenic mouse under the Tph2 promotor, specific to serotonin cells, followed by confocal imaging and automatic tracing.

Experiment 1.1 - Verification of Transgene Expression

Ex. 1.1a Genotyping, PCR, and Tapestation Analysis: Genotyping was performed using toe biopsies obtained from animals at 10 days in age. DNA extraction was completed using the QIAmp Fast DNA Tissue Kit (QIAGEN) and PCR completed using the primers listed in Table 2. TdTomato mice were kept homozygous, eliminating the need for genotyping to be

performed on this strain. Successful genetic crosses were additionally verified with IHC and confocal imaging.

Animals: This experiment utilized the transgenic mouse line: STOCK Tg (Tph2-icre/ERT2)6Gloss/J (iCre), which carries a tamoxifen-inducible Cre-recombinase under Tph2, crossed with the transgenic mouse line: B6.129(Cg)-Gt(ROSA)26Sortm4(ACTB-tdTomato,-EGFP)Luo/J, which has a Cre-recombination-dependent tdTomato construct (Jackson Laboratories). After crossing the two lines, the offspring were genotyped using the primers listed in Table 2, and only adult (4-5 months) Cre+/tdTomato+ genotypes were used. PCR-genotyping for these lines is shown in Figure 10. All mice were maintained on an artificial 12-hour light cycle and group housed in plexiglass cages with food and water ad libitum. Cre-recombination was induced at 11-12 weeks of age with intraperitoneal injections of 75 mg/kg of tamoxifen solution dissolved in corn oil (20 mg/ml) once a day for five days (Sohol et al., 2001; Madisen et al., 2010, Pelosi et al., 2015). Mice were euthanized 4 weeks following the final tamoxifen injection and the brain was immediately dissected and immersion fixed in 4% paraformaldehyde. All experimental procedures outlined were approved by the UCSB Institutional Animal Care and Use Committee (IACUC).

Primer	Forward Sequence	Reverse Sequence
iCre	5'- GCT GAG AAA GAA AAT TAC ATC -3'	5'- TGG CTT GCA GGT ACA GGA GG -3'
Control iCre	5'- CAA ATC TTG CTT GTC TGG RG -3'	5'- GTC AGT CGA GTG CAC AGT TT -3'

Table 2: Primer sequences used in PCR-genotyping.

Immunohistochemistry:

To verify expression of Cre in the raphe nuclei, sections through the DRN were rinsed in phosphate-buffered saline (PBS). Using a free-floating technique, sections were blocked to reduce background staining, followed by a 2–3-day incubation in primary antibody solution before incubation for 90 minutes in a secondary antibody solution. Once completed, sections were mounted onto gelatin/chromium-subbed slides, allowed to air-dry, and then cover-slipped using Prolong Gold antifade-reagent with DAPI (Life Technologies).

Primary: iCre tissue sections were rinsed in PBS and incubated for two days at 4°C in a primary antibody solution of 2% NDS, 0.3% Triton X-100 (TX), and rabbit anti-Cre IgG (1:1000).

Secondary: Sections were first rinsed 3 times in PBS solution for 10 minutes per rinse. Once rinsed, sections were incubated in a secondary antibody solution containing 2% NDS, and Cy3-conjugated donkey anti-rabbit IgG (1:200) for 90 minutes on a rotator at room temperature (Figure 9).

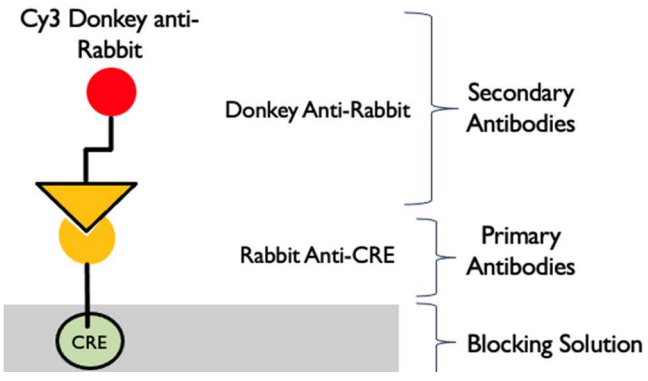

Figure 9: Schematic outlining the IHC set-up for labeling Cre-expressing soma.

Ex. 1.1a Results: The results from the first portion of this experiment yielded mixed results. The PCR results indicate that we successfully produced a transgenic mouse model (with Tapestation peaks at ~275 for Cre). However, these results were not successfully verified with IHC which lacked expression of Cre cells in the DRN. Since PCR indicated the animals were the correct genotype, IHC was attempted again with heat-induced epitope retrieval (HIER) to rule out the formaldehyde fixation as the cause for these mixed results.

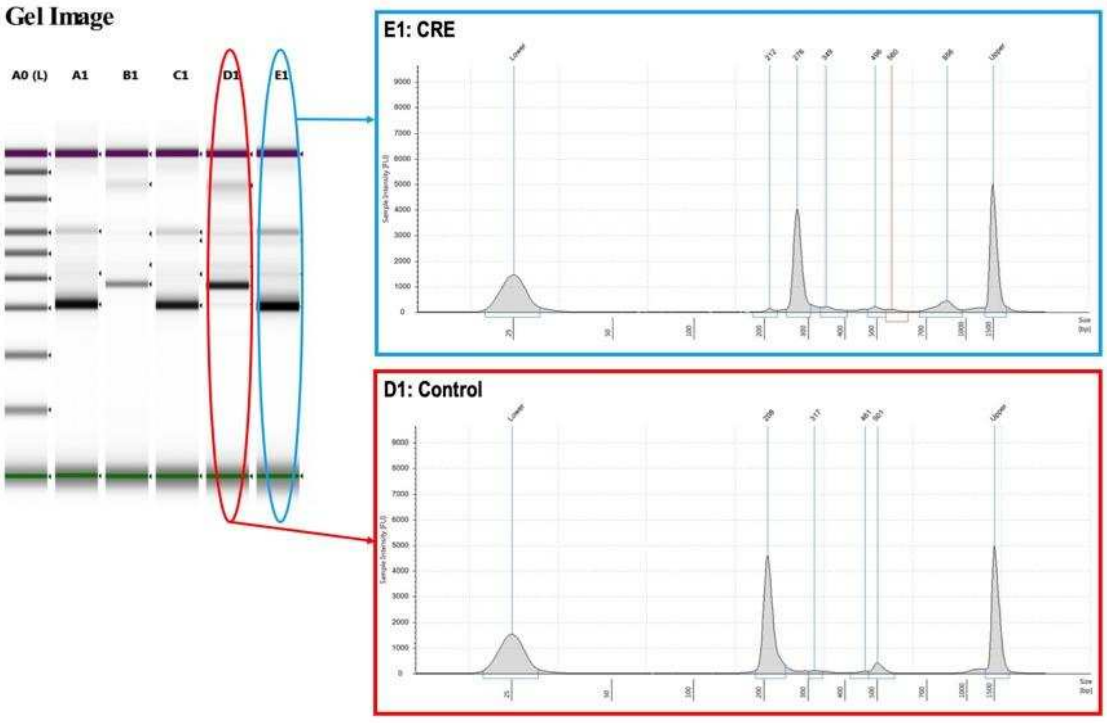

Figure 10: Tapestation results from PCR of STOCK Tg(Tph2-icre/ERT2)6Gloss/J showing DNA peaks at: 206 (control) and 276 (Cre).

Ex. 1.1b Genetic Verification with Heat-Induced Epitope Retrieval

Due to the lack of expression with standard IHC techniques, HIER was applied to the sections prior to IHC. Our tissue is fixed in paraformaldehyde which is a formalin-based fixative. These have been shown to provide excellent preservation of morphology, cytology,

and tissue architecture, but greatly diminishes the sensitivity of the IHC technique. Formaldehyde covalently binds to tissue protein and may also act to crosslink adjacent proteins or peptides to form large aggregates of proteins. This cross-linking is believed to block or "mask" the epitope and thus hinder the binding of the antibody. HIER methods involve applying heat and a buffer to the tissue which by some means reverses the formaldehyde mediated chemical modifications (possibly by breaking up the cross links with thermal energy or by removing the bound calcium ions from the cross links).

Immunohistochemistry:

HIER: Tissue sections through the DRN were microwaved for 3 minutes at 30% power (avoiding boiling) in Tris HCl buffer (pH 9) solution.

Primary: iCre tissue sections were rinsed in PBS and incubated for two days at 4°C in a primary antibody solution of 2% NDS, 0.3% Triton X-100 (TX), and rabbit anti-Cre IgG (1:1000).

Secondary: Sections were first rinsed 3 times in PBS solution for 10 minutes per rinse. Once rinsed, were incubated in a secondary antibody solution containing 2% NDS, and Cy3-conjugated donkey anti-rabbit IgG (1:200) for 90 minutes on a rotator at room temperature (Figure 11).

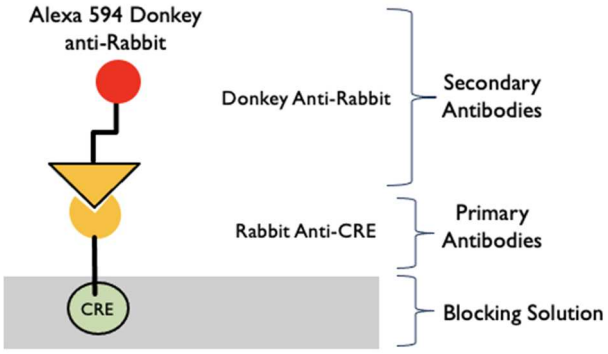

Figure 11: Schematic outlining the IHC set-up for labeling Cre-expressing soma.

Ex. 1.1b Results: We have successfully developed the Cre and tdTomato breeding colonies despite some challenges with the Cre line. An initial challenge for breeding was a founding Cre female that repeatedly cannibalized her litters—even when provided with a special diet containing Love Mash (Bio-Serv), a high calorie food that is used to increase foraging behavior in mothers. This diet has been shown to increase litter size, pup survival rate and enhance milk production (Lecker & Froberg-Fejko, 2016). Success was achieved only by using another mouse that fostered the offspring. An ongoing challenge in breeding the Cre line is the relatively small litter sizes (3-5 pups) they produce.

Verifying the expression of Cre in the DRN also posed challenges. The initial IHC revealed no signal in the DRN. However, upon review of literature (Paulsen et al., 2015) we discovered expression can be amplified using heat-induced epitope retrieval (HIER) (Figure 12). Extreme caution must be used when performing HIER as overheating (boiling) leads to tissue shredding and under-heating fails to retrieve the epitope.

Once iCre+ and tdTomato+ lines were established, the lines were crossed to produce a iCre+/TdTomato+ mouse line (Figure 13).

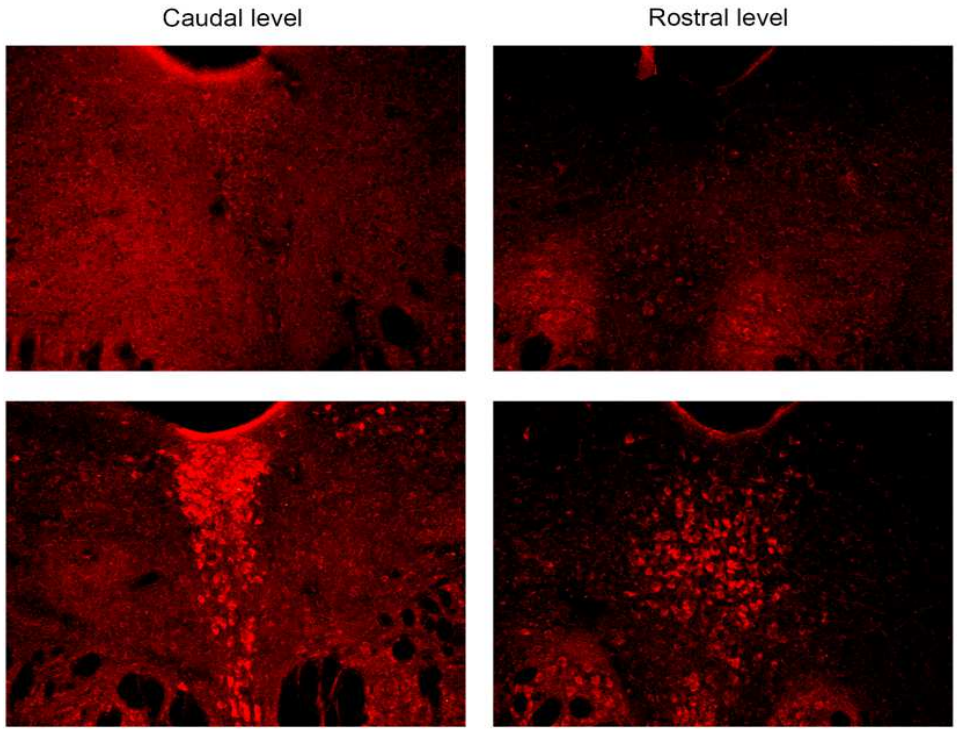

Figure 12: Epifluoresence images of the rostral and caudal DRN visualized with IHC for Cre. Top: A non-carrier mouse. Bottom: A Cre-Tph2 mouse.

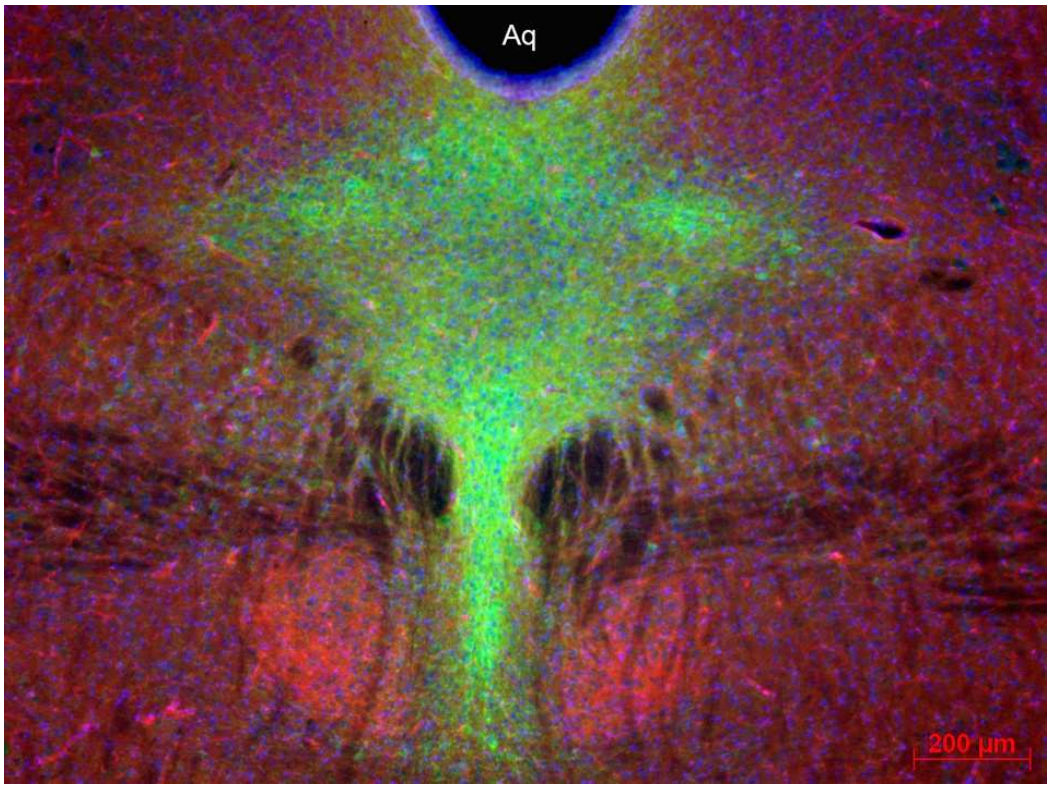

Figure 13: Epifluorescence image of the DRN in a Cre-Tph2 x tdTomato mouse. Serotonergic neurons show EGFP-fluorescence. Scale bar = 200 µm.

Experiment 1.2: Signal Amplification and Imaging

Purpose: The endogenous fluorescent level in transgenic models tends to be weak and signal amplification with IHC is a common practice when working with endogenously fluorescent tissues. In this portion of Experiment 1, the EGFP signal in Cre+/tdTomato+ tissue was amplified with IHC for GFP, and z-stack images obtained with a Leica SP8 Resonant Scanning Confocal microscope.

Signal Amplification IHC:

Primary: Tissue sections were rinsed in PBS and fluorescent signal amplified by incubation for two days at 4°C in a primary antibody solution containing 2% NDS, 0.3% Triton X-100 (TX), and rabbit anti-GFP (AbCam 1:500).

Secondary: Sections were first rinsed 3 times in PBS solution for 10 minutes per rinse. Once rinsed, sections were incubated in a secondary antibody solution containing 2% NDS, and AlexaFluor 488-conjugated donkey anti-rabbit IgG (1:200) for 90 minutes on a rotator at room temperature (Figure 14).

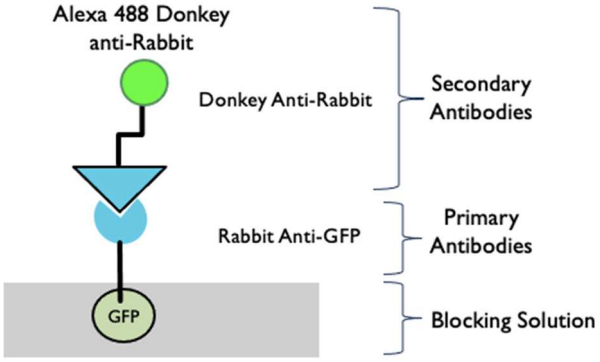

Figure 14: Schematic outlining the IHC set-up for labeling tdTomato-expressing soma.

Imaging:

High power confocal images were acquired using a Leica confocal microscope system, with a 63X oil immersion objective. Z-series of 60-70 images were obtained at a 1032x1032-pixel resolution.

Results: The IHC signal in iCre+/TdTomato+ samples were successfully amplified, and confocal images taken from the Inferior Colliculus (IC) that were used for analysis are shown in Figure 15.

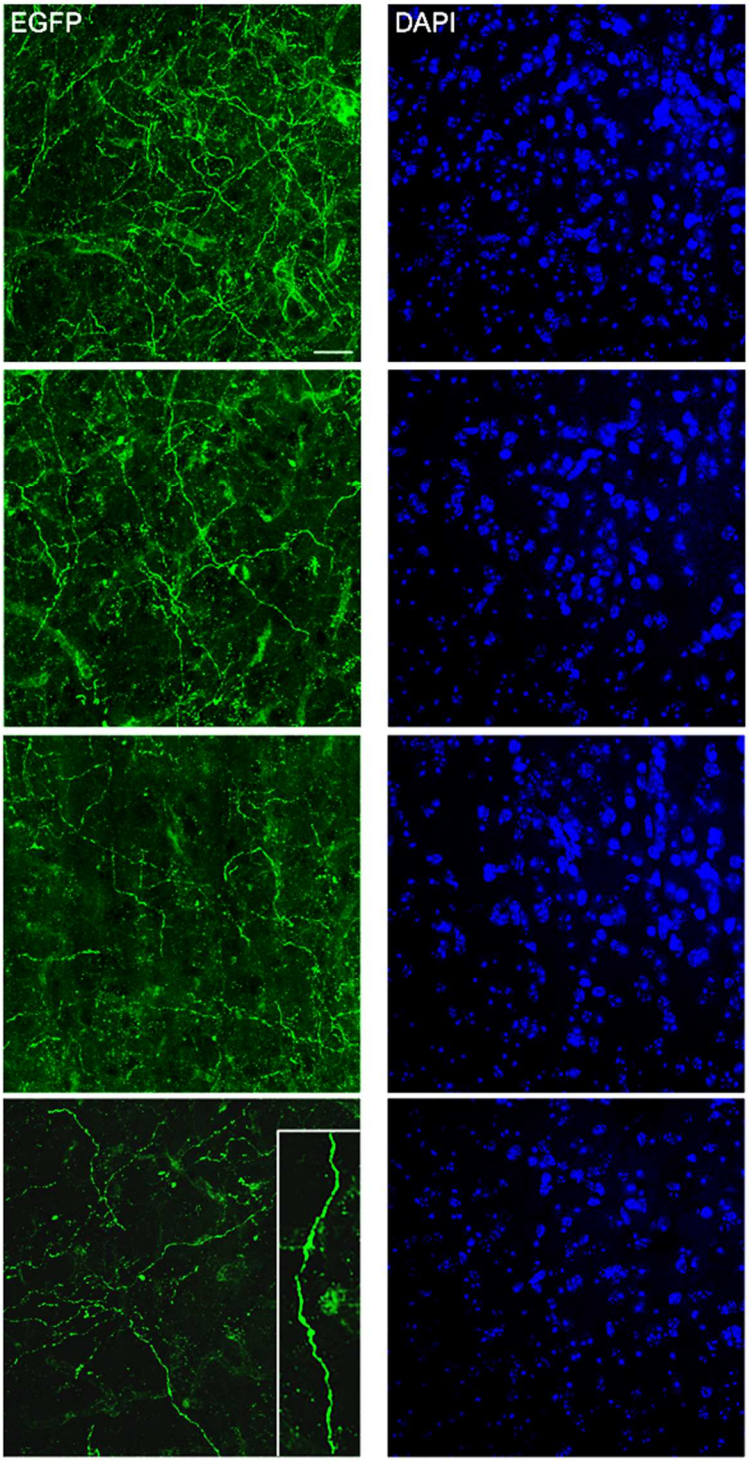

Figure 15: Confocal images of EGFP-positive serotonergic fibers in the inferior colliculus of Tph2-iCre x LoxP-EGFP mice, with the corresponding images of cell nuclei (visualized with DAPI). This transgenic approach may produce varying labeling intensities (arranged from high to low in the figure) that are partially controlled by Tamoxifen induction. This facilitates the tracing of individual axons, also because the signal is not concentrated in varicosities and is strong throughout the entire length of labeled fibers, with only short interruptions (inset). The actual ("complete") fiber densities can be easily visualized with 5-HT or SERT immunohistochemistry. Scale bar = 20 μm.

Experiment 1.3: Fiber Tracing and Analysis

Purpose: Once z-stack images were obtained, serotonergic fibers were first manually and then automatically traced using an algorithm developed in this project (outlined in Chapter 2), before analyzed using stochastic modeling.

Manual Tracing: Fibers were manually traced in motor cortex (M1) and cingulate cortex (CCX) using the Simple Neurite Tracer plugin for ImageJ and analyzed for their κ values (Figure 16).

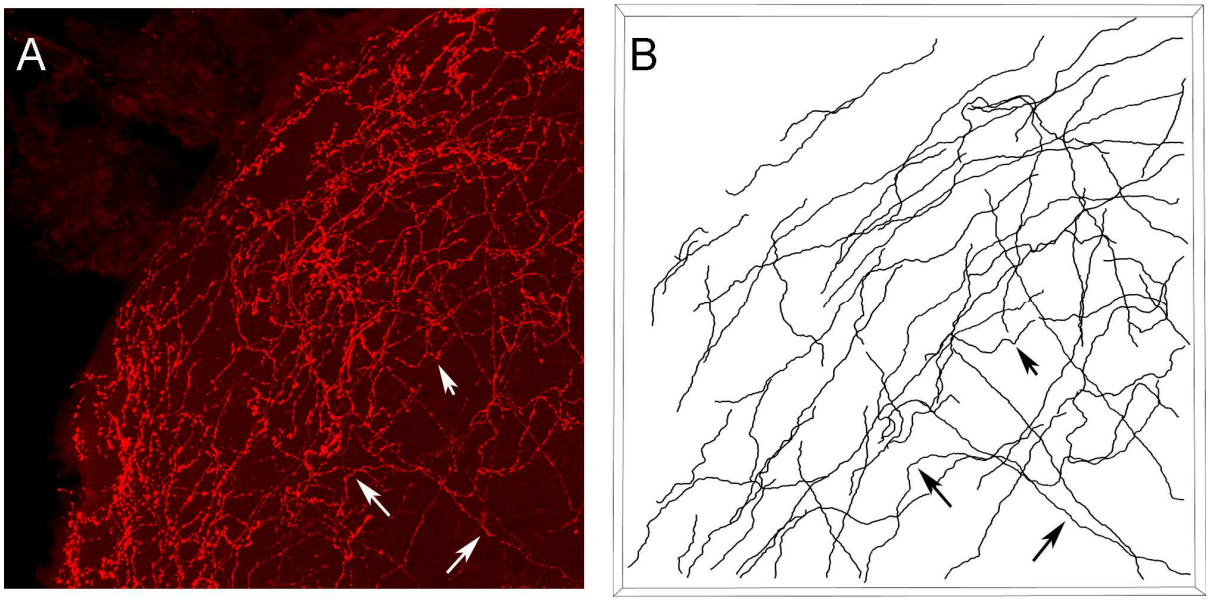

Figure 16: A) 2D-projection of a confocal z-stack of serotonergic fibers (labeled with an anti-5-HT antibody) from the mouse cingulate cortex (at the most superficial depth). The κ calculations from this scan correspond to depth 1 of the CCX shown in Table 3. B) Sample traces of serotonergic fibers from the mouse CCX. The tracing was performed manually in Fiji ImageJ in a confocal z-stack collected from a 40 µm thick brain section. κ estimates were obtained for each individual fiber based on its trajectory.

Manually Traced Results Analysis of κ values obtained using images produced two main findings. First, different κ values were obtained in different brain regions (Figure 17D, E). A significant difference was not found in κ values at different cortical depths as expected, which could simply be due to not sampling regions at a

great enough distance apart to change κ values or oversampling of D or M fibers. The second main finding is despite having multiple tracing individuals, the κ values obtained are rather consistent. We note that despite this encouraging result, the low resolution of the z-axis makes reliable tracing by human individuals difficult (especially when human tracers need to decide which fiber trajectory to follow across sections). There are several alternatives that can be explored to improve fiber tracing; however, the only way to completely remove tracing bias is to replace manual tracing with some sort of automated tracing process. Therefore, further estimations of stochastic parameters will be obtained using the new automated tracing algorithm developed in this project

Automatic Tracing: Serotonergic fibers were automatically traced in Mathematica in the IC region of adult iCre+/TdTomato+ mice.

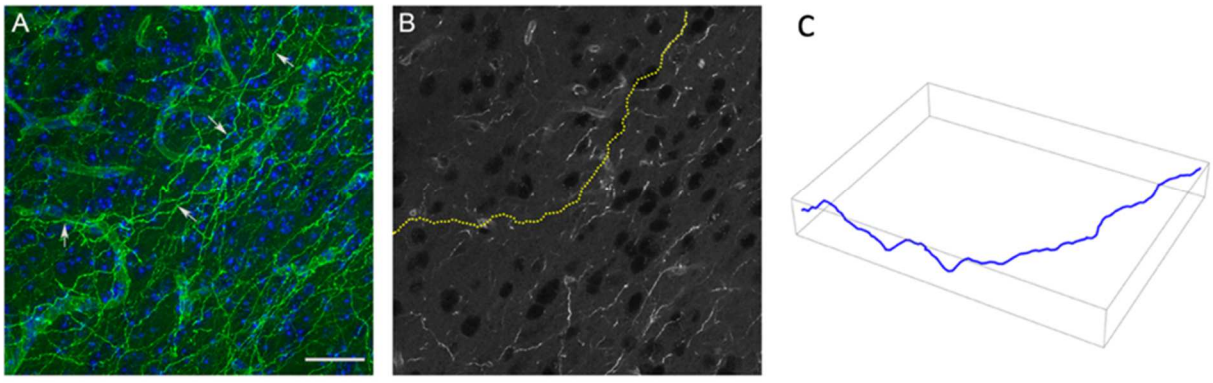

Figure 17: (A) serotonergic fibers in the inferior colliculus of a Cre+/tdTomato+ mouse. The image is a 2D-projection of a confocal z-stack with 86 optical sections. The small arrows indicate a fiber that travels in the physical section for a long distance without leaving it. The fiber is surrounded by other fibers which makes accurate tracing difficult. (B) An automatically extracted trajectory of the selected fiber, using the algorithm developed by the Janusonis laboratory. The trajectory is overlaid on a single optical section. (C) The fiber trajectory plotted as an array of 3D-coordinates. This trajectory can be analyzed as a sample path of a spatial stochastic process. Scale bar = 30 μm (A-C).

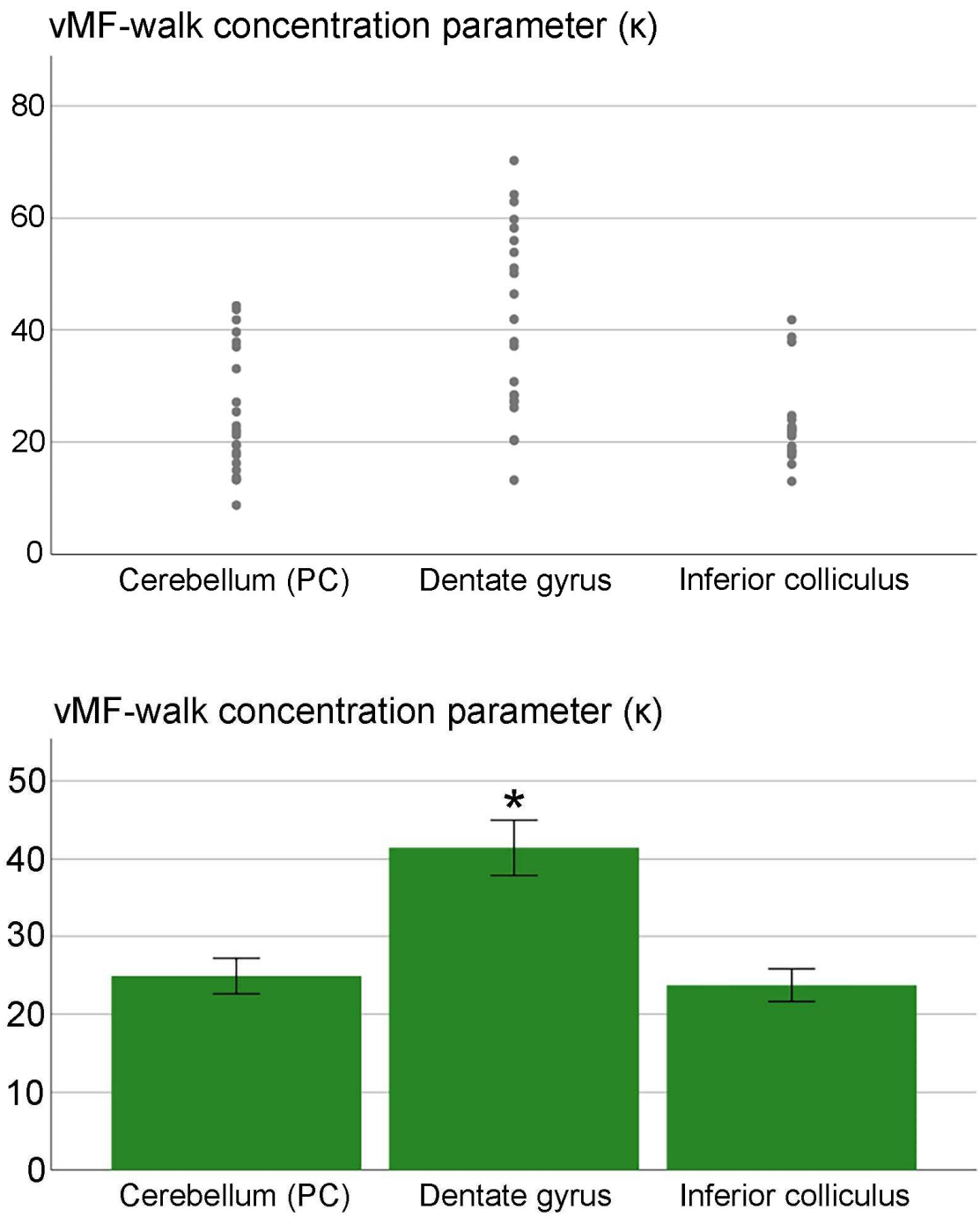

Figure 17 D/E: Estimated values of the vMF concentration parameter (κ) in the cerebellum (purkinje cell layer; PC) the dentate gyrus, and the inferior colliculus. The tracing step is 1.5 μm. The fibers appear to be significantly less tortuous in the dentate gyrus (one-way ANOVA: $F(2, 58) = 12.5$, $p < 0.001$).

EXPERIMENT 1 RESULTS

During this experiment, a transgenic mouse model specific for the serotonergic system was successfully developed. The transgenic model was successfully verified using both genotyping and fluorescent labeling with HIER required for fluorescent labeling. Signal amplification, tracing, and analysis of fibers was completed on obtained sections and this experiment shows although tracing can be completed manually, automatic tracing is faster and reduces the risk of unconscious bias and sampling. Ultimately, obtaining differing kappa values indicates this method of analysis can be used to study individual fiber behavior. However, even with the high-resolution power of confocal imaging, during the tracing process we found that with axons can pass so close to one another (even on the same plane), the algorithm sometimes favors brightness over the axon's current direction, causing mistakes in tracing to occur (Figure 18). Therefore, despite using some of the most advanced technological options at our disposal, the algorithm can still make mistakes—requiring the tedious and perhaps subjective requirement of human intervention. If this algorithm struggles with tracing due to the density of axons in Figure 18A, how could it possibly trace axons in a highly dense region such as Figure 18D? The answer is an algorithm that accurately traces axons may not be possible without solving the problem of axon differentiation.

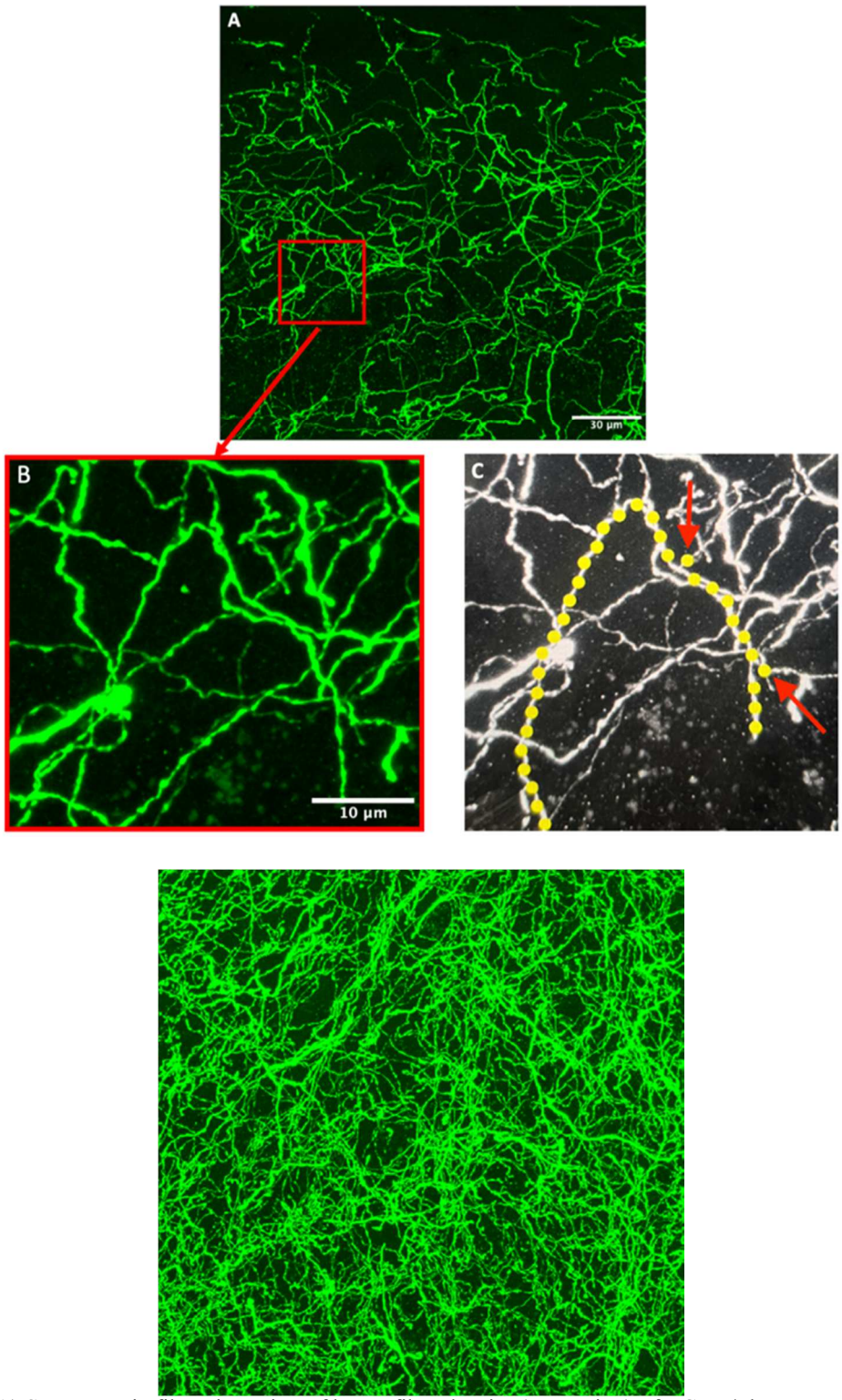

Figure 18: (A) Serotonergic fibers in region of lower fiber density (PY region) of a Cre+/tdTomato+ mouse. This image is a 2D projection of a confocal z-stack with 99 optical sections used for fiber tracing scale bar = 30µm. The red box highlights area of interest enlarged in (B) scale bar = 10 µm of an automatically traced fiber in (C) with red arrows pointing to errors in the algorithm's tracing. (D) Serotonergic fibers in a region of higher fiber density (BLA region of the amygdala) of a Cre+/tdTomato+ mouse. This image is a 2D projection of a confocal z-stack with 95 optical sections scale bar = 30µm.

Experiment 2: Creating a Model for Axon Differentiation

Purpose: The central problem discovered in Experiment 1 is that all axons are labeled with the same color. The single-color model is better than IHC as it produces continuous trajectories that can be traced in regions with low to moderate fiber densities with diligent monitoring of the tracing algorithm. The goal for Experiment 2 is to design a mouse model that improves the ability to differentiate axons. In this experiment, a transgenic mouse model is created by crossing the Brainbow 3.2 mouse line with the iCre line under the Tph2 promoter. As outlined in Chapter 3, this model can give individual neurons unique coloring and thereby improve the ability to separate individual axons which can improve tracing accuracy while also providing additional information about fiber behavior such as if fibers from a single soma (single color) produce meshworks, changing behavior/tortuosity in specific brain regions, as well as branching behaviors.

Experiment 2.1: Verification of Transgene Expression

Purpose: Genotyping was performed using toe biopsies obtained from animals at PND 10. DNA extraction was completed using the QIAmp Fast DNA Tissue Kit (QIAGEN) and PCR completed using the primers listed in Table 3. Only mice confirmed as iCre+/Brainbow 3.2+ mice were used.

Animals: The mouse model we utilized was created by crossing two separate mouse lines. The first mouse line is STOCK Tg (Thy1-Brainbow3.2)7Jrs/J, carries a Cre-recombination-dependent Brainbow 3.2 construct which was crossed with the same iCre mouse line outlined in Experiment 1. After crossing the two lines, the offspring

were genotyped using the primers listed in Table 1, and only Cre+/Brainbow+ genotypes were used. These lines have already been established, and PCR-genotyping is shown in Figure 19. Mice were euthanized using CO_2 seven days after the final injection. The brain was immediately dissected and immersion-fixed in 4% paraformaldehyde.

Primer	Forward Sequence	Reverse Sequence
iCre	5'- GCT GAG AAA GAA AAT TAC ATC -3'	5'- TGG CTT GCA GGT ACA GGA GG -3'
Control iCre	5'- CAA ATC TTG CTT GTC TGG RG -3'	5'- GTC AGT CGA GTG CAC AGT TT -3'
Brainbow	5'- CCA CCT GAT CTG CAA CTT GA -3'	5'- TGC TAG GGA GGT CGC AGT AT -3'
Control Brainbow	5'- CTA GGC CAC AGA ATT GAA AGA TCT-3'	5'- GTA GGT GGA AAT TCT AGC ATC ATC C -3'

Table 3: Primer sequences used in PCR-genotyping.

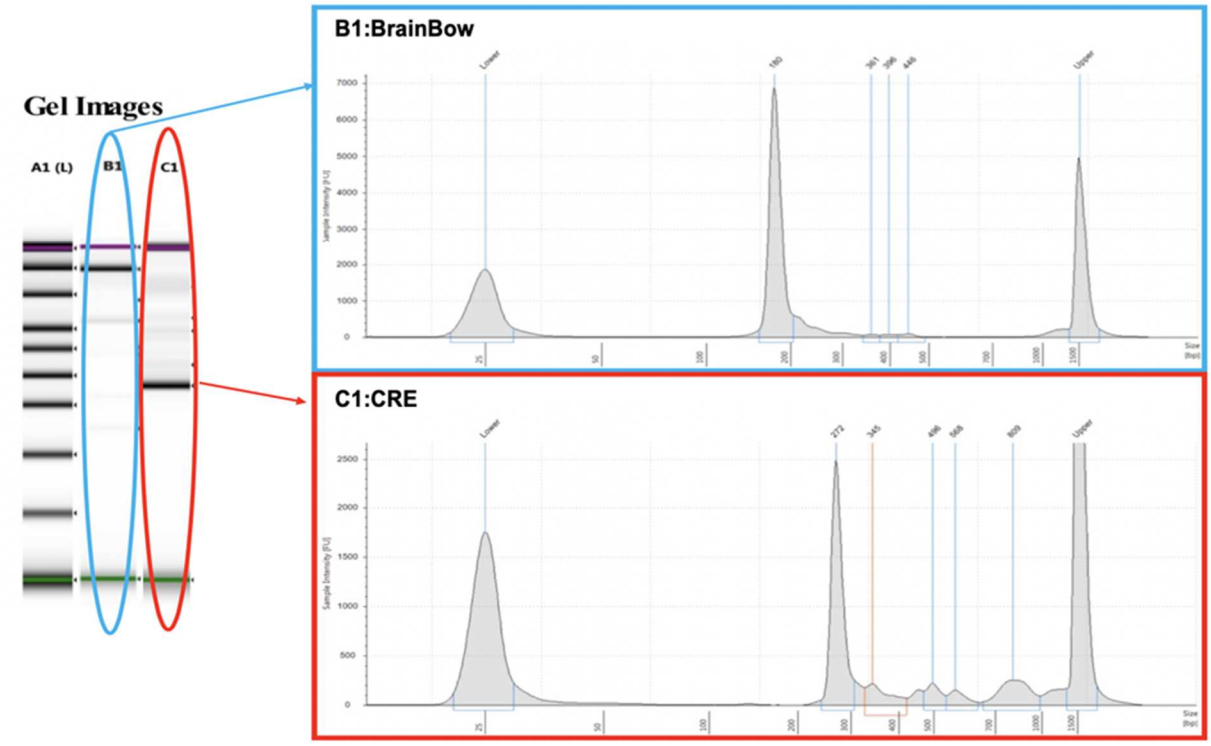

Figure 19: Tapestation results from PCR of an iCre+/Brainbow 3.2+ mouse showing DNA peaks at 180 (Brainbow) and 272 (iCre).

Immunohistochemistry*:*

To verify the expression of the Brainbow transgene, sections were rinsed in PBS and blocked to reduce background staining, followed by incubation for 2-3 days in primary antibody solution and incubated for 90 minutes in secondary antibody solution. Once completed, sections were mounted onto gelatin/chromium-subbed slides, allowed to air-dry, and then cover-slipped using Prolong Gold antifade-reagent with DAPI (Life Technologies).

Primary: Sections were rinsed with PBS and placed into microcentrifuge tubes containing a primary antibody solution of 2% NDS, 0.3% Triton X-100 (TX), and rabbit anti-PhiYFP IgG (1:500). Sections incubated for two days at 4°C.

Secondary: Sections were first rinsed 3 times in PBS solution for 10 minutes per rinse. Once rinsed, sections were incubated in a secondary antibody solution containing 2% NDS, and Cy3-conjugated donkey anti-rabbit IgG (1:200) for 90 minutes on a rotator at room temperature.

Imaging:

High power confocal images were acquired using a Leica confocal microscope system, with a 63x oil immersion objective. Z-series of 60-70 stacks were obtained at a 1032x1032-pixel resolution.

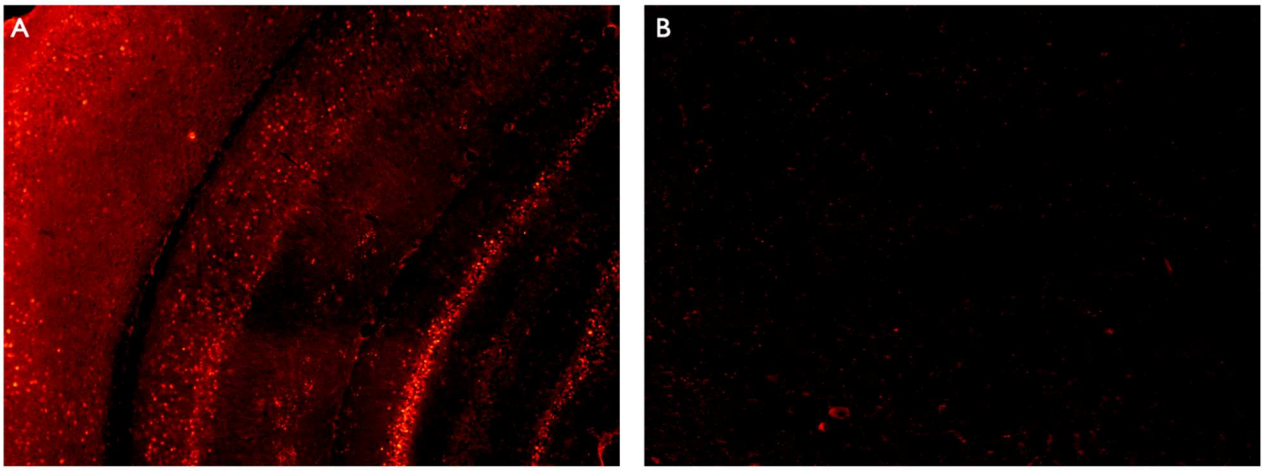

Figure 20: phi-YFP immunohistochemistry (used to verify the expression of the Brainbow transgene) in the forebrain of a Brainbow 3.2 mouse (A) and a non-carrier mouse (B).

Results: As shown in Figure 19 and confirmed by IHC in Figure 20, we successfully produced a transgenic iCre+/Brainbow 3.2+ mouse. In the next section, fluorescent signals in tissue samples were amplified and imaged for analysis.

Experiment 2.2: Signal Amplification and Imaging

Purpose: The endogenous fluorescent level in transgenic models tends to be weak and signal amplification with IHC is a common practice when working with endogenously fluorescent tissues. In this portion of Experiment 2, the fluorescent signal of iCre+/Brainbow 3.2+ tissue was amplified, and z-stack images obtained with the Leica SP8 Resonant Scanning Confocal microscope.

Immunohistochemistry:

Primary: Sections were rinsed with PBS, incubated in 2% NDS, 0.3% Triton X-100 (TX), and rabbit anti-GFP IgG, guinea pig anti-RFP IgG, and rat anti-mTFP IgG (1:500, all). Sections incubated for two days at 4°C.

Secondary: Sections were first rinsed 3 times in PBS solution for 10 minutes per rinse. Once rinsed, sections were incubated in a secondary antibody solution containing 2% NDS, and Alexa Fluor 488-conjugated donkey anti-rabbit IgG (1:1000), Alexa Fluor 647-conjugated donkey anti-guinea pig (1:500), and Alexa 594-conjugated donkey anti-rat IgG (1:500) for 90 minutes on a rotator at room temperature (Figure 21).

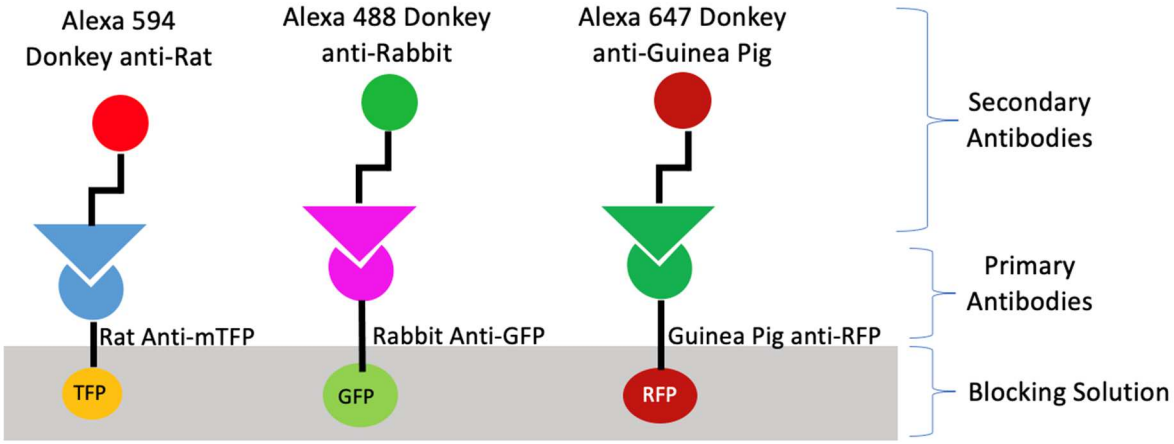

Figure 21: Schematic figure outlining the IHC set-up for labeling different Brainbow-expressing soma

Imaging:

High power confocal images were acquired using a Leica confocal microscope system, with a 63X oil immersion objective. Z-series of 60-70 stacks were obtained at a 1032x1032-pixel resolution.

Results: As outlined in Experiment 2.1, we successfully produced a transgenic mouse. However, despite the strong expression of the Brainbow 3.2 IHC results in cortical areas, expression in the DRN is not detectable (Figure 22 D-E). To be sure, iCre+/Brainbow 3.2+ tissue samples were also amplified using IHC to check for recombination and fluorescent labeling. Unfortunately, as Figure 22 A-C indicates, fluorescent labeling was not detectable

making this transgenic approach not compatible with the goals of the project. We then tested Brainbow adeno-associated viruses (AAV) that have been developed in the Sanes laboratory (Harvard University) and are commercially available from Addgene.

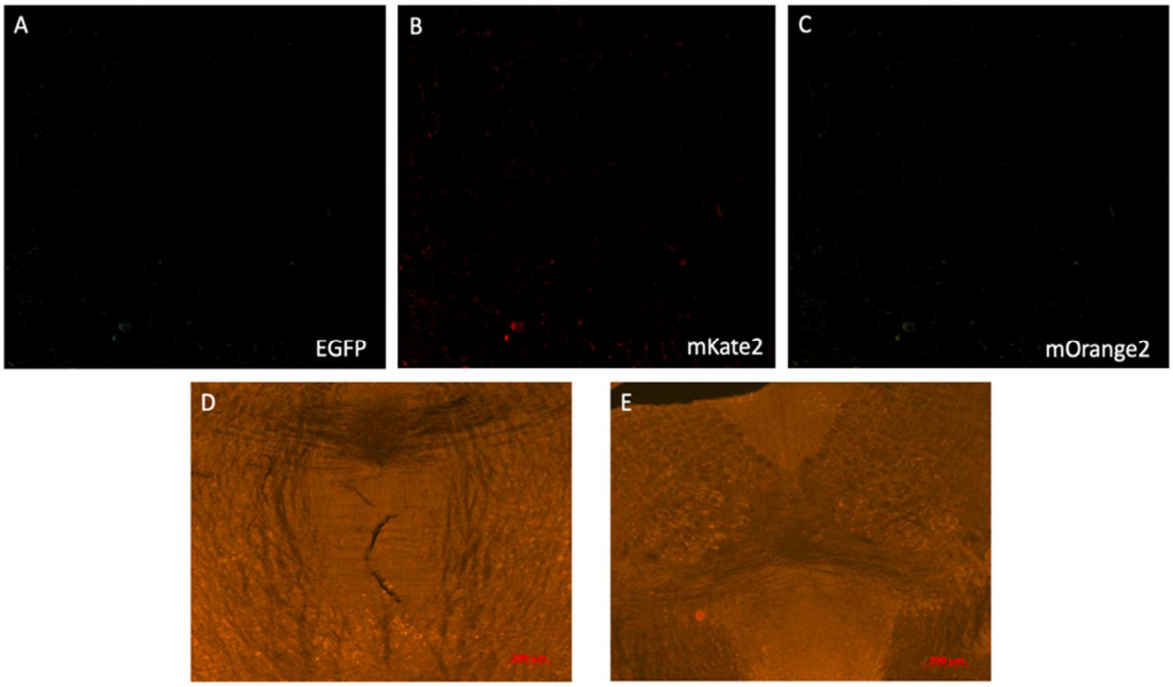

Figure 22: A-C) Fluorophore IHC in the forebrain of iCre+/Brainbow 3.2+ mice. D-E). The rostral and caudal DRN showing non-detectable levels of Brainbow 3.2 expression (visualized with IHC for PhiYFP) Scale bar = 200 µm.

Experiment 3: Creating a Model for Axon Differentiation with Brainbow AAV

Purpose: Due to the lack of expression of Brainbow 3.2 cells in the DRN, this experimental set-up takes advantage of the Brainbow-AAV by transfecting the DRN through surgical craniotomies performed on the same tamoxifen-inducible iCre line described in Experiment 1. The Brainbow AAV was generated to provide spatial and temporal control over expression and to make the method applicable to other species. Differing from the transgenic Brainbow mouse line, the AAV was designed so recombination can lead to 3

outcomes from two XFPs: XFP1, XFP2, or neither. The generation of two AAV's with two XFPs leads to a minimum of eight possible hues. Due to the AAV's ability to infect cells at high multiplicity, the true number of color expressions is greater than eight (Cai et al., 2013).

Experiment 3.1: Surgical Transfection of the Brainbow AAV

Purpose: Sterile craniotomies were performed to transfect the DRN region with the Brainbow AAVs on the same iCre mouse line outlined in Experiment 1. Post-operative care was provided for one week following surgeries before five days of tamoxifen injections were given for induction.

Animals: 18-week-old (STOCK Tg(Tph2-icre/ERT2)6Gloss/J) were used for this experiment to ensure mice were at least of adult age but not aging at the time of tissue collection (~25 weeks).

Surgery:

Stereotaxic AAV Injections: Adult mice (3-4 months) were first placed under anesthesia using an intraperitoneal injection of 0.3 mL of ketamine (200mg/kg) and xylazine (20mg/kg) cocktail. The mouse was weighed and placed onto a mouse stereotaxic apparatus. Anesthesia was maintained with (1-3%) isoflurane, and temperature was monitored and maintained at 37°C using a closed loop rectal probe/heating pad system. Once all pain responses become undetectable, the head was stabilized on the stereotaxic, and subcutaneous injections were given for pain management of 30 µl lidocaine (1:10 dilution) into the incision area of the scalp and 10 µl meloxicam (5mg/mL) into the flank. A sterile field was established, and the skull exposed using a midline incision before a small hole was made with a surgical

drill directly dorsal to the targeted brain region (DRN), based on coordinates from Paxinos et al. (2019). Then, 2.0 µl of Brainbow AAV (1.5 x 1012 vg/mL, Addgene) was slowly injected into the DRN using a Hamilton micro-syringe over 5 minutes and the needle was slowly retracted. Following surgery, the mouse was removed from the stereotaxic apparatus and closely monitored until ambulatory before transfer back into its home cage.

Post-Operative Care: Mice were visually examined at the end of the day of surgery, and at least once a day for the next four days. During examination, mice were assessed for symptoms of persistent pain (e.g., depressed, or lethargic behavior) and for the condition of the surgical wound (clean versus showing signs of dehiscence or infection). Mice were provided with analgesic of Meloxicam at appropriate intervals (at least every 24 hours) for the first 48 hours after surgery, or if assessed as being in pain, and/or at the recommendation of the attending veterinarian. Detailed post-operative records were kept as mandated by the IACUC. Mice were provided with seven days of recovery time before beginning TMX injections for Cre induction using the same methods as outlined in Experiment 1.1.

Experiment 3.2: Signal Amplification and Imaging

Purpose: The endogenous fluorescent level in transgenic models tends to be weak and signal amplification with IHC is a common practice when working with endogenously fluorescent tissues. In this portion of Experiment 3, fluorescent signal of iCre+/Brainbow AAV tissue was amplified, and z-stack images obtained with a Leica SP8 Resonant Scanning Confocal microscope.

Immunohistochemistry:

Primary: Sections were rinsed with PBS, then placed into microcentrifuge tubes containing a primary antibody solution of 2% NDS, 0.3% Triton X-100 (TX), and rabbit anti-GFP IgG, guinea pig anti-RFP IgG, and rat anti-mTFP IgG (1:500, all). Sections incubated for two days at 4°C.

Secondary: Sections were first rinsed 3 times in PBS solution for 10 minutes per rinse. Once rinsed, sections were incubated in a secondary antibody solution containing 2% NDS, and Alexa Fluor 488-conjugated donkey anti-rabbit IgG (1:1000), Alexa Fluor 647-conjugated donkey anti-guinea pig (1:500), and Alexa 594-conjugated donkey anti-rat IgG (1:500) for 90 minutes on a rotator at room temperature (Figure 21).

Imaging:

High power confocal images were acquired using a Leica confocal microscope system, with a 63x oil immersion objective. Z-series of 60-70 stacks were obtained at a 1032x1032-pixel resolution.

Results: By surgically transfecting the DRN with the Brainbow AAV, a transgenic model was successfully created. Three separate channels are used for imaging (Blue, Green, Red; Figure 23 A-C), and the combination of these channels (Figure 23, D-F) results in the individual colors of somata in the DRN (Figures 23-26).

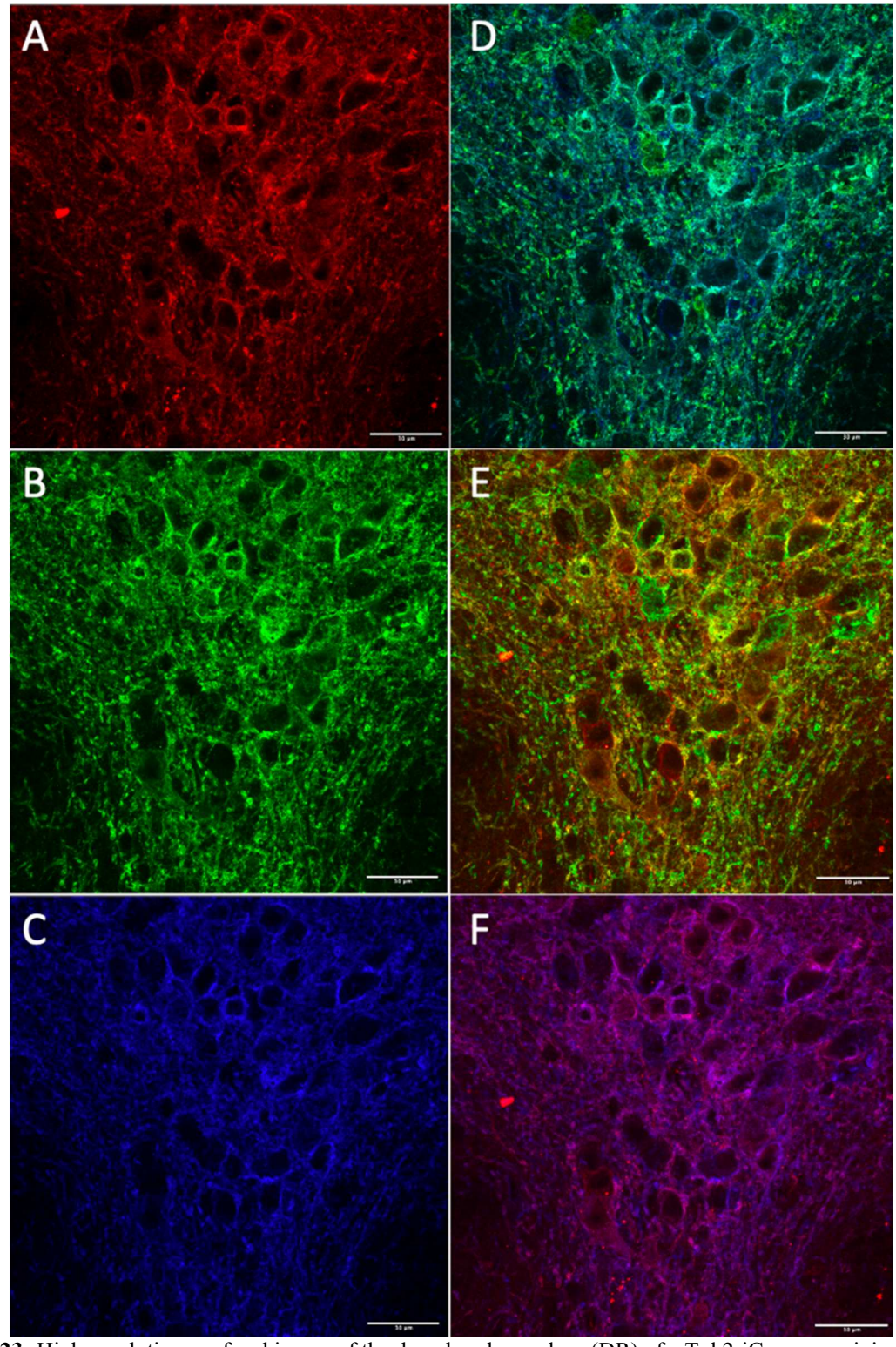

Figure 23: High-resolution confocal image of the dorsal raphe nucleus (DR) of a Tph2-iCre mouse injected with the AAV-packaged Brainbow construct, with three fluorophores: Alexa Fluor 647 (pseudocolored red, on TagRFP) (A), Alexa Fluor 488 (pseudocolored green, on GFP) (B), Alexa Fluor 594 (pseudocolored blue, on mTFP) (C). D) Combination of Green and Blue channels. E) Combination of Green and Red channels. F) Combination of Red and Blue channels.

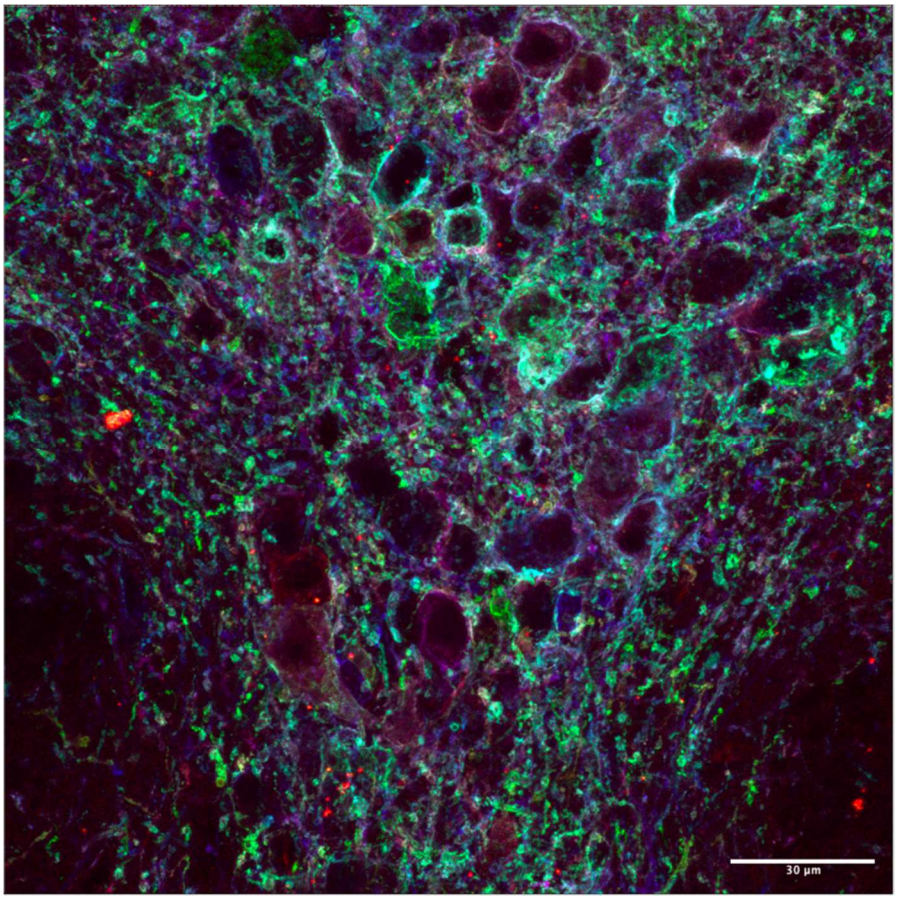

Figure 24: Serotonergic neurons in the DRN of a Cre+/Brainbow AAV mouse. This image is a 2D projection of a confocal z-stack with 68 optical sections. Alexa Fluor 647 (pseudocolored red, on TagRFP), Alexa Fluor 488 (pseudocolored green, on GFP), Alexa Fluor 594 (pseudocolored blue, on mTFP).

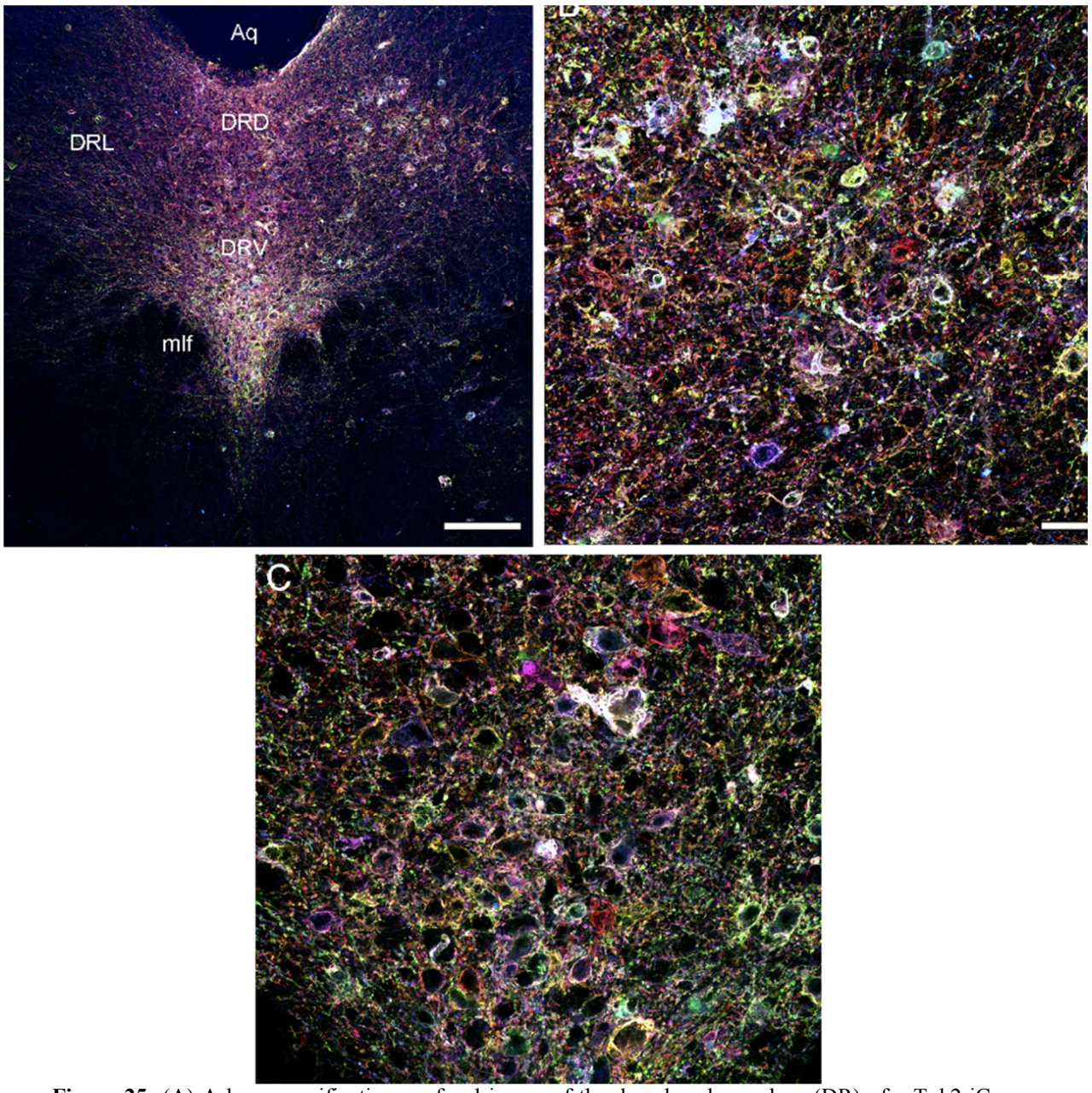

Figure 25: (A) A low-magnification confocal image of the dorsal raphe nucleus (DR) of a Tph2-iCre mouse injected with the AAV-packaged Brainbow construct, with three fluorophores: Alexa Fluor 488 (pseudocolored green, on GFP), Alexa Fluor 594 (pseudocolored blue, on mTFP), Alexa Fluor 647 (pseudocolored red, on TagRFP). (B) A high-resolution image of the lateral DR (DRL). (C) A high-magnification image of the ventromedial DR (DRV). Aq, aqueduct; mlf, medial longitudinal fasciculus. Scale bars = 150 μm (A), 30 μm (B&C).

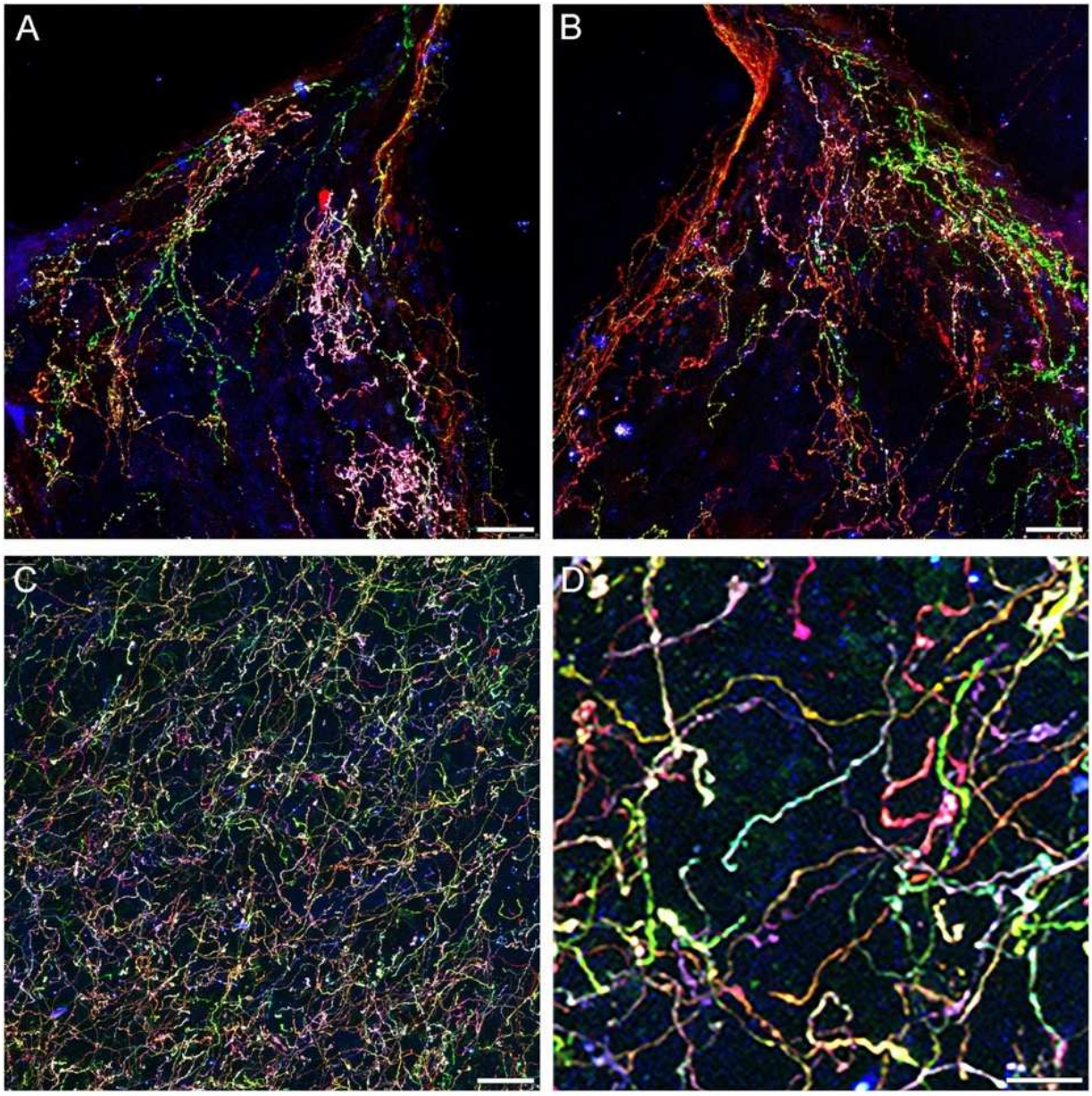

Figure 26: (A&B) Confocal images of the two habenulas in the same a Tph2-iCre mouse injected with the AAV-packaged Brainbow construct. (C) A confocal image of the basolateral amygdala of a Tph2-iCre mouse injected with the AAV-packaged Brainbow construct. (D) A digitally enlarged area of (C). Three fluorophores were used: Alexa Fluor 488 (pseudocolored green, on GFP), Alexa Fluor 594 (pseudocolored blue, on mTFP), Alexa Fluor 647 (pseudocolored red, on TagRFP). Scale bars = 20 μm (A-C), 5 μm (D).

EXPERIMENT 3 RESULTS

As shown in Figures 23-26, we have been able to successfully produce a transgenic mouse and induce recombination with Brainbow labeling—giving rise to the ability for axon differentiation. This addresses the problem of differentiation, yet it does not address the challenges of imaging and tracing across longer distances.

Experiment 4: Visualization of Serotonergic Fibers in a 3D environment

Purpose: An inherent limitation of using sectioned tissue is the challenges around recreating the brain's natural 3D environment from the thin sections of tissue required for standard microscopy imaging. Precise sectioning and imaging alignment are needed to reconstruct larger volumes, however since individual sections are processed separately, tissue distortions may occur, further limiting the ability to recreate the natural environment. A challenge seen in the previous outlined experiments is despite the fact that superior fluorescent labeling was used, due to the innate random behavior of serotonergic axons and the thin sections required for imaging, long traces were difficult to obtain as fibers would quickly escape the depth of the section. The goal of this experiment is to address this problem by keeping the original 3D tissue volume intact by employing tissue clearing methods (outlined in detail in Chapter 3). A recent improvement in clearing methods has been achieved by Ueda and colleagues, called CUBIC (Clear, Unobstructed Brain/Body Imaging Cocktails; Mano et al., 2018). CUBIC is a method that is gentle on biological tissue and causes limited shrinkage or expansion of tissue while preserving the fluorescent signals. Another advantage of CUBIC over other clearing methods is that it is able to remove heme pigments from samples, resulting in a more complete clearing and an overall improved RI (Mano et al., 2018). Once tissue has been

cleared, it can be imaged without sectioning using light-sheet microscopy. By combining tissue clearing with our advanced fluorescent mouse models, this approach can provide unprecedented information about the trajectories and dynamics of individual serotonergic fibers, across a spectrum of spatial scales and conditions. For instance, a brain region with higher fiber density could simply have more fibers occupying this space, or in theory, the elevated density can be produced by the same number of fibers whose trajectories show an altered stochastic dynamic (to meet the requirements of the region).

Experiment 4.1: Tissue Clearing

Purpose: The overall clarity of cleared tissue is dependent upon methods/regents used as well as clearing times. Tissue clearing timeframes differ as well based on tissue size and type. Therefore, in this experiment, the process and optimal timeframe to clear whole mouse brain samples was tested.

Animals: Adult iCre+/tdTomato+ mice were used for this experiment.

Tissue Clearing: Mice were euthanized using CO_2 and anesthesia was verified using eye-blink, toe and tail-pinch response methods with the brain dissected and fixed overnight in 4% paraformaldehyde at 4°C. Following fixation, brain samples were rinsed in PBS for 24 hours and pre-treated in 50% CUBIC-L + PBS solution in a water bath at 37°C overnight. Next, brain samples were incubated in 100% CUBIC-L solution in a water bath at 37°C, while replacing the solution every 2 days until clarity is reached. Once cleared, tissue is rinsed in PBS for 24 hours and then can optionally have immunohistochemistry performed on the tissue before completing the clearing process by placing the tissue into a RI matching solution.

Verification of clarity: Multiple factors can influence the overall transparency of a sample and thereby, how it reacts in a RI matched solution. Factors such as regents used to clear the tissue, overall protocol, fixation, dehydration, as well as incubation times and temperatures can all influence the overall transparency thus when optimizing a protocol, it is important to evaluate the outcome using a metric for transparency (Weiss et al., 2021). A few methods can be used to evaluate the tissue clarity, first is volumetric imaging—a series of fluorescent images from increasing depth into the tissue where change of signal to noise ratio can be analyzed. Another method that can be used to assess tissue transparency is to image tissue overlaid on text or grid pattern to see if the text is readable throughout tissue or if line sizes or text distortions occur. In the absence of grid or imaging data, the final and simplest way to assess the tissue is to visually examine it for the following:

- Ability to see through the sample.
- Check for a glassy appearance of the tissue in RI matched solution which can indication bulk RI matching is off or incomplete.
- If the surface details of the sample are not easily discernible, then the RI match was likely successful.

For this experiment, text/grid analysis was used to check for transparency of tissue with printed size 18 font used for larger (whole brain) samples, printed size 12 font used for smaller blocks of tissue (e.g., the whole brainstem), and size 8 font used for thin, (40 μm thick) tissue sections. Improving light penetration for imaging depth does not necessarily mean that the entire tissue will be perfectly transparent—in fact, it is often not possible in larger tissue samples without extended protocol durations or tissue damage. Another

important factor to consider is that the remaining proteins in the tissue may still yield a slight yellow/brownish tint to the tissue. This does not necessarily inhibit imaging and may be beneficial as it represents good protein retention (Weiss et al., 2021).

Results: The major limitations in tissue clearing are long clearing times and limits in clearing penetration depth (in our tests, brains remained opaque at the center even after a month of clearing). Despite this challenge, brain tissue samples were successfully rendered transparent (Figure 27). We next asked if fluorescent labeling can be successfully achieved in cleared tissue.

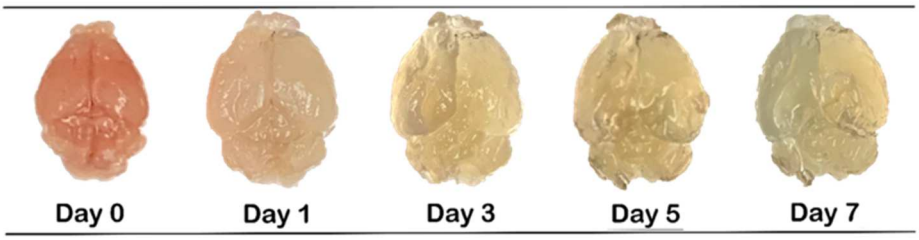

Figure 27: A sequence of images of a mouse brain at different times during the CUBIC tissue clearing process.

Experiment 4.2: Testing Immunohistochemistry on Cleared Tissue

Purpose: To test compatibility of IHC with clearing methods, IHC targeting serotonin (a method we have used previously with success), was performed on cleared tissue.

Immunohistochemistry:

Primary: Sections were rinsed with PBS and placed into microcentrifuge tubes containing a primary antibody solution of 2% NDS, 0.3% Triton X-100 (TX), and goat anti-5-HT IgG (ImmunoStar 1:500). Sections incubated for two days at 4°C.

Secondary: Sections were first rinsed 3 times in PBS solution for 10 minutes per rinse. Once rinsed, sections incubated in a secondary antibody solution containing 2%

NDS, and Cy3-conjugated donkey anti-goat IgG (1:200) for 90 minutes on a rotator at room temperature.

Imaging: High power confocal images were acquired using a Leica confocal microscope system, with a 63x oil immersion objective. Z-series of 60-70 stacks were obtained at a 1032x1032-pixel resolution.

Results: Despite previous success with IHC protocols targeting 5-HT, this method appears to be incompatible with cleared tissues (Figure 28B). These results were perplexing since a recent publication by Ueda and colleagues demonstrates the compatibility of this clearing method with IHC techniques (Kim et al., 2018). To improve this approach, we first performed IHC against different (non-serotonin) epitopes. As shown in Figure 29, we were able to obtain results utilizing these techniques. Therefore, we next attempted to label serotonin fibers by using a different marker, SERT. As shown in Figure 28C, we were able to produce a strong signal in cleared tissue and hypothesize that smaller molecules, such as serotonin, could be removed during the clearing process. Future studies using this method should consider this factor when selecting IHC targets.

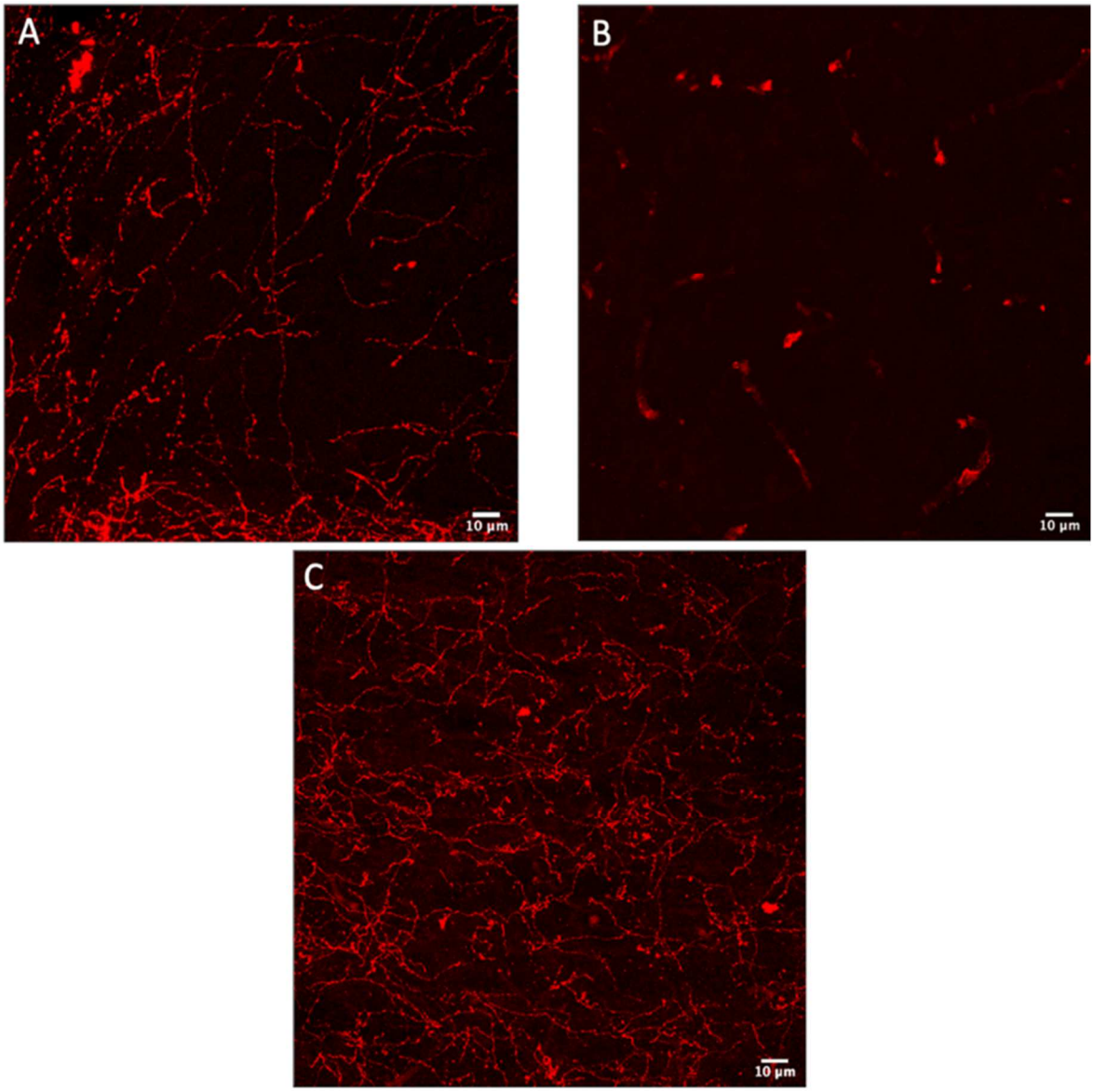

Figure 28: Images of serotonergic fibers using immunohistochemistry. A) Serotonergic fibers labeled with anti-5-HT in a section of uncleared mouse cortex. B) Serotonergic fibers labeled with anti-5-HT in a section of cleared mouse cortex. C) Serotonergic fibers labeled with anti-SERT in a section of cleared mouse cortex.

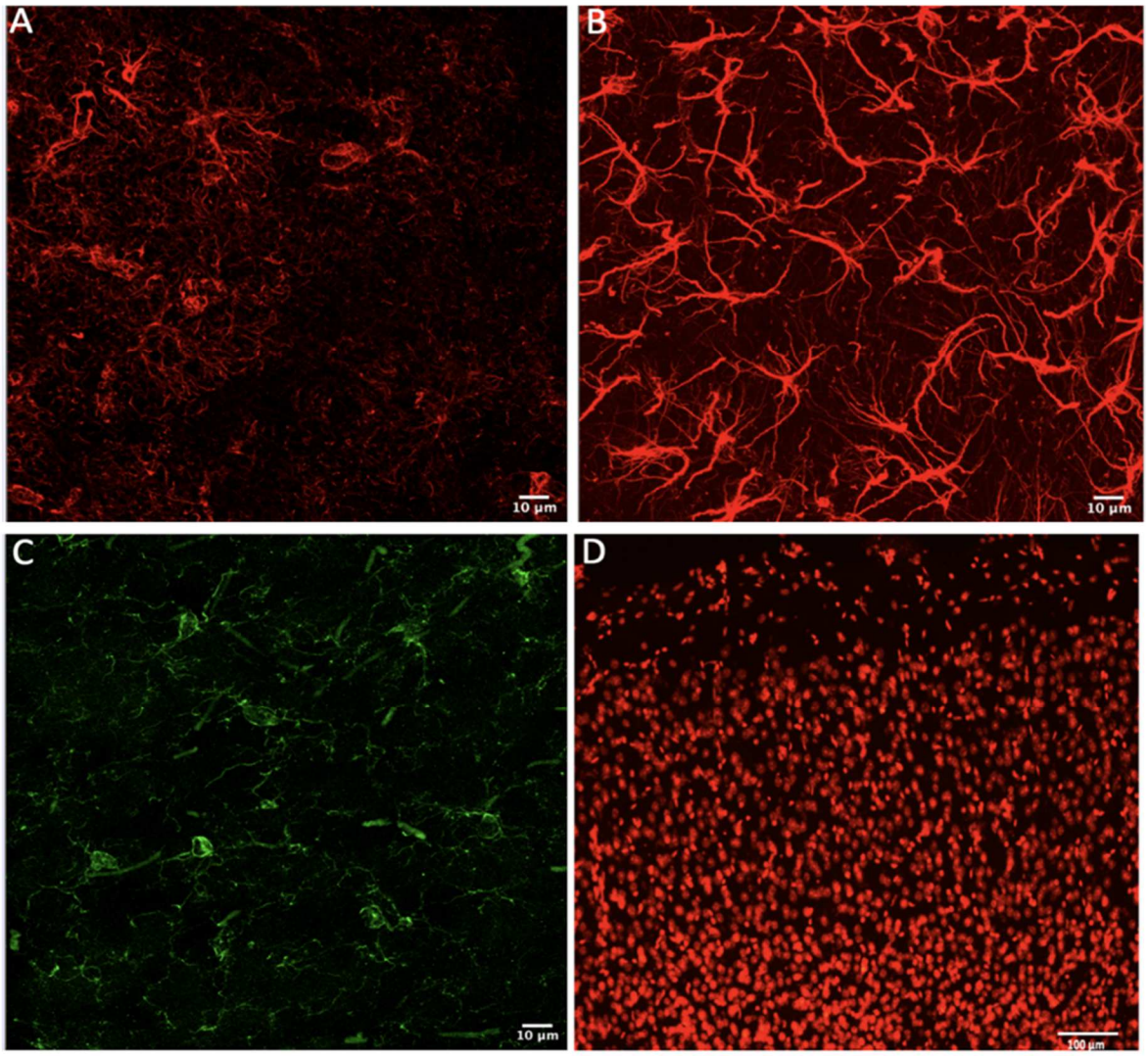

Figure 29: Immunohistochemistry of CUBIC cleared brain sections in the mouse cortex. A) Protoplasmic astrocytes labeled with anti-GFAP. B) Fibrous astrocytes labeled with anti-GFAP. C) Microglia labeled with anti-Iba1. D) Cell bodies labeled with propidium iodide. Scale bars = 10 µm (A-C) and 100 µm (D).

Experiment 4.3: Light-sheet Imaging

Purpose: After successfully clearing and fluorescently labeling cleared tissue, the next step is to image the tissue for tracing and analysis.

Ex. 4.3a Light-sheet Troubleshooting: Multiple challenges arose before a successful imaging session was achieved and a stable protocol established for imaging cleared tissue. The challenges faced and steps taken to overcome these challenges are outlined here.

Refractive Index Matching: During the first light-sheet imaging attempt, we were not able to bring the tissue into focus due to a mismatch between the RI produced by CUBIC and the RI requirements of the Zeiss Z.1 light-sheet microscope (the chamber windows support a RI=1.45). These windows can only be adjusted up to RI=1.49, and unfortunately, the RI solution that was part of the CUBIC protocol produced a RI of 1.54. This led to contacting the Principal Investigator of the group that created CUBIC, Dr. Hiroki Ueda, who suggested using a cocktail they had previous developed, *scale*CUBIC (RI= 1.49). The new cocktail was not commercially available and had to be produced in the lab which led to a high number of bubbles (which can obstruct view using the light-sheet microscope), and only lasted around 2 weeks before deterioration with an intense odor (as the cocktail contains urea). Finally, after researching commercially available solutions, a different RI solution was found with a compatible RI—Easy Index (LifeCanvas Technologies; RI=1.45) which was used for the final tissue clearing protocol.

Tissue Mounting and Imaging: When using a light-sheet microscope, special care needs to be taken when preparing samples as these systems operate differently than most standard microscopes. Samples are submerged in a chamber that is filled with the same RI solution used in the RI matching step of the tissue clearing protocol. Because of this, tissue either has to be embedded in agarose gel in a 1cc syringe, glued to a syringe, or a special stage needs to be purchased to image larger tissue samples.

To create an agarose gel for imbedding, the powder must be dissolved in the same RI solutions, so a RI mismatch does not occur and obstruct imaging. These solutions are generally highly viscous and sticky, making dissolving the agarose powder in them difficult to achieve. After careful testing, we found that in order to obtain proper gelling without bubbles, the powder + RI solution must first be placed in a water bath overnight, followed by mixing the solution on a vortexer to remove crystallizations, then placed again in the water bath overnight. However, this still only allows for smaller tissue samples that can fit within the 1cc syringe to be imaged. Since the ultimate goal is to image the entire brain, not small pieces, we next attempted to superglue whole brains onto capillary tubes for imaging. However, with the tissue immersion requirement for light-sheet imaging, this method was unstable (samples fell off during the imaging process). Therefore, smaller pieces of tissue that can fit within the syringe were used in the final protocol.

Results: From these problem-solving steps, we were able to produce the following protocol (Figure 30) for imaging transparent tissue samples with the light-sheet microscope.

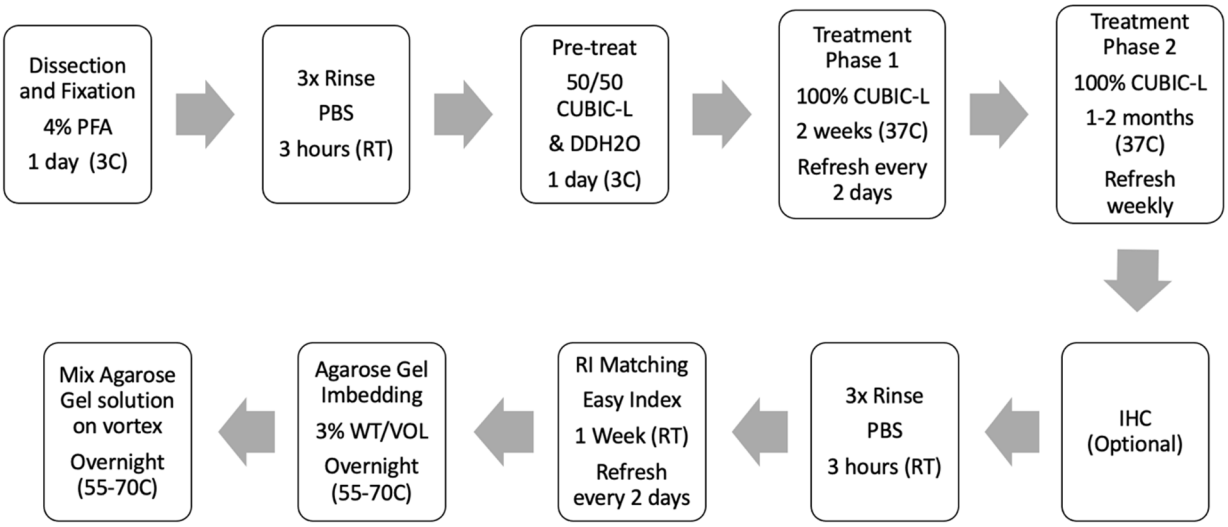

Figure 30: Protocol for tissue clearing and embedding of transparent tissue samples for lightsheet microscopy.

Ex. 4.3b Imaging and Trailmap: Due to the size and number of serotonergic fibers contained in these images, tracing was completed using a machine-learning system, TrailMap (Friedmann et al., 2020). This system uses a convolutional neural network based on the 3D U-Net architecture. The system is designed for a lower resolution (typically used in light-sheet microscopy), but we adapted it for our high-resolution images.

Animals*:* Adult Cre+/tdTomato+ mice (Experiment 1.1) were used for this experiment.

Imaging: Z-stack images were obtained using a Zeiss Z.1 light-sheet microscope with a 20x CLARITY objective compatible with the RI used in this study (Our laboratory has recently purchased this objective specifically for this study). Image samples were gathered from the primary somatosensory cortex, and basal nuclei.

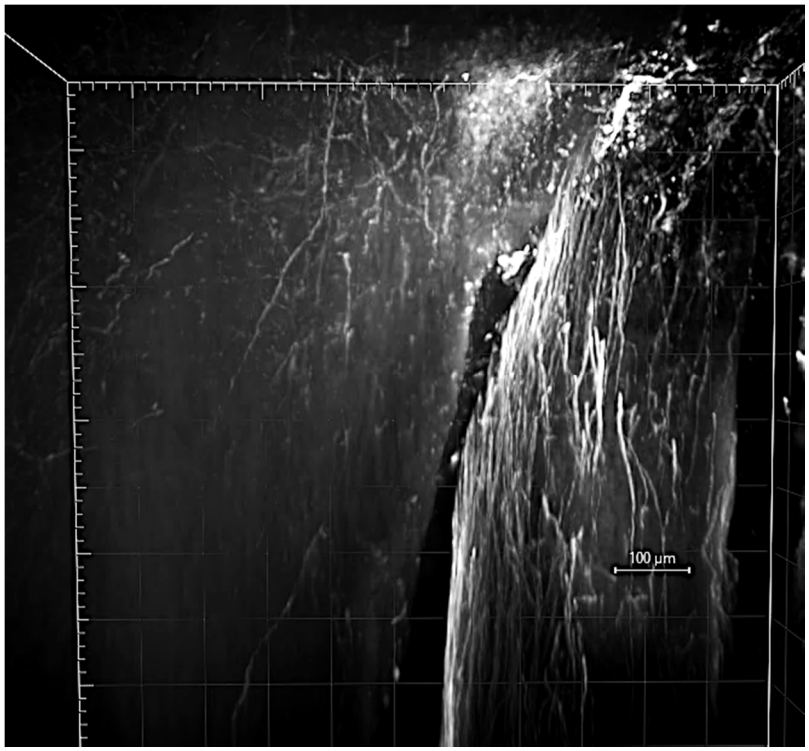

Figure 31: 3D image of serotonergic fibers in the caudate-putamen region of a iCre+/tdTomato+ mouse enhanced with GFP IHC. Scale bar = 100 µm.

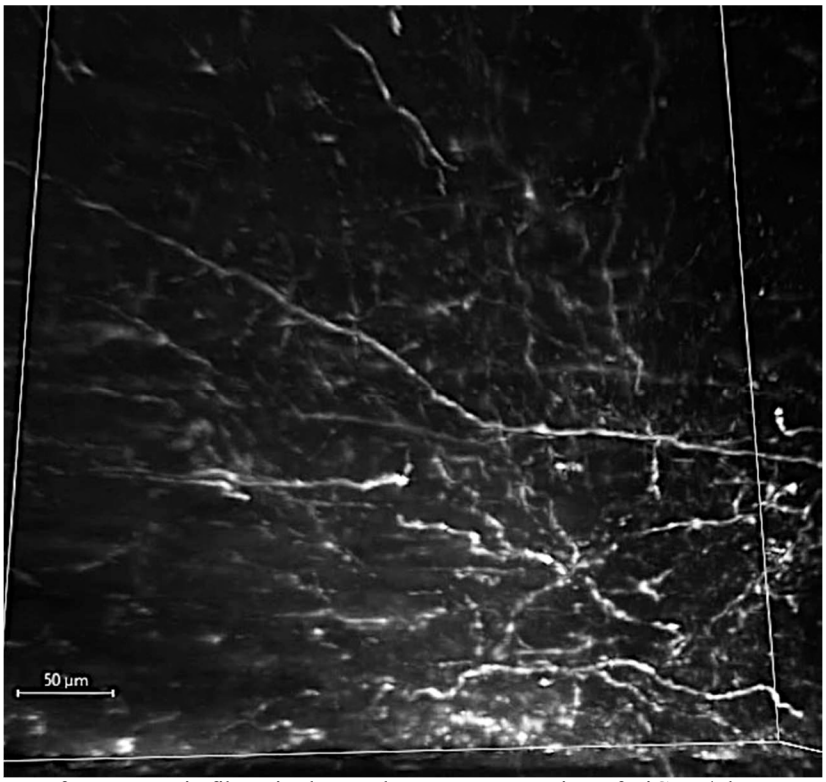

Figure 32: 3D image of serotonergic fibers in the caudate-putamen region of a iCre+/tdTomato+ mouse enhanced with GFP IHC. Scale bar = 50 µm

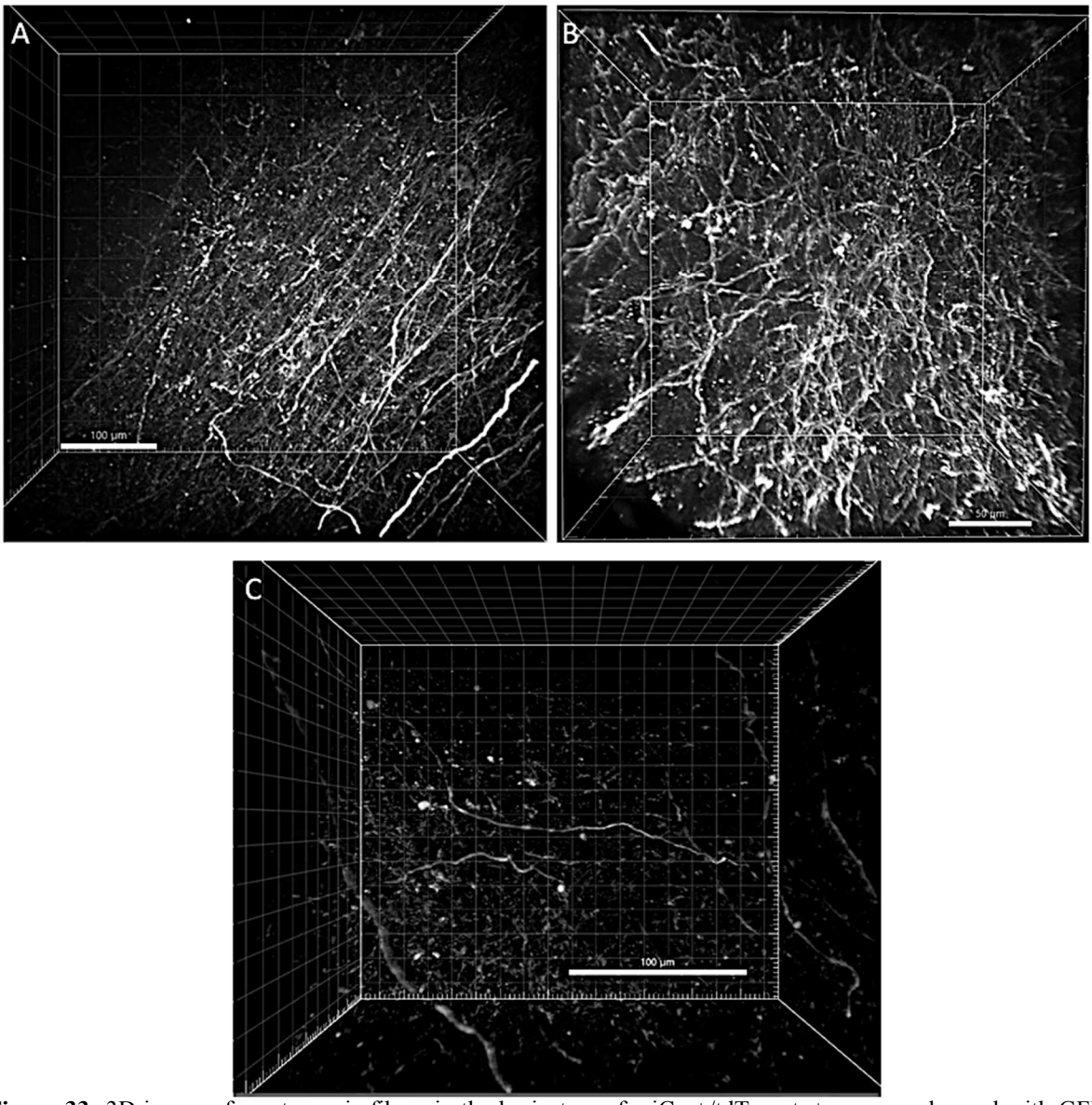

Figure 33: 3D image of serotonergic fibers in the brainstem of a iCre+/tdTomato+ mouse enhanced with GFP IHC. Scale bar (A) = 100 µm, (B) 50 µm, (C) 100 µm.

Results: Tissue clearing presents several challenges: from long clearing times (in our tests, brains remained opaque at the center after up to a month of clearing), to RI matching solution incompatibility, to preparation and mounting of the tissue for imaging. Despite these challenges, we have successfully obtained the first high-resolution images of serotonergic fibers using the light-sheet microscope (Figures 31-33).

Despite our ability to obtain results using this method, performance of IHC on cleared tissue is not ideal due to limitations with penetration depth without sectioning. Use of a transgenic mouse model with strong endogenous fluorescent labeling could solve these issues and will be explored in the future.

CHAPTER 5: DISCUSSION

The main goal for this research was to design methods for studying individual monoaminergic fiber behaviors in the brain. This effort began by using a single-color fluorescent mouse model for fiber visualization. An inducible Cre mouse model (iCre+/TdTomato+) under the Tph2 promoter (for serotonin) was established and verified, the fluorescent signal amplified, and fibers automatically traced with a novel algorithm. The obtained κ values were around 20-40, at the sampling step of 1.5 μm. The current (proof-of-principle) region set is small, but it can now be easily expanded to any brain region.

This progress is important, but the single-color mouse model is not ideal for analysis of individual fiber behavior as errors can still occur in the automatic tracing algorithm, even in areas with moderate fiber density. This requires close monitoring of the results and manual adjustments to traces–overall limiting the ability to study fiber behavior in high-density regions. These challenges necessitate the development of more advanced experimental approaches.

To address the problem of fiber differentiation, we next sought to establish a transgenic mouse model by utilizing the Brainbow 3.2 mouse line that endows neurons with around 100 different colors through random recombination of four unique fluorophores. An inducible Cre mouse line (under the Tph2 promoter) was successfully crossed with the

mouse line carrying the Brainbow 3.2 transgene and genetically verified. Unfortunately, serotonergic fibers could not be visualized with this approach due to an absence of Brainbow expression in an essential region for this research, the brainstem (including the raphe nuclei). Although the Brainbow 3.2 line was not tested with other monoaminergic Cre lines, it is expected that these would encounter a similar problem due to the overall lack of Brainbow 3.2 expression in cells within the brainstem region, where the somata of other monoaminergic systems are located.

Due to the absence of Brainbow expression, the next experiment pursued using the Brainbow AAV (which allows one to transfect the gene into regions of interest) as an alternative method toward obtaining separation of fibers. The DR region of an iCre mouse was transfected with the Brainbow AAV, creating the transgenic model that provides the differentiation required for more detailed analysis of the axons. Following transfection, fluorescent signal was amplified, and a model was finally uncovered that produces excellent separation of fibers, allowing for highly advanced analysis of individual fiber trajectories within monoaminergic systems.

With the ability to differentiate axons at our disposal, the final challenge to overcome—and the main goal of the final experiment—is imaging axons across larger distances without physically disrupting the brain's natural 3D space. Imaging tissue while maintaining the 3D space can be completed with the performance of tissue clearing processes which break down lipid rafts, remove endogenous pigments and homogenize the RI of the tissue. Once the tissue is rendered transparent, it can then be imaged without sectioning using light-sheet microscopy. First, clearing methods were tested by clearing thin sections of tissue to assess the efficacy of immunostaining and found that IHC can be used on cleared tissue,

albeit, with careful consideration of targets as small molecules (such as 5-HT) may be removed during the clearing process. Next, these clearing methods were used in an endogenously fluorescent mouse model to obtain images of axons across the brain. Following extensive testing and troubleshooting various issues with the tissue clearing process (outlined in section 4.3a), a reliable protocol for preparing and imaging cleared tissue was developed and light-sheet images of serotonergic fibers were obtained for future analyses with machine learning-based segmentation methods (e.g., TrailMap).

In summary, we have developed an advanced tool kit for studying the monoaminergic system that may finally bring the hidden intricacies of this system into the light with an iCre/Brainbow AAV model that bestows the ability of fiber differentiation along with light-sheet microscopy methods for studying axons across different regions of the brain. There are two additional directions for this line of research and many additional applications that can be explored in the near future. In the first direction, the iCre/Brainbow AAV model can be combined with light-sheet imaging so analysis of individual axons across greater distances can be achieved while preserving the natural 3D space. The second furute direction is for improvements and alternatives in automatic tracing methods to be explored. For example, a frequent challenge for the algorithm developed in this project was the prioritization of pixel brightness over current direction when tracing, which can lead to tracing errors when two fibers cross each other in close proximity. We now know, based on a large set of images and extensive testing, that the fiber brightness tends to be relatively stable throughout the imaged stack. We therefore recommend a simple improvement to the algorithm's accuracy by future including a rule that still prioritizes brightness but constrains pixel brightness possibilities to only one standard deviation from the mean brightness. Another option is to pursue machine

learning algorithms; however, it should be noted that current available artificial neural networks (ANNs), have been trained on images with a much lower resolution than those required for imaging serotonergic fibers. A novel ANN architecture that is custom-designed for objects that are both thread-like and strongly stochastic, would be particularly promising.

The true power of this work stems from how it could be applied to numerous other lines of future research. For example, this toolkit could be used to refine and improve previous studies of serotonergic systems, as it operated at the single-fiber resolution and offers unprecedented tracing capabilities. Uncovering this fine-grained information can help to unlock the causal factors that lead to altered fiber densities. One direct application for these methods is in anatomical research. Serotonergic fibers branch, as all axons, but the extent of this ramification remains largely implied (based on resultant densities) rather than directly observed. Due to the stochastic and intertwining trajectories, previous studies could not confidently separate true branches from fibers passing each other at very small distances. The ability to differentiate fibers with individual colors effectively solves this problem, even where the distance between two fibers falls below the limit of optical resolution. A related application of these methods is in the question of serotonergic fiber subtypes. The possibility of serotonergic fiber subtypes was first suggested in 1987 by Kosofsky and Molliver who proposed that they differ based on the site of their origin. Dorsal or "D" fibers were described as more abundant with homogenous and tapering shaped varicosities, while the median or "M" fibers were described as less abundant, thicker, and containing larger varicosities. Fiber subtypes have since remained an open question, including their fundamental existence, the number of subtypes, and the association with morphological and neurochemical properties (caliber, neurotransmitter co-expression, expression of transcription factors, or dynamics). A

recent publication by Huang (2019) used retrograde tracing for fiber visualization in the mouse DR and ultimately suggested the existence of 18 neuronal subtypes and 5 different fiber subtypes. So, do true fiber subtypes exist, or are fiber differences based on something else? For instance, the lack of expression of certain receptors (WNT) or changes in expression of guidance molecules can change the resulting growth and innervation patters of these fibers (Fenstermaker, 2010). Overall, the biggest limitation of this research line is its narrow scope that focused on reliably tracing individual fibers and disregarding the possibility of their behaviors based off interactions. With the potential of the Brainbow method developed in this project, we can now perform high-throughput analyses, allowing for a more holistic study into the entire fiber system, from their high-resolution individual trajectories to large-scale densities. By combining this method with other experimental manipulations, we may be able to finally have answers to a question 35 years in the making—are there true fiber subtypes? The possibilities for answers to this question are expansive, ranging from the existence of subtypes based on physical characteristics (fiber size, branching behaviors, or varicosity size), the serotonergic neurons in which they originate from, their expression levels (neurotransmitters, receptors, transcription factors), or a combination of these. Perhaps we could find fibers have no true subtype and adapt to needs of the environment in which they are innervating, or that there are no true fiber subtypes and that differing fiber morphologies ultimately random (reflecting the stochastic architecture of neural tissue). Regardless of what the future holds, this method will pave the way toward new discoveries and a better understanding of the serotonergic system.

A frequently used analytic measurement for serotonergic fibers is optic densities, or the cumulative signal density above background level in an area. This method of

measurement has been used in anatomical studies, to create distribution maps, in studies of evolutionary differences, and in research of neuropsychiatric disorders (Foote & Morrison, 1984; Vertes, 1991; Voigt & De Lima, 1991; Morin & Meyer-Bernstein, 1999; Leger et al., 2001; Lew et al., 2019; Awasthi et al., 2020; Awasthi et al., 2021). Although this method of analysis can provide some useful information, it fails to provide deeper insights such as the overall composition of the axons contributing to these density variations. We may know that the amygdala the bonobo has a higher density of serotonergic fibers than that of the chimpanzee, but why are these different? Is there a true increase in the number of fibers in that region, or do the fibers simply behave different here? What about the overall composition of the fibers in the region? Do fibers innervate the area and freely intermix with each other or are fibers from one neuronal cell dominating the area and forming possible meshworks (e.g., Figure 26)? Previous studies using traditional labeling methods have not been able to answer these questions with confidence due to the inability to differentiate fibers—but with the employment of our models, the answers to these questions are finally within reach.

When it comes to understanding specific developmental patters of serotonergic fibers, research by Maddaloni (2017) is a key article outlining specific innervation patterns as well as tracking the overall length of fibers throughout development (growth beginning at PND 14 and peaking at PND 28 while remaining largely unchanged throughout adulthood). However, this research was limited to length measurements within individual 3D image stacks as opposed to the overall length across the brain. Employment of the Brainbow AAV+/iCre+ line could be beneficial to developmental studies, but there are a couple obstacles that must be overcome before it can be applied in this way. The most challenging of these hurdles is

time. The Brainbow AAV requires surgical transfections along with tamoxifen injections for Cre induction, it may not be possible to achieve expression before PND 14 and 28. However, some groups have been successful in conducting surgical AAV transfections in pups as young as PND 1 (He et al., 2018). For instance, one group has successfully conducted viral injections of a calcium indicator, GCAMP, AAV in newborn mice by utilizing a dissecting microscope and blunt-tipped ear bars to stabilize the head. Since then, a mouse neonatal stereotaxic adaptor has also been created that may increase ease and success for these surgeries (Olivetti et al., 2020). Complete instructions for each of these proposed methods can be found in the cited articles. If the surgical transfections do not work, another possible option would be the creation of a transgenic Brainbow line that does expresses the Brainbow gene in the raphe nuclei. If this can be achieved, the total lengths of fibers in a given volume, as well as precise innervations patterns, can be studied with confidence.

Even though we may not be able to use these methods in their current state for early developmental studies, they can have an impact on other developmental experimentation such as changes in fiber growth and innervation patterns occurring due to altered expressions of guidance molecules. An example is research by Fenstermaker (2010) that has found abnormal arborizations in serotonergic fibers after PCDA was knocked out. Using the information on true branching frequency and patterns in iCre/+Brainbow AAV+ mice, we can compare this data to those in PCDA-knockout mice, causally bridging these single-fiber properties and the resultant densities of fiber meshworks.

Serotonergic fiber regrowth following TBI is another future application this method can contribute to. Research by Kajstura (2018) has found that fibers not only regrow following injury, but they also appear to grow to form a similar density to what the region

had prior to the TBI and without following the prior axonal pathways. Again, the dynamics of this process can be studied in much greater detail with the Brainbow approach.

Looking at possible differences in fiber behaviors across different psychological disorders in which serotonin has been implicated is another possible direction for this research that should be explored. However, a limitation for the methods outlined here is the inability to apply Brainbow method to human tissue samples. Nevertheless, it is important to note that even without the Brainbow extension, the other developed methods (tissue clearing, improved tracing methods, and advanced stochastic models) can still be applied to human tissue samples to glean insights into possible differences in individual fiber behavior. A couple specific psychological disorders that should be explored are MDD and ASD—which have options for using both animal models and human samples. With regard to MDD, previous research has implicated a possible decrease in serotonergic fiber densities (Austin et al., 2002). Therefore, this can be further explored in several ways: depressive-like behavior can be induced in mice (Iniguez et al., 2014; Iniguez et al., 2018; Petkovic & Chaudhury, 2022), mouse models for depression such as forebrain glucocorticoid receptor (GR) knockout mouse can be crossed with an inducible Cre mouse and then injected with the Brainbow AAV to obtain fiber differentiation, and finally human tissue samples can be obtained, and compared (using a single fluorophone) with results obtained in mouse models. performed independently of, and later, compared to analyses from the animal models. All of these approaches, taken separately, have drawbacks (e.g., mouse models may not accurately reflect human psychological disorders), but together they may achieve a reliable "triangulation" of the underlying biological deficiencies. Similar approaches can be used to study the dynamic changes induced by SSRIs.

Research with ASD is less straight-forward due to the spectrum of behaviors that are associated with the disorder. A recent publication looked at the differences of connectivity using fMRI scans and found spectrum-like variability across 16 different ASD mouse models (Zerbi et al., 2021). The developed methods can be used to achieve fiber differentiation in these models, which can again be combined with the analysis of human tissue samples from individuals diagnosed with ASD.

Importantly, these new methods do not need to be exclusive to serotonin research and can be applied to other monoaminergic systems to verify and expand on results of previous studies. For example, to study individual axon behavior of dopaminergic cells, the iCre mouse line, B6;129-Th$^{Tm1(cre/Esr1)Nat}$/J (from JAX) could be used and transfected with the Brainbow AAV. Similarly, the Cre lines of B6;129-Cckbr$^{Tm1.1(Cre)Mgmj}$/J and B6.Dbh$^{Tm3.2(Cre)Pjen}$/J (also from JAX) could be used to study adrenaline and noradrenaline, respectively.

Overall, this research will greatly improve our ability to analyze and understand the components of monoaminergic systems, by answering questions about how the dynamics of fibers change across distances, whether it is determined by the requirements of different brain regions, the local microarchitecture of brain tissue, or other factors. It may ultimately allow us to understand how this massive system becomes what it is, a vast and dense matrix in which our cognitive lives are forever embedded (Figure 34).

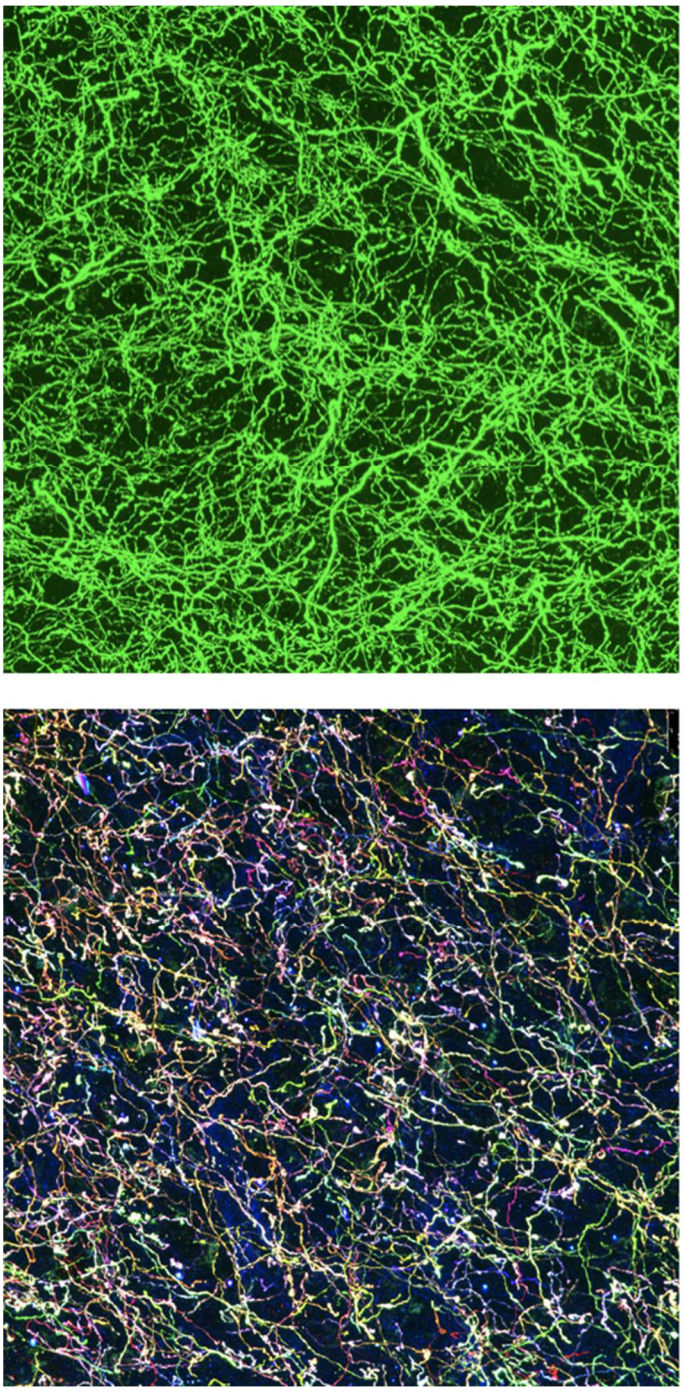

Figure 34: Confocal images comparing the BLA region of the amygdala in a (top) single-color transgenic model and (bottom) Tph2-iCre mouse injected with the AAV-packaged Brainbow construct. Three fluorophores were used in the left image: Alexa Fluor 488 (pseudocolored green, on GFP), Alexa Fluor 594 (pseudocolored blue, on mTFP), Alexa Fluor 647 (pseudocolored red, on TagRFP).

REFERENCES

Abela AR, Browne CJ, Sargin D, Prevot TD, Ji XD, Li Z, Lambe EK, Fletcher PJ (2020) Median Raphe Serotonin Neurons Promote Anxiety-like Behavior via Inputs to the Dorsal Hippocampus. *Neuropharmacology* 15(168): 107985

Austin MC, Whitehead RE, Edgar CL, Janosky JE, Lewis DA. (2002) Localized Decrease in Serotonin Transporter-Immunoreactive Axons in the Prefrontal Cortex of Depressed Subjects Committing Suicide. *Neuroscience* 114(3): 807-815

Awasthi, JR, Tamada K, Overton ETN, Takumi T. (2020) Development of Serotonergic Projections to the Suprachiasmatic Nucleus in the Mouse Brain. *Neuroscience letters*, 739, 135438.

Awasthi JR, Tamada K, Overton ETN, Takumi T. (2021) Comprehensive Topographical Map of the Serotonergic Fibers in the Male Mouse Brain. *Journal of Comparative Neurology,* 529(7), 1391–1429.

Azmitia EC, Singh JS, Whitaker-Azmitia PM. (2011) Increased Serotonin Axons (Immunoreactive to 5-HT Transporter) in Postmortem Brains from Young Autism Donors. *Neuropharmacology* 60: 1347-1354

Banasr M, Hery M, Printemps R, Daszuta A. (2004) Serotonin-Induced Increases in Adult Cell Proliferation and Neurogenesis Are Mediated Through Different and Common 5-HT Receptor Subtypes in the Dentate Gyrus and the Subventricular Zone *Neuropsychopharmacology.* 29:450–460.

Barlow R, Alsio J, Jupp B. *et al.* (2015) Markers of Serotonergic Function in the Orbitofrontal Cortex and Dorsal Raphe Nucleus Predict Individual Variation in Spatial-Discrimination Serial Reversal Learning. *Neuropsychopharmacol.* 40: 1619–1630.

Baroncelli L, Sale A, Viegi A *et al.,* (2010) Experience-Dependent Reactivation of Ocular Dominance Plasticity in the Adult Visual Cortex. *Exp Neurol* 226: 100–109.

Becker K, Jahrling N, Saghafi S, Weiler R, Dodt HU (2012) Chemical Clearing and Dehydration of GFP Expressing Mouse Brains. *PLoS ONE* 7:e33916

Benzekhroufa K, Liu B, Tang F, Teschemacher AG, Kasparov S (2009) Adenoviral Vectors for Highly Selective Gene Expression in Central Serotonergic Neurons Reveal Quantal Characteristics of Serotonin Release in the Rat Brain. *BMC Biotechnology* 3(19): 9-23

Berger M, Gray JA, Roth BL. (2009) The Expanded Biology of Serotonin. *Annu Rev Med.* 60: 355-66.

Betancur C. (2011) Etiological Heterogeneity in Autism Spectrum Disorders: More than 100 Genetic and Genomic Disorders and Still Counting. *Brain Research*. 1380: 42-77

Biagini F, Hu Y, Oksendal B, Zhang T. (2010). *Stochastic Calculus for Fractional Brownian Motion and Applications.* London: Springer.

Bockaert J, Claeysen S, Becamel C, Dumuis A, Marin P. (2006) Neuronal 5-HT Metabotropic Receptors: Fine-Tuning of Their Structure, Signaling, and Roles in Synaptic Modulation. *Cell and Tissue Research*. 326(2) 553-572.

Bockaert J, Becamel C, Chaumont-Dubel S, Claeysen S, Vandermoere F, and Marin P. (2021) Novel and Atypical Pathways for Serotonin Signaling. *Faculty Reviews*. 10:52.

Bonnin A, Levitt P. (2012) Placental Source for 5-HT that Tunes Fetal Brain Development *Neuropsychopharmacology* 37(1): 299-300

Bright FM, Byard RW, Vink R, Paterson DS. (2017) Medullary Serotonin Neuron Abnormalities in an Australian Cohort of Sudden Infant Death Syndrome. *Journal of Neuropathology and Experimental Neurology.* 76(10): 864-873

Brocard J, Warot X, Wendling O, Messaddeq N, Vonesch JL, Chambon P, Metzger D. (1997) Spatio-temporally controlled site-specific somatic mutagenesis in the mouse. Proc Natl Acad Sci. 94(26): 14559–14563.

Bunin MA, Wightman RM. (1998) Quantitative evaluation of 5-hydroxy-tryptamine (serotonin) neuronal release and uptake: an investigation of extrasynaptic transmission. *J Neurosci.*18: 4854–4860

Burri A, Hysi P, Clop A, Rahman Q, Spector TD. (2012) A Genome-Wide Association Study of Female Sexual Dysfunction. *PLoS One*. 7(4): e35041.

Cai D, Cohen K, Luo T, Lichtman J, Sanes J (2013) New Tools for the Brainbow Toolbox. *Nat Methods* 10(6): 540-547

Chen J, Condron B. (2009) *Drosophila* Serotonergic Varicosities are not Distributed in a Regular Manner. *J. Comp. Neurol.* 515 (4): 441-453

Chollet F, Tardy J, Albucher JF et al (2011) Fluoxetine for Motor Recovery After Acute Ischaemic Stroke (FLAME): a Randomised Placebo-Controlled Trial. *Lancet Neurol* 10: 123–130.

Chung K, Wallace J, Kim SY, Kalyanasundaram S, Andalman AS, Davidson TJ, Mirzabekov JJ, Zalocusky KA, Mattis J, Denisin AK, Pak S, Bernstein H, Ramakrishnan C, Grosenick L, Gradinaru V, Deisserroth K (2013) Structural and Molecular Interrogation of Intact Biological Systems. *Nature* 497:332-337

Codling EA, Plank MJ, Benhamou S. (2008) Random Walk Models in Biology. *Journal of Royal Society Interface* 5(25): 813-834.

Commons KG. (2009) Locally Collateralizing Glutamate Neurons in the Dorsal Raphe Nucleus Responsive to Substance P Contain Vesicular Glutamate Transporter 3 (VGLUT3). *J. Chem. Neuroanat.* 38, 273–281

Cook Jr EH, Arora RC, Anderson GM, Berry-Kravis EM, Yan SY, Yeoh HC, Sklena PJ, Charak DA, Leventhal BH. (1993) Platelet Serotonin Studies in Hyperserotonemic Relatives of Children with Autistic Disorder. *Life Science.* 52: 2005-2015.

Curtin PC, Medan V, Neumeister H, Bronson DR, Preuss T. (2013) The 5-HT5A Receptor Regulates Excitability in the Auditory Startle Circuit: Functional Implications for Sensorimotor Gating. *J Neurosci.* 33:10011–10020.

D'Amato RJ, Blue ME, Largent BL, Lynch DR, Ledbetter DJ, Molliver ME, et al. (1987). Ontogeny of the Serotonergic Projection to Rat Neocortex: Transient Expression of a Dense Innervation to Primary Sensory Areas. *Proc. Natl. Acad. Science.* 84, 4322–4326.

Dahlstroem A, Fuxe K. (1964) Evidence for the Existence of Monoamine-containing Neurons in the Central Nervous System Demonstration of monoamines in the Cell Bodies of Brain Stem Neurons. *Acta Physiol. Scand. Suppl.* 232, S231–S255

De Jong TR, Veening JG, Waldinger MD, Cools AR & Olivier B. (2006) Serotonin and the Neurobiology of the Ejaculatory Threshold. *Neurosci Biobehav Rev.* 30: 893–907.

Deltheil T, Guiard BP, Guilloux JP, Nicolas L, Delomenie C, Reperant C, Le Maitre E, Leroux-Nicollet I, Benmansour S, Coudore F, David DJ, Gardier AM. (2008)

Consequences of Changes in BDNF Levels on Serotonin Neurotransmission, 5-HT Transporter Expression and Function: Studies in Adult Mice Hippocampus. *Pharmacol. Biochem. Behav.* 90(2): 174-183.

Deneris E, Gaspar P. (2018) Serotonin Neuron Development: Shaping Molecular and Structural Identities. *WIREs Dev Biol.* 7(1): e301

Dias MB, Li A, Nattie E. (2008) Focal CO2 Dialysis in Raphe Obscurus does not Stimulate Ventilation but Enhances the Response to Focal CO_2 Dialysis in the Retrotrapezoid Nucleus. *J Appl Physiol.* 105: 83–90.

Donovan SL, Mamounas LA, Andrews AM, Blue ME, JS MC. (2002) GAP-43 is Critical for Normal Development of the Serotonergic Innervation in Forebrain. *J Neuroscience.* 22: 3543– 3552.

Donovan SL, Spencer WC, Kitt MM, Eastman BA, Lobur KJ, Jiao K, Silver J, Deneris ES. (2019) Lmx1b is Required at Multiple Stages to Build Expansive Serotonergic Axon Architectures. *eLife* 8:e48788

Dubert EA, Heffron DS, Mandell JW, Condron BG (2011) Serotonergic Dystrophy Induced by Excess Serotonin. *Mol Cell Neuroscience.* 44(3) 297-306.

Feldman JL, Mitchell GS, Nattie EE. (2003) Breathing: Rhythmicity, Plasticity, Chemosensitivity. *Annu Rev Neurosci.* 26: 239–266.

Fenstermaker AG, Prasad AA, Bechara A, Adolfs Y, Tissir F, Goffinet A, Zou Y Pasterkamp RJ. (2010) Wnt/Planar Cell Polarity Signaling Controls the Anterior–Posterior Organization of Monoaminergic Axons in the Brainstem. *Journal of Neuroscience* 24 30 (47) 16053-16064.

Fernandez SP, Muzerelle A, Scotto-Lomassese S, Barik J, Gruart A, Delgado-García JM, Gaspar P. (2017) Constitutive and Acquired Serotonin Deficiency Alters Memory and Hippocampal Synaptic Plasticity. *Neuropsychopharmacology.* 42(2): 512-523.

Fink LH, Anastasio NC, Fox RG, Rice KC, Moeller FG, Cunningham KA. (2015) Individual Differences in Impulsive Action Reflect Variation in the Cortical Serotonin 5-HT2A Receptor System. *Neuropsychopharmacology.* 40(8): 1957-1968.

Foote SL, Morrison JH. (1984) Postnatal Development of Laminar Innervation Patterns by Monoaminergic Fibers in Monkey (Macaca fascicularis) Primary Visual Cortex. *J Neurosci*. (11):2667-80.

Gagnon D and Parent M. (2014) Distribution of VGLUT3 in Highly Collateralized Axons from the Rat Dorsal Raphe Nucleus as Revealed by Single-Neuron Reconstructions. *PLoS One.* 9(2):e87709.

Gardier AM. (2009) Mutant Mouse Models and Antidepressant Drug Research: Focus on Serotonin and Brain-Derived Neurotrophic Factor. *Behav Pharmacol.* 20(1): 18-32.

Gardiner C. (2010). Stochastic Methods (4th ed.). Berlin: Springer-Verlag.

Goldberg J, Anderson GM, Zwaigenbaum L, Hall GB, Nahmias C, Thompson A, Szatmari P (2009) Cortical Serotonin Type-2 Receptor Density in Parents of Children with Autism Spectrum Disorders. *Journal of Autism Developmental Disorders*. 39: 97-104

Gonzalez R, Chavez-Pascacio K, Meneses A. (2013) Role of 5-HT5A Receptors in the Consolidation of Memory. *Behav Brain Res.* 252:246–251.

Gras C, Herzog E, Bellenchi GC, Bernard V, Ravassard P, Pohl M, Gasnier B, Giros B, El Mestikawy S. (2002) A Third Vesicular Glutamate Transporter Expressed by Cholinergic and Serotoninergic Neurons. *J. Neurosci.* 22, 5442–5451

Groman SM, James AS, Seu E, Crawford MA, Harpster SN, Jentsch JD. (2013) Monoamine Levels Within the Orbitofrontal Cortex and Putamen Interact to Predict Reversal Learning Performance. *Biol Psychiatry.*73: 756–762.

Gryglewski G, Lanzenberger R, Kranz GS, Cumming P. (2014) Meta-Analysis of Molecular Imaging of Serotonin Transporters in Major Depression. *Journal of Cerebral Blood Flow & Metabolism.* 34: 1096-1103

Gu H, Zou YR, Rajewsky K. (1993) Independent Control of Immunoglobulin Switch Recombination at Individual Switch Regions Evidenced Through Cre-loxP-Mediated Gene Targeting. *Cell* 73: 1155-1164.

Gu H, Marth JD, Orban PC, Mossmann H, Rajewsky K. (1994) Deletion of a DNA Polymerase Beta Gene Segment in T Cells Using Cell Type-Specific Gene Targeting. *Science* 265: 103-106.

Guidotti G, Calabrese F, Auletta F *et al.,* (2012) Developmental Influence of the Serotonin Transporter on the Expression of Npas4 and GABAergic Markers: Modulation by Antidepressant Treatment. *Neuropsychopharmacol* 37: 746–758.

Guirado R, Perez-Rando M, Sanchez-Matarredona D, Castren E, Nacher J. (2014) Chronic Fluoxetine Treatment Alters the Structure, Connectivity and Plasticity of Cortical Interneurons, *Internatl. Journal of Neuropsychopharmacol.* 17(10): 1635–1646.

Guirado R, La Terra D, Bourguignon M *et al.,* (2016) Effects of PSA Removal from NCAM on the Critical Period Plasticity Triggered by the Antidepressant Fluoxetine in the Visual Cortex. *Front Cell Neurosci.* 10: 1–9.

Hall B, Limaye A, Kulkarni AB. (2009) Overview: Generation of Gene Knockout Mice. *Curr. Protoc. Cell Biol.* 44: 19.12.1-19.12.17.

Hama H, Kurokawa H, Kawano H, Ando R, Shimogori T, Noda H, Fukami K, Sakaue-Sawano A, Miyawaki A. (2011) Scale: A Chemical Approach for Fluorescence Imaging and Reconstruction of a Transparent Mouse Brain. *Nat. Neurosci* 14: 1481-1488

Hawthorne AL, Hu H, Kundu B, Steinmetz MP, Wylie CJ, Deneris ES, Silver J. (2011) The Unusual Response of Serotonergic Neurons After CNS Injury: Lack of Axonal Dieback and Enhanced Sprouting Within the Inhibitory Environment of the Glial Scar. *J Neuroscience* 31: 5605– 5616.

He CX, Arroyo ED, Cantu DA, Goel A, Portera-Cailliau C. (2018) A Versatile method for Viral Transfection of Calcium Indicator in the Neonatal Mouse Brain. *Frontiers in neural circuits,* 12:56.

Hennessy ML, Corcoran AE, Brust RD, Chang YJ, Nattie EE, Dymecki SM. (2017) Activity of tachykinin1-expressing Pet1 Raphe Neurons Modulates the Respiratory Chemoreflex. *J. Neurosci.* 37, 1807–1819

Herzog E, Gilchrist J, Gras C, Muzerelle A, Rayassard P, Giros B, Gaspar P, El Mestikawy S. (2004) Localization of VGLUT3, the Vesicular Glutamate Transporter type 3, in the Rat Brain. *Neuroscience* 123, 983–1002

Hioki H, Nakamura H, Ma YF, Konno M, Hayakawa T, Nakamura KC, Fujiyama F, Kaneko T. (2010) Vesicular Glutamate Transporter 3-expressing Non-serotonergic Projection Neurons Constitute a Subregion in the Rat Midbrain Raphe Nuclei. *J. Comp. Neurol.* 518, 668–686

Hodges MRR, Wehner M, Aungst J, Smith JC, Richerson GB. (2009) Transgenic Mice Lacking Serotonin Neurons Have Severe Apnea and High Mortality during Development. *J Neuro.* 29(33) 10341-10349.
Homberg JR, Molteni R, Calabrese F, Riva MA. (2014) The Serotonin–BDNF Duo: Developmental Implications for the Vulnerability to Psychopathology. *Neurosci & Biobehav Reviews.* 43: 35-47.
Huang EJ, Reichardt LF. (2001) Neurotrophins: Roles in Neuronal Development and Function. *Annu Rev Neurosci*. 24:677-736.
Huang KW, Ochandarena NE, Philson AC, Hyun M, Birnbaum JE, Cicconet M, Sabatini BL. (2019) Molecular and Anatomical Organization of the Dorsal Raphe Nucleus. *eLife*, 8: e46464.
Hurst HE. (1951). Long-term Storage Capacity in Reservoirs. *Trans. Amer. Soc. Civil Eng.* 116, 770-799.
Hyman JM, Zilli EA, Paley AM, Hasselmo ME (2005) Medial Prefrontal Cortex Cells Show Dynamic Modulation with the Hippocampal Theta Rhythm Dependent on Behavior. *Hippocampus* 15: 739–749.
Iniguez SD, Riggs LM, Nieto SJ, Dayrit G, Zamora NN, Shawhan KL, Cruz B, & Warren BL. (2014). Social Defeat Stress Induces a Depression-like Phenotype in Adolescent Male c57BL/6 Mice. *Stress* 17(3), 247–255.
Iniguez SD, Flores-Ramirez FJ, Riggs LM, Alipio JB, Garcia-Carachure I, Hernandez MA, Sanchez DO, Lobo MK, Serrano PA, Braren SH, & Castillo SA. (2018). Vicarious Social Defeat Stress Induces Depression-Related Outcomes in Female Mice. *Biological psychiatry,* 83(1), 9–17.
Jacobs BL, Azmitia EC. (1992) Structure and Function of the Brain Serotonin System. *Physiological Reviews*. 72(1): 165-229
Janusonis S, Mays KC, Hingorani MT (2019) Serotonergic Axons as 3D Walks *ACS Chem. Neurosci.* 10(7): 3064-3067
Janusonis S, Detering, N (2018) A Stochastic Approach to Serotonergic Fibers in Mental Disorders. *Biochimie,* in press.
Jensen P, Farago AF, Awatramani RB, Scott MM, Deneris ES, Dymecki SM. (2008) Redefining the serotonergic system by genetic lineage. *Nat. Neurosci.* 11, 417–419
Jin Y, Dougherty SE, Wood K, Sun L, Cudmore RH, Abdalla A, Kannan G, Pletnikov M, Hashemi P, Linden DJ. (2016) Regrowth of Serotonin Axons in the Adult Mouse Brain Following Injury. *Neuron.* 91(4): 748-762
Jones MW, Wilson MA. (2005) Theta Rhythms Coordinate Hippocampal-Prefrontal Interactions in a Spatial Memory Task. *PLoS Biol* 3: e402.
Kajstura TJ, Dougherty SE, Linden DJ. (2018) Serotonin Axons in the Neocortex of the Adult Female Mouse Regrow After Traumatic Brain Injury. *J Neurosci Res.* 96(4): 512-526
Kania A, Klein R. (2016) Mechanisms of Ephrin–Eph Signaling in Development, Physiology and Disease. *Nat Rev Mol Cell Biol.* 17, 240–256.
Kim H, Kim M, Im SK, Fang S. (2018) Mouse Cre-LoxP system: General Principles to Determine Tissue-Specific Roles of Target Genes. *Lab Anim Res.*34(4): 147-159.
Kim JH, Jang MJ, Choi J, Lee E, Song KD, Cho J, Kim KT, Cha HJ, Sun W. (2018) Optimizing Tissue-Clearing Conditions Based on Analysis of the Critical Factors Affecting Tissue-Clearing Procedures. *Sci Rep*. 8:12815.

Kosofsky BE, Molliver ME. (1987) The Serotoninergic Innervation of Cerebral Cortex: Different Classes of Axon Terminals Arise from Dorsal and Median Raphe Nuclei. *Synapse* 1(2):153-168

Lecker J, Froberg-Fejko K. (2016) Using Environmental Enrichment and Nutritional Supplementation to Improve Breeding Success in Rodents. *Lab Animal* 45: 406-407

Lee YS, Choi SL, Lee SH, Kim H, Park H, Lee N, Lee SH, Chae YS, Jang DJ, Kandel ER, Kaang BK. (2009) Identification of a Serotonin Receptor Coupled to Adenylyl Cyclase Involved in Learning-Related Heterosynaptic Facilitation in Aplysia. *PNAS* 106 (34): 14634-14639.

Leger L, Charnay Y, Hof PR, Bouras C, Cespuglio R. (2001) Anatomical distribution of serotonin-containing neurons and axons in the central nervous system of the cat. *J Comp Neurol*. 433(2):157-8

Lew CH, Hanson KL, Groeniger KM, Greiner D, Cuevas D, Hrvoj-Mihic B, Schumann CM, Semendeferi K. (2019) Serotonergic Innervation of the Human Amygdala and Evolutionary Implications. *Am J Phys Anthropol.* 170(3): 351-360

Lew CH, Groeniger KM, Hanson KL, Cuevas D, Greiner DMZ, Hrvojmihic B, Bellugi U, Schumann CM, Semendeferi K. (2020) Serotonergic Innervation of the Amygdala is Inceased in Autism Spectrum Disorder and Decreased in Williams Syndrome. *Molecular Autism.* 11(1):12

Li A, Li R, Ouyang P, Li H, Wang S, Zhang X, Wang D, Ran M, Zhao G, Yang Q, Zhu Z, Dong H, Zhang H. (2021) Dorsal Raphe Serotonergic Neurons Promote Arousal from Isoflurane Anesthesia. *CNS* 27(8): 941-950.

Lidov HGW, Molliver ME. (1982) Immunohistochemical Study of the Development of Serotonergic Neurons in the Rat CNS. *Brain Research Buletin.* 9:559–604

Linley SB, Hoover WB, Vertes RP. (2013) Pattern of Distribution of Serotonergic Fibers to the Orbitofrontal and Insular Cortex in the Rat. *J. Chemical Neuroscience* 48-49: 29-45

Maddaloni G, Bertero A, Pratelli M, Barsotti N, Boonstra A, Giorgi A, Migliarini S, Pasqualetti M. (2017). Development of Serotonergic Fibers in the Post-Natal Mouse Brain. *Frontiers in Cellular Neuroscience 11*, 202

Madisen L, Zwingman TA, Sunkin SM, Oh SW, Zariwala HA, Gu H, Ng LL, Palmiter RD, Hawrylycz MJ, Jones AR, Lein ES, Zeng H. (2010) A Robust and High Through-put Cre Reporting and Characterization System for the Whole Mouse Brain. *Nat. Neuroscience* 13(1): 133-140

Maggioni M, Boracchi G, Foi A, Egiazarian K. (2012) Video Denoising, Deblocking, and Enhancement through Separable 4-D Nonlocal Spatiotemporal Transforms. *IEEE Transactions on Image Processing.* 21(9): 3952–66.

Maia G, Soares J, Almeida S, Leite J, Baptista H, Lukoyanova A, Brazete C, Lukoyanov N. (2019) Altered Serotonin Innervation in the Rat Epileptic Brain. *Brain Research Bulletin* 152: 95-106

Mamounas LA, Altar CA, Blue ME, Kaplan DR, Tessarollo L, Lyons WE. (2000) BDNF Promotes the Regenerative Sprouting, but not Survival, of Injured Serotonergic Axons in the Adult Rat Brain. *J Neurosci.* 20(2):771-82.

Mano T, Albanese A, Dodt HU, Erturk A, Gradinaru V, Treweek JB, Miyawaki A, Chung K, Ueda H. (2018) Whole-Brain Analysis of Cells and Circuits by Tissue Clearing and Light-Sheet Microscopy. *J Neurosci* 38 (44): 9330-9337

Matias S, Lottem E, Dugue GP, Mainen ZF. (2017) Activity Patterns of Serotonin Neurons Underlying Cognitive Flexibility. *eLife* 6: e20552.
McBride PA, Anderson GM, Hertzig ME, Sweeney JA, Kream J, Cohen DJ, Mann JJ. (1989) Serotonergic Responsivity in Male Young Adults with Autistic Disorder. *Archives of General Psychiatry.* 46: 205-212
McCorvy JD, Harland AA, Maglathlin R, Nichols DE. (2011) A 5-HT(2C) Receptor Antagonist Potentiates a Low Dose Amphetamine-Induced Conditioned Place Preference. *Neurosci Lett.* 505:10–13.
McCorvy JD, Roth BL. Structure and Function of Serotonin G Protein-Coupled Receptors. (2015) *Pharmacol Ther.* 150:129-42.
McLellan MA, Rosenthal NA, Pinto AR. (2017) Cre-loxP-Mediated Recombination: General Principles and Experimental Considerations. *Curr Protoc Mouse Biol.* 7(1):1–12.
Metzger D, Chambon P. (2001) Site- and Time-Specific Gene Targeting in the Mouse. *Methods.* 24(1): 71–80.
Mandelbrot BB, Van Ness JW. (1968) Fractional Brownian Motions, Fractional Noises and Applications. *SIAM Review* 10, 422-437.
Legg LA, Tilney R, Hsieh CF, Wu S, Lundstrom E, Rudberg AS, Kutlubaev MA, Dennis M, Soleimani B, Barugh A, Hackett ML, Hankey GJ, Mead GE. (2012) Selective Serotonin Reuptake Inhibitors (SSRIs) for Stroke Recovery (Review). *Cochrane Database Syst Rev* 11:1–306.
Meltzer HY, Roth BL. (2013) Lorcaserin and Pimavanserin: Emerging Selectivity of Serotonin Receptor Subtype-Targeted Drugs. *J Clin Invest.* 123(12):4986-91.
Miranda M, Morici JF, Zanoni MB, Bekinschtein P. (2019) Brain-Derived Neurotrophic Factor: A Key Molecule for Memory in the Healthy and the Pathological Brain. *Front. Cell Neuroscience.*10: 33-89.
Moll JL, Brown CS. (2011) The Use of Monoamine Pharmacological Agents in the Treatment of Sexual Dysfunction: Evidence in the Literature. *J Sex Med.* 8(4): 956-70.
Morin LP, Meyer-Bernstein EL. (1999) The Ascending Serotonergic System in the Hamster: Comparison with Projections of the Dorsal and Median Raphe Nuclei. *Neuroscience.* 91(1): 81-105.
Mosienko V, Beis D, Pasqualetti M, Waider J, Matthes S, Qadri F, Bader M, Alenina N. (2015) Life Without Brain Serotonin: Reevaluation of Serotonin Function with Mice Deficient in Brain Serotonin Synthesis. *Behavioural Brain Research.* 277: 78-88.
Murphy DG, Daly E, Schmitz N, Toal F, Murphy K, Curran S, Erlandsson K, Eersels J, Kerwin R, Ell P, Travis M. (2006) Cortical Serotonin 5-HT2A Receptor Binding and Social Communication in Adults with Asperger's Syndrome: An in-vivo SPECT Study. *American Journal of Psychiatry.* 163: 934-936
Muller CL, Anacker AMJ, Veenstra-Vanderweele J. (2016) The Serotonin System in Autism Spectrum Disorder: From Biomarker to Animal Models. *Neuroscience.* 321: 24-41
Nagy A. (2000) Cre Recombinase: The Universal Reagent for Genome Tailoring. *Genesis.* 26(2): 99–109.
Naso MF, Tomkowicz B, Perry WL 3rd, Strohl WR. (2017) Adeno-Associated Virus (AAV) as a Vector for Gene Therapy. *BioDrugs.*31(4): 317-334.

Nattie EE, Li A, Richerson GB, Richerson G, Lappi DA. (2004) Medullary Serotonergic Neurones and Adjacent Neurones that Express Neurokinin-1 Receptors are both Involved in Chemoreception *in-vivo*. *J Physiol.* 556(Pt 1): 235-53.

Nautiyal KM, Hen R. (2017) Serotonin Receptors in Depression: From A to B. *F1000Research Faculty Review*: 123

Naumer M, Sonntag F, Schmidt K, Nieto K, Panke C, Davey NE, Popa-Wagner R, Kleinschmidt JA. (2012) Properties of the Adeno-Associated Virus Assembly-Activating Protein. *J Virol.* 86(23): 13038–13048.

Nayyar T, Bubser M, Ferguson MC, Diana Neely M, Shawn Goodwin J, Montine TJ, Deutch AY, Ansah TA. (2009) Cortical Serotonin and Norepinepherine Denervation in Parkinsonism: Prefrontal loss of the Beaded Serotonin Innervation. *Eur. J. Neurosci.* 30: 208-216.

Ng KL, Gibson EM, Hubbard R et al. (2015) Fluoxetine Maintains a State of Heightened Responsiveness to Motor Training Early After Stroke in a Mouse Model. *Stroke* 46: 2951–2960.

Niederkofler V, Asher TE, Okaty BW, Rood BD, Narayan A, Hwa LS, Beck SG, Miczek KA, Dymecki SM. (2016) Identification of serotonergic neuronal modules that affect aggressive behavior. *Cell Rep.* 17, 1934–1949.

Oblak A, Gibbs TT, Blatt GJ. (2013) Reduced Serotonin Receptor Subtypes in a Limbic and a Neocortical Region in Autism. *Autism Research*. 6: 571-583.

Ohira K, Takeuchi R, Iwanaga T, Miyakawa T. (2013) Chronic Fluoxetine Treatment Reduces Parvalbumin Expression and Perineuronal Nets in Gamma-Aminobutyric Acidergic Interneurons of the Frontal Cortex in Adult Mice. *Mol Brain* 6: 43–53.

Okaty, BW, Freret ME, Rood BD, Brust RD, Hennessy ML, deBairos D, Kim JC, Cook MN, Dymecki SM. (2015) Multi-Scale Molecular Deconstruction of the Serotonin Neuron System. *Neuron* 88, 774–791.

Okaty BW, Commons KG, Dymecki SM. (2019) Embracing Diversity in the 5-HT Neuronal System. *Nature Reviews: Neuroscience* 20: 397-424.

Olivetti PR, Lacefield CO, Kellendonk C. (2020) A Device for Stereotaxic Viral Delivery into the Brains of Neonatal Mice. *Biotechniques*. 69(4): 307-312.

Olivier B, Chan JSW, Snoeren EM, Olivier JDA, Veening JG, Vinkers CH, Waldinger MD, Oosting RS. (2010) Differences in Sexual Behaviour in Male and Female Rodents: Role of Serotonin. *Biological Basis of Sex Differences in Psychopharmacology.* 116(8).

Pasquale ED, Morin D, Monteau R, Hilaire G. (1992) Serotonergic Modulation of the Respiratory Rhythm Generator at Birth: An *in vitro* Study in the Rat. *Neuroscience Letters.* 143: 91-95.

Paterson DS, Trachtenberg FL, Thompson EG, Belliveau RA, Beggs AH, Darnall R, Chadwick AE, Krous HF, Kinney HC. (2006) Multiple Serotonergic Brainstem Abnormalities in Sudden Infant Death Syndrome. *Journal of the American Medical Association.* 296(17): 2124-2143.

Paulsen IMS, Dimke H, Frische S. (2015) A Single Simple Procedure for Dewaxing, Hydration and Heat-Induced Epitope Retrieval (HEIR) for Immunohistochemistry in Formalin-Fixed Paraffin-Embedded Tissue. *Eur J Histochem* 59(4): 2532.

Pelloux Y, Dilleen R, Economidou D, Theobald D, Everitt BJ. (2012) Reduced Forebrain Serotonin Transmission is Causally Involved in the Development of Compulsive Cocaine Seeking in Rats. *Neuropsychopharmacology.* 37(11): 2505-14.
Pelosi B, Pratelli M, Migliarini S, Pacini G, Pasqualetti M. (2015) Generation of Tph2 Conditional Knockout Mouse Line for Time-and-Tissue-Specific Depletion of Brain Serotonin. *PLoS ONE* 8:e0136422.
Petkovic A, Chaudhury D. (2022). Encore: Behavioral Animal Models of Stress, Depression and Mood Disorders. *Frontiers in behavioral neuroscience,* 16, 931964.
Quintero-Villegas A, Valdés-Ferrer SI. (2022) Central Nervous System Effects of 5-HT_7 Receptors: A Potential Target for Neurodegenerative Diseases. *Mol Med.* 28(1): 70.
Rapport MM, Green AA, Page IH. (1948) Serum Vasoconstrictor (Serotonin). IV. Isolation and characterization. *Journal of biology and chemistry*. 176: 1243-1251.
Richerson GB, Wang W, Tiwari J, Bradley SR (2001) Chemosensitivity of Serotonergic Neurons in the Rostral Ventral Medulla. *Respiration Physiology*. 129: 175-189.
Robinson C, Apgar C, Shapiro LA (2016) Astrocyte Hypertrophy Contributes to Aberrant Neurogenesis after Traumatic Brain Injury. *Neural Plasticity*. 1347987.
Roossien DH, Sadis BV, Yan Y, Webb JW, Min LY, Dizaji AS, Bogart LJ, Mazuski C, Huth RS, Stecher JS, Akula S, Shen F, Li Y, Xiao T, Vandenbrink M, Lichtman JW, Hensch TK, Herzog ED, Cai D. (2019) Multispectral Tracing in Densely Labeled Mouse Brain with nTracer. *Bioinformatics.* 35(18): 3544–3546.
Samulski RJ, Muzyczka N. (2014) AAV-Mediated Gene Therapy for Research and Therapeutic Purposes. *Annu Rev Virol.* 1(1): 427–451.
Sauer B, Henderson N. (1988) Site-Specific DNA Recombination in Mammalian Cells by the Cre Recombinase of Bacteriophage P1. *Genetics.* 85: 5166-5170.
Schmidt H, Rathjen FG. (2010) Signaling Mechanisms Regulating Axonal Branching *in-vivo. BioEssays*: *news & reviews in mol., cell. and dev. biology* 32: 977–985.
Simon HH, Scholz C, O'Leary DD. (2005) Engrailed Genes Control Developmental Fate of Serotonergic and Noradrenergic Neurons in Mid- and Hindbrain in a Gene Dose-Dependent Manner. *Mol. Cell Neurosci.* 28, 96–105.
Snoeren MS, Veening JG, Olivier, B, Oosting RS. (2014) Serotonin 1A Receptors and Sexual Behavior in Female Rats: A Review. *Review Pharmacol Biochem Behav.* 121:43-52.
Sohal DS, Nghiem M, Crackower MA, Witt SA, Kimball TR, Tymitz KM, Penninger JM, Molkentin JD. (2001) Temporally Regulated and Tissue-Specific Gene Manipulations in the Adult and Embryonic Heart Using a Tamoxifen-Inducible Cre Protein. *Circulation Research* 89(1): 20-25.
Song G, Poon CS. (2009) Lateral Parabrachial Nucleus Mediates Shortening of Expiration and Increase of Inspiratory Drive During Hypercapnia. *Respir Physiol Neurobiol.* 165(1): 9-12.
Sos KE, Mayer MI, Cserep C, Takacs FS, Szonyi A, Freund TF, Nyiri G. (2017) Cellular Architecture and Transmitter Phenotypes of Neurons of the Mouse Median Raphe Region. *Brain Struct Funct* 222: 287– 299.
Spalteholz W. (1914) About Transparency of Human and Animal Preparations and its Theoretical Conditions. *Leipzig: S. Hirzel*

Sternberg N, Hamilton D. (1981) Bacteriophage P1 Site-Specific Recombination: I. Recombination Between LoxP Sites. *J. Mol. Biol.* 150: 467-486.
Storm-Mathisen J, Leknes AK, Bore AT, Vaaland JL, Edminson P, Haug FM, Ottersen OP. (1983) First Visualization of Glutamate and GABA in Neurons by Immunocytochemistry. *Nature* 301, 517–520.
Sun C, Qi L, Cheng Y, Zhao Y, Gucor C. (2022) Immediate Induction of Varicosities by Transverse Compression but not Uniaxial Stretch in Axon Mechanosensation. *Acta Neuropathol Commun.*10:7.
Susaki EA, Tainaka K, Perrin D, Yukinaga H, Kuno A, Ueda HR. (2015) Advanced CUBIC Protocols for Whole-Brain and Whole-Body Clearing and Imaging. *Nature Protocols*. 10: 1709-1727.
Tainaka K, Kuno A, Kubota SI, Murakami T, Ueda H. (2016) Chemical Principles in Tissue Clearing and Staining Protocols in Whole-Body Cell Profiling. *Annu. Rev. Cell Dev. Biol.* 32: 713-741
Teng T, Gaillard A, Muzerelle A, Gaspar P. (2017) EphrinA5 Signaling is Required for the Distinctive Targeting of Raphe Serotonin Neurons in the Forebrain. *eNeuro.* 6: 4(1).
Thomas DR, Hagan JJ. (2004) 5-HT7 Receptors. *Curr Drug Targets CNS Neurol Disord*. 3(1):81-90.
Thomsen WJ, Grottick AJ, Menzaghi F, Reyes-Saldana H, Espitia S, Yuskin D, *et al.* (2008) Lorcaserin, a Novel Selective Human 5-Hydroxytryptamine2C Agonist: in Vitro and in Vivo Pharmacological Characterization. *J Pharmacol Exp Ther.* 325:577–587.
Tritsch NX, Ding JB, Sabatini BL. (2012) Dopaminergic Neurons Inhibit Striatal Output Through Non-Canonical Release of GABA. *Nature.* 490, 262–266.
Tyler WJ, Alonso M, Bramham CR, Pozzo-Miller LD. (2002) From Acquisition to Consolidation: on the Role of Brain-Derived Neurotrophic Factor Signaling in Hippocampal-Dependent Learning. *Learning and Memory*. 9(5):224-37.
Vahid-Ansari F, Daigle M, Manzini MC, Tanaka KF, Hen R, Geddes SD, Beique JC, James J, Merali Z, Albert PR. (2017) Abrogated Freud-1/Cc2d1a Repression of 5-HT1A Autoreceptors Induces Fluoxetine-Resistant Anxiety/Depression-Like Behavior. *J Neurosci* 37(49): 11967-11978.
Varea E, Castillo-Gomez E, Gomez-Climent MA. *et al.* (2017) Chronic Antidepressant Treatment Induces Contrasting Patterns of Synaptophysin and PSA-NCAM Expression in Different Regions of the Adult Rat Telencephalon. *European Neuropsychopharmacology.* 17(8): 546–557.
Yan R, Huang T, Xie Z, Xia G, Qian H, Zhao X, Cheng L. (2013) Lmx1b Controls Peptide Phenotypes in Serotonergic and Dopaminergic Neurons. *Acta Biochim. Biophys. Sin.* 45, 345–352.
Yan Y, Roossien DH, Sadis BV, Corso JJ, Cai D. (2018) A Recurrent Neural Network Approach for Automated Neural Tracing in Multispectral 3D Images. *bioRxiv.* 230441.
Varga V, Losonczy A, Zemelman BV, Borhegyi Z, Nyiri G, Domonkos A, Hangya B, Holderith N, Magee JC, Freund TF. (2009) Fast Synaptic Subcortical Control of Hippocampal Circuits. *Science* 326, 449–453.
Vertes RP. A PHA-L. (1991) Analysis of Ascending Projections of the Dorsal Raphe Nucleus in the Rat. *J Comp Neurol.* 313(4):643-68.

Vertes RP, Linley SB, Hoover WB. (2010) Pattern of Distribution of Serotonergic Fibers to the Thalamus of the Rat. *Brain Struct. Funct.* 215: 1-28.
Vetencourt JFM, Sale A, Viegi A, Baroncelli L, De Pasquale R, O'Leary OF, Castren E, Maffei L. (2008) The Antidepressant Fluoxetine Restores Plasticity in the Adult Visual Cortex. *Science* 320: 385–388.
Vialou V, Thibault M, Kaska S. *et al.* (2015) Differential Induction of FosB Isoforms Throughout the Brain by Fluoxetine and Chronic Stress. *Neuropharmacol.* 99: 28–37.
Vitalis T, Ansorg M, Dayer AG. (2013) Serotonin Homeostasis and Serotonin Receptors as Actors of Cortical Construction: Special Attention to the 5-HT3A and 5-HT6 Receptor Subtypes *Front. Cell. Neurosci.* 7:93.
Voigt T, Dolabela De Lima A. (1991) Serotoninergic Innervation of the Ferret Cerebral Cortex. *Jour Comp Neurology* 314: 415-428.
Vojta T, Halladay S, Skinner S, Janusonis S, Guggenberger T, Metzler R. (2020) Reflected Fractorial Brownian Motion in one and Higher Dimensions. *Phys Rev E.* 102(3-1): 032108.
Volosin M, Song W, Almeida RD, Kaplan DR, Hempstead BL, Friedman WJ. (2006) Interaction of Survival and Death Signaling in Basal Forebrain Neurons: Roles of Neurotrophins and Proneurotrophins. *J Neurosci.* 26(29): 7756-66.
Wallace JA, Lauder JM. (1983) Development of the Serotonergic System in the Rat Embryo: An Immunocytochemical Study. *Brain Research Bulletin.* 10(4):459–79.
Wardle RA, Poo MM. (2003) Brain-Derived Neurotrophic Factor Modulation of GABAergic Synapses by Postsynaptic Regulation of Chloride Transport. *J Neurosci.* 23(25):8722-32.
Wihan J, Grosch J, Kalinichenko L, Muller C, Winkler J, Kohl Z. (2019) Layer-Specific Axonal Degeneration of Serotonergic Fibers in the Prefrontal Cortex of Aged A54T α-synuclein—Expressing Mice. *Neurobiology of Aging.* 80: 29-37.
Weiss KR, Voigt FF, Shepherd DP, Huisken J. (2021) Practical Considerations for Tissue Clearing and Imaging. *Nature Protocols* 16: 2732-2748.
Wu Y, Wang W, Diez-Sampedro A, Richerson GB. (2007) Nonvesicular inhibitory neurotransmission via reversal of the GABA transporter GAT-1. *Neuron* 56, 851–865.
Wyler SC, Spencer WC, Green NH, Rood BD, Crawford L, Craige C, Gresch P, McMahon DG, Beck SG, Deneris E. (2016) Pet-1 Switches Transcriptional Targets Postnatally to Regulate Maturation of Serotonin Neuron Excitability. *J Neurosci* 36: 1758– 1774.
Zerbi V, Pagani M, Markicevic M, *et al.* (2021) Brain Mapping Across 16 Autism Mouse Models Reveals a Spectrum of Functional Connectivity Subtypes. *Mol Psychiatry*. 26: 7610-7620.
Zhang G, Stackman RW. (2015) The Role of Serotonin 5HT2A Receptors in Memory and Cognition. *Front. Pharmacol.* 6:225.
Zhao ZQ, Scott M, Chiechio S, Wang JS, Renner KJ, Gereau RW, Johnson RL, Deneris ES, Chen ZF. (2006) Lmx1b is Required for Maintenance of Central Serotonergic Neurons and Mice Lacking Central Serotonergic System Exhibit Normal Locomotor Activity. *J. Neurosci.* 26(49):12781-12788.